



Analysis, Design, Optimization and Realization of Compact High Performance Printed RF Filters

Dissertation

zur Erlangung des akademischen Grades

**Doktoringenieur
(Dr.-Ing.)**

von **M.Sc. Atallah Balalem**

geb. am 15. January 1978 in Nablus, Palestine

genehmigt durch die Fakultät für Elektrotechnik und Informationstechnik
der Otto-von-Guericke-Universität Magdeburg

Gutachter:

Prof. Dr.-Ing Abbas S. Omar

Prof. Dr.-Ing Marco Leone

Prof. Ing Jan Machac, DrSc.

Promotionskolloquium am: 15. März 2010

Dedications

*This work is dedicated to my Father and to the memory of
my Mother*

Atallah

Acknowledgement

First of all, I would like to thank God, who gives us every thing and without him nothing can be done.

First and foremost, I would like to thank my advisor, Professor Abbas S. Omar for his constant help and advising me. His encouragement and insight were extremely valuable throughout my graduate career. I would also like to thank Professor Jan Machac from Czech Technical University for his cooperation and discussions, and for allowing me to join his research group in Prague for six month. My thanks also go to Professor Wolfgang Menzel from the University of Ulm for his cooperation, discussions and for the fabrication of my structures at his department. I also thank Professor Samin Amari from Royal Military Collage in Canada for his cooperation and his discussions.

I would like to thank all of my colleagues and friends who have helped me through the difficult task of creating this Thesis, namely: Ali R. Ali, Ihab Hamad, Abdallah Fared, Julia Braun, Hasan Salem, Michael Maiwald, Mohammed Salah, Adel Abdel-Rahman, Fawzy Abujarad and his wife Raesa.

Last not least it is my pleasure to thank my father, brothers and sisters for their support, love, and their prayers. I should never forget to thank my wife Razan and my daughter Samia for their love and patience.

Kurzfassung

In der vorliegenden Arbeit wird ein modifizierter Querschnitt der mehrschichtigen Koplanarleitung und seine Anwendung fuer Filterzwecke untersucht. Mit Hilfe dieses Querschnittes wurde ein Tiefpass entworfen, der durch das Anbringen von breiten Patches auf dem klassischen Koplanar Waveguide (CPW) Tiefpassfilter realisiert wird. Die Patches sind auf der Ruckseite des Substrates und unter dem kapazitiven Streifen angebracht. Weitere Filter mit Bandpasscharakteristik sind so aufgebaut, dass sie Mikrostreifenleitung, CPW oder aus beiden beinhalten. Ein in der Mitte des Hohlleiters angebrachtes Streifenleitungs-Ultrabreitband-Bandpassfilter mit einem breiten Sperrbereich basiert auf einem Tiefpassfilter, das mit Ein/Aus- Versorgungsleitungen kapazitiv gekoppelt wird.

In dieser Arbeit wird auch ein interdigitaler Defected Ground Schlitz vorgestellt und untersucht. Zwei Tiefpassfilter werden dargestellt, die diesen Schlitz benutzen und dabei die Vorteile von kompakten Slots aufzeigen. Es wird eine Losung gezeigt, die die Schwierigkeiten beim Aufbau von Gehausen reduziert, indem die Grundplatte der Schaltung voll metallisiert wird und Schlitze auf dem Substrat geätzt werden. Das Metall des Substrates ist mit der Grundplatte mit Hilfe von Durchganglochern verbunden.

Es konnte ein erster Mikrostreifen-Resonators realisiert werden, der drei Resonanzfrequenzen besitzt. Dieser Resonator ist so aufgebaut, dass eine zusatzliche Maander-Mikrostreifenleitung von halber Wellenlange hinzugefugt wurde, die an den zwei gegenuberliegenden Ecken des originalen quadratischen Mikrostreifen- Zweimodenresonators verbunden ist. Zwei Bandpassfilter wurden realisiert mit Hilfe dieses Resonators, der erste mit einer Nullstelle in seinem Sperrbereich und der zweite mit drei Nullstellen. Weiterhin wird auf der Basis von Streifenleitungen ein Hohlleiter-Zweimodenresonator vorgestellt, es ist der erste Zweimodenresonator in dieser Technologie.

Zwei weitere kompakte Filter werden entworfen, gefertigt und getestet, die zwei Durchlassbereiche besitzen und auf dem Einsatz eines Zweimodenresonators aufbauen. Der erster Filter ist ein Mikrostreifen- Filter, er wurde realisiert durch das Einfugen von Nullstellen im Durchlassband eines Breitbandfilters durch die Benutzung eines quadratische scheifen Zweimodenresonator. Der zweite Filter ist ein Filter mit

bereits vorher vorgestellten Hohlleiter-Streifenleitungen. Der Filter wurde realisiert durch die Aufteilung der Moden von Zweimodenresonator in zwei Frequenzbander.

Abstract

This thesis introduces and investigates different multilayer structures and their filter applications. Compact quasi-lumped filters are introduced using this technology. Low-pass filter is designed using this structure by adding wide patches to the classical coplanar waveguide low-pass filter at the back side of the substrate and under the capacitive lines. Bandpass filters are introduced, these filters are constructed to be integrated with microstrip line, coplanar waveguide, and both. Moreover, a suspended stripline ultra-wideband bandpass filter with very wide stopband is introduced by coupling low-pass filter capacitively with the I/O feeding lines. The thesis also introduces and investigates an interdigital defected ground slot. The slot is very compact compared to the other known slots. Two low-pass filters are presented using this slot showing advantages of the compact slot. Moreover, the thesis presents a solution to reduce the packaging difficulties by keeping the ground plane of the circuit fully metallized and etching the slots on the superstrate, which is directly laying on the top of the substrate. The metal of the superstrate is connected by via holes to the ground plane. Further more, the thesis also introduces the first microstrip realization of triple-mode resonator. This resonator was realized by adding an additional meander half wavelength microstrip line connected to two opposite corners of the original microstrip square-loop dual-mode resonator. Two bandpass filters are realized using this resonator, the first one with a transmission zero in its stopband, and the second one with three transmission zeroes in its stopband. Moreover, a realization of suspended stripline dual-mode resonator is presented in this thesis, which is the first dual-mode resonator for this technique. Very compact bandpass filters are designed fabricated and tested using this resonator. Dual-band bandpass filters are realized by using dual-mode resonators. The first filter is a microstrip one is realized by introducing transmission zero in the passband of a broadband bandpass filter by using square-loop dual-mode resonator. The second introduced filter is a suspended stripline one. The filter is realized by splitting the modes of the dual-mode resonator into two frequency bands.

Table of Contents

Dedications	i
Acknowledgement	iii
Kurzfassung	v
Abstract	vii
Table of Contents	vi
List of Figures	viii
1 Introduction	1
1.1 Planar Resonators	3
1.2 Planar Lowpass Filters	5
1.3 Planar Bandpass Filters	7
1.3.1 Narrowband and Wideband Bandpass Filters	7
1.3.2 Ultra-Wideband Bandpass Filters	8
1.3.3 Dual-Band Bandpass Filters	9
1.4 Contributions and Thesis Organization	9
2 Background	11
2.1 Filter Types	12
2.1.1 Butterworth Response	12
2.1.2 Chebyshev Response	12
2.1.3 Elliptic Response	13
2.2 Elements Realization for Lowpass Prototype Filters	13
2.2.1 Butterworth Lowpass Prototype Filters	13
2.2.2 Chebyshev Lowpass Prototype Filters	14
2.2.3 Elliptic Lowpass Prototype Filters	15
2.2.4 Elements Transformations	16
2.3 Bandpass Transformation	17
2.4 Coupling Matrix and Cross Coupled Resonators	23
2.5 Planar Transmission Lines	26
2.5.1 Microstrip Line	26

2.5.2	Coplanar Waveguide	27
2.5.3	Suspended Stripline	28
2.5.4	Multilayer Transmission Lines	29
3	Multilayer Structures and Filter Applications	31
3.1	Multilayer Coplanar Line Cross Section	31
3.2	Quasi-Lumped Elements	34
3.3	Lowpass Filters	38
3.4	Microstrip Bandpass Filters Using Multilayer Line	41
3.5	CPW Bandpass Filters Using Multilayer Line	45
3.6	Bandpass Filter with Microstrip-CPW Feed Lines	48
3.7	Suspended Stripline Ultra-Wideband Bandpass Filter	50
4	Defected Ground Structures	57
4.1	Interdigital DGS Slot	60
4.2	Quasi Elliptic Microstrip Lowpass Filters	65
4.3	Defected Ground Structure and Packaging	66
5	Dual and Triple-Mode Resonators and Filters	73
5.1	Triple-Mode Microstrip Resonator	75
5.1.1	Resonator Topology	75
5.1.2	Modes and Perturbations p, r	76
5.1.3	Triple-Mode Resonator and Filter Realization	79
5.1.4	Broadband Equivalent Circuit	84
5.1.5	Experimental Results	87
5.2	Dual-Mode Suspended Stripline Filters	90
5.2.1	Quasi-Lumped Parallel Resonator	90
5.2.2	Open-Loop Resonator	90
5.2.3	Resonators Combination	91
6	Dual-Band Bandpass Filters Using Dual-Mode Resonator	99
6.1	Dual-Band Microstrip Filter	100
6.1.1	Filter Topology	100
6.1.2	Center Frequency and Bandwidth Control	101
6.1.3	Experimental Results	104
6.2	Dual-Band Suspended Stripline Filters Using Dual-Mode Resonator .	105
7	Conclusions and Future Work	111
7.1	Thesis Summary	111
7.2	Suggestions for Future Work	112
	List of Publications	127

List of Figures

1.1	Simplified schematic of a basic radio transmitter (up) and receiver (down).	1
1.2	Simplified schematic of a doppler radar.	1
1.3	Two possible shapes of open-loop resonator.	3
1.4	Dual-mode resonator fed by perpendicular feeding lines	4
1.5	Return loss of dual-mode bandpass filter using one dual-mode resonator.	4
1.6	Top layout of stepped impedance microstrip lowpass filter.	5
1.7	Low-pass filter structure (a) with quarter-wavelength stub, (b) with stepped-impedance stub.	6
1.8	Low-pass filter structure with extending the low-impedance line sections in parallel to the high-impedance section	7
1.9	Layout of microstrip bandpass filter using half-wavelength end coupled resonators [1].	7
1.10	Layout of microstrip bandpass filter using half-wavelength side coupled resonators.	8
2.1	Two forms of odd order lowpass prototype filter, inductance as first element (up), capacitance as first element (down).	14
2.2	Two forms of even order lowpass prototype filter, inductance as first element (up), capacitance as first element (down).	14
2.3	Elliptic lowpass prototype filter by using parallel resonators, even order (up), odd order (down).	16
2.4	Elliptic lowpass prototype filter by using series resonators, even order (up), odd order (down).	17
2.5	Bandpass filter prototype.	18
2.6	Admittance inverters used to convert a series inductance into its equivalent circuit with shunt capacitance.	19
2.7	Admittance inverters used to convert a shunt capacitance into its equivalent circuit with series inductance.	19
2.8	Low-pass filter structure using impedance inverters.	20
2.9	Low-pass filter structure using admittance inverters	20
2.10	Bandpass filter built with impedance inverters and series resonators	21
2.11	Bandpass filter built with admittance inverters and parallel resonators.	21

2.12	Bandpass filter using distributed elements connected to impedance inverters.	22
2.13	Bandpass filter using distributed elements connected to admittance inverters.	23
2.14	n -coupled resonators [2].	23
2.15	Microstrip line cross section.	26
2.16	Coplanar waveguide cross section.	27
2.17	Suspended stripline cross section.	28
3.1	(a) Cross section of MCL , (b) the MCL compatible with CPW , (c) the MCL compatible with microstrip line	32
3.2	coupling two 50 Ω lines structure (a) microstrip-microstrip, (b) CPW-CPW, and (c) CPW-slotted microstrip line.	33
3.3	Calculated capacitive coupling values between the two ends of 50 Ω strips of particular lines: CPW- CPW, microstrip-microstrip (ML-ML), and broadside coupling CPW-slotted microstrip line.	33
3.4	Characteristic impedance of slotted microstrip line as function of w for different slot width s	34
3.5	Characteristic impedance of slotted microstrip line as function of the width of the ground plane a	35
3.6	Layouts of shunt capacitance for (a) CPW , (b) microstrip.	36
3.7	3D view of suspended stripline shunt capacitance.	36
3.8	Layouts of shunt inductance for (a) CPW , (b) microstrip.	36
3.9	3D view of suspended stripline shunt inductance.	37
3.10	Layout of microstrip interdigital capacitance.	37
3.11	Top (up) and backside (down) layouts of a CPW lowpass filter, all dimensions are in mm	39
3.12	Insertion loss of CPW lowpass filter built on one layer of the substrate and Insertion loss of CPW lowpass filter with wide patches under the capacitive transmission line.	40
3.13	Measured (solid) and simulated (dashed) insertion and return loss of a CPW lowpass filter with patches.	40
3.14	Top (up) and backside (down) layout of the CPW lowpass filter with additional stubs.	41
3.15	Measured (solid) and simulated (dashed) insertion and return loss of a CPW lowpass filter with two transmission zeros.	42
3.16	Topside (up), and backside (down) layout of an MCL bandpass filter compatible with the microstrip line.	43
3.17	Equivalent circuit model of the bandpass filter.	43
3.18	Simulated return loss of the filter with inductive strip length l vary from 4.7 to 0.6 mm.	44

3.19	EM (solid) and Circuit (dashed) simulation of the insertion and return loss of the filter and its equivalent circuit.	44
3.20	Simulated and measured insertion and return loss of the ML bandpass filter.	45
3.21	Topside (up), and backside (down) layout of an MCL bandpass filter with additional capacitive coupling between the resonators.	46
3.22	Equivalent circuit model of the bandpass filter with additional capacitive coupling between the resonators.	46
3.23	Measured (solid) and simulated (dashed) insertion and return loss of the microstrip filter with additional transmission zero.	47
3.24	Top (up) and backside layouts (down) of an MCL bandpass filter with CPW feed lines,(all dimensions are in mm).	47
3.25	The equivalent circuit of the of CPW bandpass filter.	48
3.26	Measured (solid) and simulated (dashed) insertion and return loss of the CPW bandpass filter with transmission zero.	48
3.27	Top (up) and backside (down) layouts of a bandpass filter with microstrip-CPW feeding lines.	49
3.28	Simulated insertion and return loss of the Microstrip- CPW filter. . .	50
3.29	Top layer CPW-microstrip filter connected to patch antenna.	51
3.30	Return loss of the patch antenna itself and the patch antenna with the filter.	51
3.31	Cross-section of SSL (a) used in simulation process, (b) realized in practice.	52
3.32	Top (up), and backside (down) layouts of an SSL lowpass filter. . . .	53
3.33	Simulated insertion and return loss of a SSL lowpass filter.	54
3.34	Top (up) and backside (down) layouts of the SSL UWB filter using a coupled lowpass filter.	54
3.35	Equivalent circuit of the ultra-wideband bandpass filter using a coupled lowpass filter structure.	54
3.36	Photograph of the ultra-wideband bandpass filter with opened mount. . .	55
3.37	Simulated (dashed) and measured (solid) insertion and return loss of the UWB filter.	55
3.38	Simulated and measured insertion loss at the passband of the UWB filter.	56
4.1	Layouts of defected ground slots, (a) dumb bell structure with square head, (b) dumb bell structure with circular head, (c) U shape DGS structure.	58
4.2	Simulated insertion and return loss of a dumb-bell slot etched under 50-ohm transmission line.	58
4.3	ivalent circuit of a DGS slot etched under 50 Ω transmission line. .	58

4.4	Current density distribution on the slot metallization (a) at 2.5 GHz, (b) at 9 GHz.	59
4.5	Representation for the wave propagating on the slot metallization (a) at frequency lower than the resonant frequency, (b) at frequency higher than the resonant frequency.	59
4.6	Backside layout of the interdigital slot.	61
4.7	Equivalent circuit of the interdigital DGS slot etched under 50 Ω transmission line.	61
4.8	Simulated insertion and return loss of the interdigital slot.	61
4.9	Current density distribution (a) at 1 GHz, (b) 9.5 GHz.	63
4.10	Relation between the interdigital slot resonant frequency and the length of the metallic fingers.	63
4.11	Relation between the interdigital slot resonant frequency and the number of the metallic fingers.	64
4.12	Relation between the interdigital slot resonant frequency and the spacing between metallic fingers.	64
4.13	Top (above) and rear (below) layouts of a fifth order lowpass filter with apertures under the high-impedance transmission lines.	67
4.14	backside Layout of a fifth order lowpass filter with one interdigital DGS slot.	67
4.15	Simulated (dashed) and measured (solid) return and insertion loss of a fifth order lowpass filter with one transmission zero.	67
4.16	backside Layout of a fifth order lowpass filter with two interdigital DGS slots.	68
4.17	Simulated (dashed) and measured (solid) return and insertion loss of a fifth order lowpass filter with two transmission zeroes.	68
4.18	3D view of suspended DGS structure.	68
4.19	Calculated relation between the resonance frequency of the interdigital slot and the depth of the recessed region under DGS.	70
4.20	3D view of the proposed structure with an interdigital slot.	70
4.21	Simulated insertion and return loss of the proposed structure (solid) in comparison with the standard DGS structure (dashed).	71
4.22	Top layout of a fifth order lowpass filter, the rear of the substrate is fully metallized.	71
4.23	2 Metallization of the additional substrate, which contains two slots with finger lengths 3.55, and 2.45 mm, and one aperture.	71
4.24	Photograph of the fabricated lowpass filter.	72
4.25	Simulated (dashed) and measured (solid) insertion and return loss of a lowpass filter with the proposed DGS structure.	72

5.1	Dual-mode circular loop, patch resonator (a), square loop, patch resonator (b), square meander loop resonator (c).	74
5.2	Dual-mode triangular patch resonator (a), triangular closed loop (b), meander loop resonator (c).	74
5.3	(a) Dual-mode filter with inner corner cut perturbation, (b) dual-mode filter with inner corner patch perturbation, (c) dual-mode filter with outer corner patch perturbation[3].	75
5.4	Layout of a microstrip (a)dual-mode resonator, (b) triple-mode resonator coupled by perpendicular feeding lines and perturbed by outer patch.	76
5.5	Reflection coefficient of un-perturbed resonator using perfect magnetic wall at the symmetry plane.	77
5.6	Reflection coefficient of un-perturbed resonator using perfect electric wall at the symmetry plane.	78
5.7	Reflection coefficient of un-perturbed resonator fed by two perpendicular feeding lines.	78
5.8	Relation between the size of the perturbation element p and the triple-mode resonance frequencies, perturbation r is not presented ($r=0$).	79
5.9	Relation between the size of the perturbation element r and the triple-mode resonance frequencies, perturbation p is not presented ($p=0$).	80
5.10	Coupling and routing scheme of the triple-mode filter.	80
5.11	flow chart of the used optimization method.	82
5.12	EM simulation (solid) synthesized (dashed) reflection and transmission coefficients of a triple-mode bandpass filter.	84
5.13	Transmission coefficient of a triple-mode bandpass filter with various a values.	85
5.14	EM simulation (solid) synthesized (dashed) reflection and transmission coefficients of triple-mode bandpass filter with three transmission zeros.	85
5.15	Broadband equivalent circuit of the triple- mode microstrip filter. The inset shows the circuit used to determine C_s	86
5.16	Transmission coefficient of the Broad-band equivalent circuit for different values of C_{Ports}	87
5.17	EM simulation (solid) and equivalent circuit simulation (dashed) when $C_{Ports}=0.01$ pF.	88
5.18	Photograph of a third order bandpass filter using the proposed triple-mode resonator.	88
5.19	Simulated(dashed) and measured (solid) insertion and return loss of trip-mode bandpass filter with one transmission zero.	89
5.20	Simulated(dashed) and measured (solid) insertion and return loss of trip-mode bandpass filter with three transmission zeroes	89

5.21	(a) Layout of suspended stripline quasi-lumped resonator, (b) equivalent circuit of the suspended stripline resonator	91
5.22	Coupling structures for microstrip open-loop resonator (a) capacitive coupling structure, (b) inductive coupling structure, (c) mixed coupling structure, (d) mixed coupling structure [4].	91
5.23	Suspended stripline open-loop resonator.	92
5.24	Suspended stripline open-loop resonator.	93
5.25	Simulated return loss of the dual-mode resonator (dashed) in comparison with the return loss of the open-loop (solid).	93
5.26	3D view of a second order bandpass filter using SSL dual-mode resonator intensively coupled with the feeding lines.	94
5.27	Simulated insertion and return loss of a second order bandpass filter using SSL dual-mode resonator intensively coupled with the feeding lines.	94
5.28	3D view of fourth order bandpass filter using two dual-mode resonators.	95
5.29	Simulated insertion and return loss of a fourth order bandpass filter using SSL dual-mode resonator.	95
5.30	3D sketch of a fourth order SSL bandpass filter using two dual-mode resonators with parallel inductive strips on one side.	96
5.31	Photograph of fourth order bandpass filter structure.	96
5.32	Measured (solid) and simulated (dashed) return and insertion losses of the fourth order bandpass filter with additional transmission zero.	97
6.1	Layout of the broadband bandpass filter using multiple-mode resonator with a square-loop dual-mode resonator at the center of the filter.	100
6.2	Insertion loss of the broadband bandpass filter with $l_D = l_T = 10$ mm.	100
6.3	Layout of the dual-band bandpass filter using multiple-mode resonator with a square-loop dual-mode resonator at the center of the filter.	101
6.4	Insertion loss on dual-band bandpass filter with dimensions $l_D = l_T = 10$ mm, the width of all transmission lines is 0.3 mm.	101
6.5	Simulated return loss of a dual-band bandpass filter with $l_D = l_T = 5, 10, 15$ mm.	102
6.6	Simulated insertion loss of the dual-band bandpass filter with different l_T values, with $l_D = 10$ mm.	103
6.7	Simulated insertion loss of the dual-band bandpass filter with different l_D values with $l_T = 10$ mm.	103
6.8	Simulated insertion loss of the dual-band bandpass filter with different p values, with $l_D = l_T = 10$ mm.	104
6.9	Simulated and measured return and insertion loss of a dual-band bandpass filter with dimensions $l_D = l_T = 10$ mm.	105

6.10	Top (up) and backside of dual-bandpass filter using splitted mode of suspended stripline dual-mode resonator.	106
6.11	Insertion loss of the dual-band bandpass filter with deferent inductive stripline widths (w).	107
6.12	Insertion loss of the dual-band bandpass filter with deferent x dimension values.	107
6.13	Simulated (dashed) and measured (solid) Insertion loss and return loss of the dual-band bandpass filter.	108
6.14	Top (up) and backside (down) layouts of a suspended stripline filter with inductive stripline at one side of the substrate.	109
6.15	Simulated (dashed) and measured (solid) insertion and return loss of the dual-band bandpass filter with additional transmission zero.	109

Chapter 1

Introduction

The increasing scale of modern wireless communication applications and radar systems in today's technology has boosted the demand for RF and microwave filters; as they are playing an essential role in Transmit-Receive systems. Such as radio and television broadcasting, mobile communications, satellite communications, traffic radar, air traffic radar, automotive radar, and synthetic aperture radar. Fig. 1.1 shows a simple scheme of the radio system, while Fig. 1.2 shows a simple scheme of the doppler radar.

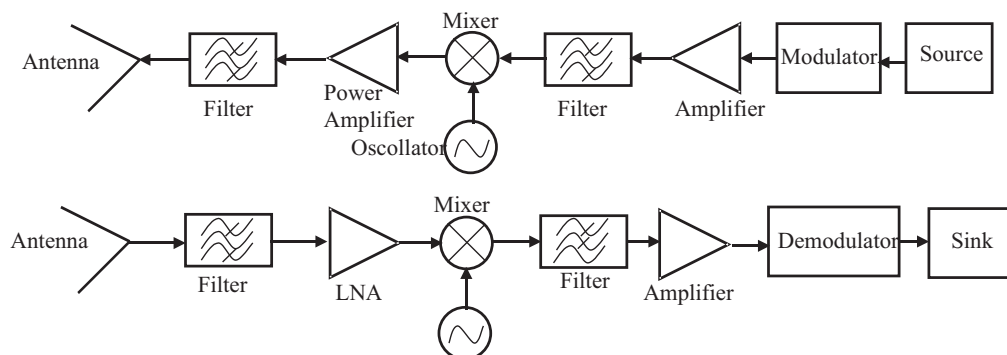


Figure 1.1: Simplified schematic of a basic radio transmitter (up) and receiver (down).

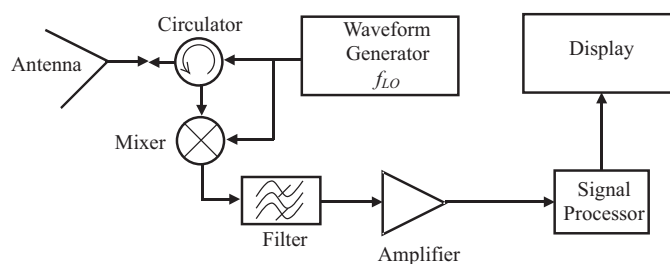


Figure 1.2: Simplified schematic of a doppler radar.

The microwave and RF filters are two-port frequency selective networks [1, 2, 5]. The main application of the filter is to reject the unwanted signal frequencies while permitting a good transmission for the required frequencies. These networks are classified according to their application. There are four main filter classes. The first class is lowpass filters which provide good transmission for low frequencies and reject the high frequencies, this kind of filters are used to suppress harmonics and spurious, which is necessary in designing power amplifiers, mixers, and voltage-controlled oscillators [1]. The second one is highpass filter which rejects the low frequency and provides a good transmission for high frequency, this filter has many applications such as removing the DC offsets and removal of low-frequency noise. The third one is bandpass filter that provides good transmission for a certain frequency band and rejects the lower and upper frequency bands, this kind of filters is used in many applications to select certain frequency band. The fourth and last common filter is bandstop filter which provides rejection at certain frequency band and provides good transmission at lower and upper frequency bands [1], [2] and [5].

Another application for filters is to separate between different frequency bands as it is in the case of diplexers and multiplexers. which are multiple port components. These components are realized by connecting two or more filters - each operates on different frequency band - in parallel or in series, see e.g. [1], [6]. By using the diplexers and multiplexers as multiple output and single input. It can also be used for different application, which is summing the signals that have different frequency bands, by using it as multiple input single output device.

RF and microwave filters are also classified by technology used for the filter realization into active and passive filters. Active filters are realized by using active elements such as transistors, diodes and amplifiers, in addition to the passive components. These filters are simple to realize, they provide gain, high quality factor, and can be easily integrated with the other system components. However, due to the active elements used in the filter, the filter requires a power supply, which may increase the complexity to the system. Moreover, the internal feedback is required, that may increase the sensitivity of the filter [7].

Passive filters are realized by using passive elements such as capacitors and inductors. This kind of filters has many advantages over active filters, they are more stable than the active filters, no power supply is required, and less expensive.

For microwave range higher than 500 MHz, the passive filters are mostly realized by using either planar transmission lines, or waveguides. Although waveguide components have low losses, and can handle higher power than the planar transmission lines, it is not preferable in new communications systems that require the mobility, because of their large size and their heavy weight. Moreover, fabrication processes of the waveguide components are more expensive than that for planar transmission lines. Therefore, most of microwave filters are designed using the planar transmission lines.

1.1 Planar Resonators

Modern systems require high performance filters with very low losses, small size, sharp cut-off, and high rejection at the stopband. Thus, different resonators and techniques have been introduced for RF and microwave filters to achieve different filters with this performance using the planar transmission line. The main used resonators and techniques are:

1. *Folded Transmission Line Resonator*: It is the simplest resonator, it is basically a transmission line section that resonates when its length corresponds to half a wavelength [1].
2. *Stepped Impedance Resonators*: This type of resonators consists of high and low impedance sections, or in other words wide and narrow width transmission lines. This resonator resonates when its length corresponds to half a wavelength [1], [2], and [5].
3. *Open-Loop Resonators*: It is a modified version of folded transmission line resonator, it is also known as U-shaped resonator and hairpin resonator, it looks like a loop which open from one side, see Fig. 1.3. This type of resonators has great advantages in reducing filter size, in addition, it has different coupling nature depending on the coupling sides [2], [4], and [8]. The main disadvantage of these resonators is that the higher order harmonic does not allow for wide stopband.



Figure 1.3: Two possible shapes of open-loop resonator.

4. *Dual-Mode Resonators*: This type of resonators is considered to be one of the most compact resonators used for the filter design these days. This is because, e.g., a second order filter can be realized by using a single resonator, in turn the size of the filter can be reduced to the half of that in case of single resonance resonators, such as half-wavelength folded line resonator. In addition, quasi-elliptic filter responses are easily achieved using such resonators without main change on the filter structure [9], [10] and [11]. The traditional dual-mode

resonators are realized by using a square or circular desks or loops, these resonators are normally fed by perpendicular feeding lines, see Fig.1.4. Fig. 1.5 resemble two minima that corresponds to the resonance of the structure.

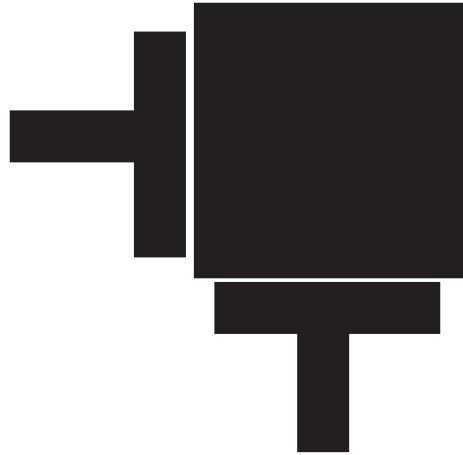


Figure 1.4: Dual-mode resonator fed by perpendicular feeding lines .

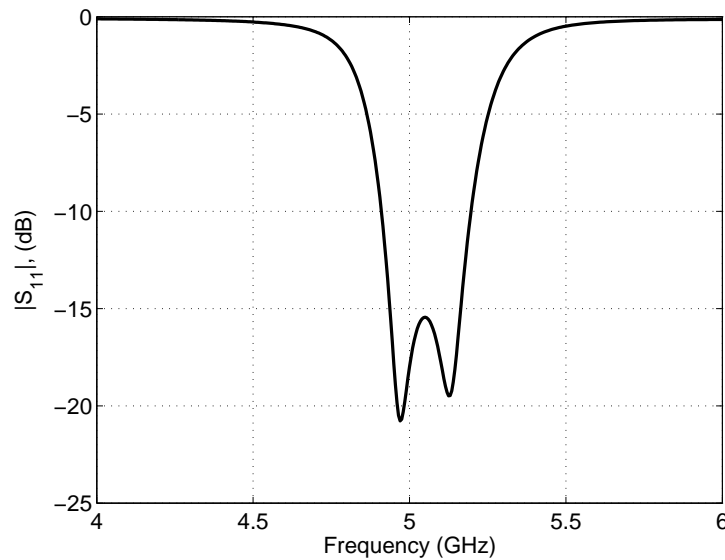


Figure 1.5: Return loss of dual-mode bandpass filter using one dual-mode resonator.

5. *Multiple-Mode Resonators*: This type of resonators has multiple resonance behavior in its passband. Many resonators of this type have been introduced. In [12] a multiple-mode resonator was introduced by using half-wavelength transmission line connected with pair of open end stubs, the resonator has been modified in [13] by replacing the open-stubs by shunted stubs. A multiple-mode resonator has been introduced by using pair of coupled rings with two open stubs symmetrically tapped to the inner ring [14]. A simple resonator of

this type was realized by stepped-impedance transmission line with length of λ at the center frequency in [15].

6. *Defected Ground Resonators*: It is a technique that has been recently introduced for microstrip and coplanar waveguide. It simply introduces resonances by etching slots in the ground plane of the microstrip and coplanar waveguide. different slot shapes have been introduced for filter applications, such as square head dumb-bell [16], rounded head dumb-bell [17], U-shape slots [18], and many other slot shapes [19–23]. The main advantages of this technique are reducing the size of the filter, increasing the degree of freedom since the resonator can be built on ground plane. However, this technique enlarges the packaging efforts.
7. *Quasi-Lumped Resonators*: Quasi-lumped elements and resonators have been introduced some years ago by using very small transmission line section [24–27]. Since the filter is realized by short line sections, the over all filter structure becomes small, and therefore the filters designed using quasi-lumped elements have low losses and wide stopband. Different filters with different bandwidths were introduced using the quasi-lumped elements technique [25–27].

1.2 Planar Lowpass Filters

Stepped impedance transmission lines have been first known structure for lowpass filter design [1, 2, 5]. Lowpass filters are normally realized by cascading high and low-impedance transmission lines. each of these lines must have very short length. The number of the used line section represents the order of the filter [28]. Fig. 1.6 shows a seventh order stepped impedance microstrip lowpass filter. The rejection at the stopband of such filters is not sufficient, and since most of the filter applications require filters with sharper cut-off, many techniques have been introduced in order to increase the rejection of the filter at the stopband.



Figure 1.6: Top layout of stepped impedance microstrip lowpass filter.

According to the basics of the filter, sharper cut-off slop and better rejection can be obtained by increasing the order of the filter. However, the higher the filter order, the higher the losses. Another way to increase the cut-off sharpness is introducing

transmission zeros at the stopband of the filter response, which can be done by two approaches. The first approach is realized by introducing series resonator instead of shunt capacitance. This approach can be achieved using the planar technology by different ways. First one is done by implementing open-circuited quarter-wavelength stubs instead of the low-impedance transmission line sections, e.g. [1, 2, 5], see Fig. 2.17a. The open stub act as a short circuit when its length corresponds to quarter a wavelength, so a transmission zero can be introduced at that frequency. To reduce the length of the stubs, stepped-impedance stubs have been introduced [29], [30], see Fig. 2.17b.

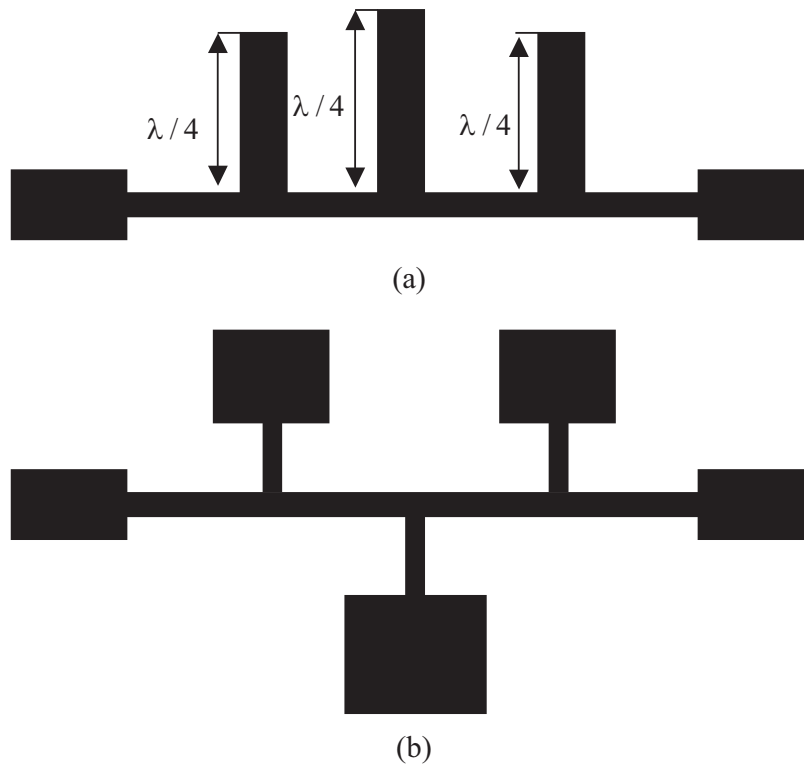


Figure 1.7: Low-pass filter structure (a) with quarter-wavelength stub, (b) with stepped-impedance stub.

The second approach is realized by introducing parallel resonators instead of series inductance. In the planar techniques, this has been realized by increasing the coupling between the low-impedance transmission line sections, by either extending the low-impedance line sections in parallel to the high-impedance line section [31, 32], as shown in Fig. 1.8, or by using snaked high impedance transmission line [33].

Transmission zeros can be easily introduced to the filter response without main change on the filter structure, by using defected ground structure technique (DGS). For lowpass filter, slots are mostly etched under the high impedance transmission lines, to introduce series capacitance in parallel to the inductive transmission line,

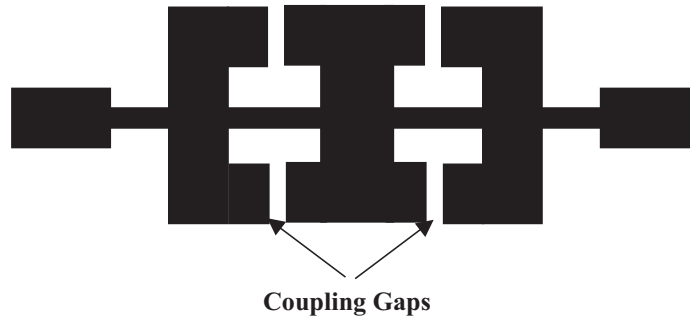


Figure 1.8: Low-pass filter structure with extending the low-impedance line sections in parallel to the high-impedance section .

which in turn introduces transmission zero. Normally the number of transmission zeros introduced for the lowpass response is equal to the number of the slots etched in ground plane, see [16], [17], [23], and [34–37].

1.3 Planar Bandpass Filters

Bandpass filters is one of the most important filters in the communication systems, they are classified by their bandwidth to narrowband, wideband and ultra-wideband filters. The main challenges that face the filter designers are to design a bandpass filter with compact size, low losses, and wide stopband.

1.3.1 Narrowband and Wideband Bandpass Filters

The early efforts were introducing end-coupled transmission line resonators [38]. It basically consists of transmission line sections having a length of half-wavelength at the corresponding center frequency. These transmission lines are coupled to each other by a small gap, as shown in Fig 1.9. The gap between the resonators is introducing a capacitive coupling between the resonators, which can be represented by a series capacitance [2].

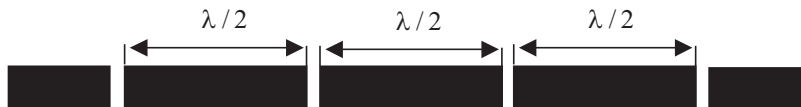


Figure 1.9: Layout of microstrip bandpass filter using half-wavelength end coupled resonators [1].

Side coupled half-wavelength transmission lines filter is a another bandpass filter structure [39]. The resonators are sidely coupled along of their length, as shown in

Fig. 1.10. Using this configuration, higher coupling is obtained and therefore wider bandwidth can be achieved.



Figure 1.10: Layout of microstrip bandpass filter using half-wavelength side coupled resonators.

Many other filters and resonators have been introduced and designed, such as stub type resonators. Filters of this type are designed using this resonator by either shunt open-circuited half-wavelength stubs or shunt short-circuited quarter-wavelength stubs [1, 2, 5]. A more compact bandpass filter is combline and quasi-combline filters. These filters are realized by having array of coupled resonators. The input and output are connected to the first and last array element which are not considered to be resonators [2]. Another resonator is hairpin-resonator that is also known as U-shape resonator, or open-loop resonator. It resonates at half-wavelength of the corresponding frequency. This resonator is more compact than the previous two resonators. Many other compact filters and resonators have been introduced in the past. In the next chapters we will discuss some other resonator types that have small size and high performance.

Wideband bandpass filters with fractional bandwidth greater than 25% are mostly realized by increasing the coupling between the resonators. To increase the coupling for the end-coupled resonators, multilayer structure has been used [40]. For the side-coupled resonator filters, apertures have been opened under the coupling area [41].

1.3.2 Ultra-Wideband Bandpass Filters

Ultra-wideband systems are defined as those systems that operate with fractional bandwidth greater than 40%. These systems have main advantages in transmitting high data rate with low power. In the recent years, ultra-wideband communication system specification has been defined for indoor applications, this system operates on 3.1-10.6 GHz [42]. For such systems, bandpass filters with fractional bandwidth of 110% is needed. The available filter theory however is not valid for this specification. Furthermore, the available resonators have not succeeded in providing such bandwidth. Therefore new resonator structures have been proposed, which is multiple-mode resonator [15]. In order to let the resonator give such wide passband, the coupling strength between the resonator and the feeding line has been increased by using locating the feeding lines and the resonator on the opposite sides of the substrate [43]. The main challenge for this class of resonators is to have wide stopband,

therefore different modifications have been done on this resonator, such as using defected ground structure under the resonator [44], the most successful one is done by using stepped impedance [45]. However, with these modifications some of these filters are suffering from bad matching the passband, some others suffer from high group delay variations in the passband.

1.3.3 Dual-Band Bandpass Filters

Some of the modern multi functional communication systems work with signals spread at the same time with several frequency bands, therefore these systems must incorporate dual-band, triple-band or multi-band filters. Thus, different efforts have been made on designing filters with this specification. The most known dual-band filter is realized by designing two individual bandpass filters, each operates on different frequency band, and connecting both sides of these two filters together by two T-junctions [46]. Using basic structure of bandstop filter with multiple shunt stubs with unequal length introduces the dual-band performance with transmission zeros [47], [48], stepped impedance resonator has been a successful approach [49–52], however it suffers from high losses, many other dual-band resonators and filter have been introduced in the recent years, we will discuss about them in details in the next chapters.

1.4 Contributions and Thesis Organization

The outlines of the thesis and authors contributions are organized as the following:

Chapter 2 consists of two parts, in the first part we are going to give a brief introduction to filter design theory. Second part gives a brief introduction to the different planar techniques.

Chapter 3 discusses quasi-lumped elements that are built on multilayer transmission line, in the first section we will give a brief introduction about the multilayer transmission lines, their characteristic impedance, and the capacitive coupling that these transmission lines provide by making use of both sides of the substrate. The second section discusses the realization of quasi-lumped elements and quasi-lumped resonators using these multilayer transmission lines. Section 3.3 introduces a coplanar waveguide lowpass filter using this technology, while section 3.4 introduces a compact quasi-lumped microstrip bandpass filter using these transmission lines. The same filter is reconstructed in section 3.5 to realize a coplanar waveguide bandpass filter. In section 3.6 the same filter is used as microstrip-CPW transition in addition to its filtering function. Section 3.7 introduces a simple ultra-wideband bandpass filter with very wide stopband using suspended stripline.

Chapter 4 investigates defected ground structures (DGS) for microstrip line. At the beginning of the chapter, an introduction to DGS is given. Section 4.1 introduces

a compact DGS slot in the shape of interdigital element. Section 4.2 introduces the interdigital slot for lowpass filter application. Section 4.3 investigates of the integration and packaging difficulties of DGS components and proposes a solution for that purpose.

Chapter 5 discusses the dual-mode and multiple-mode resonators and filters. An introduction to the available planar dual-mode resonators is give in this chapter. Section 5.1 introduces a microstrip triple-mode resonator, this resonator is used to design quasi-elliptic bandpass filters with one and three transmission zeros, an equivalent circuit is also proposed. Section 5.2 introduces a compact suspended stripline dual-mode resonator by combining the open-loop resonator with the quasi-lumped parallel resonator.

Chapter 6 investigates dual-band bandpass filters. A brief introduction is given about the available dual-band filter structures in this chapter. Section 6.1 introduces a dual-band bandpass filter by introducing transmission zeros in the passband of broadband bandpass filter using dual-mode resonator. Section 6.2 introduces a suspended stripline dual-band bandpass filter by splitting the modes of the dual-mode resonator that is introduced in section 5.2.

Chapter 7 gives conclusions of this work in addition to some suggestions for future work.

Chapter 2

Background

RF filters are two-port networks that provide frequency selectivity for the system. This device is characterized by its amplitude-squared transfer function, which is described mathematically as [1]

$$|s_{21}(j\omega)|^2 = \frac{1}{1 + \varepsilon^2 F_n^2(\omega)}, \quad (2.1)$$

where ε is a ripple constant, $F_n(\omega)$ represents the filtering or characteristic function. It is to let ω represents the radian frequency variable of a lowpass filter that has a cut-off frequency at $\omega = \omega_c$ for $\omega = 1$ (rad/s)

Another important parameter that characterizes the two-port network, such as filter, is called group delay, which is describes the actual delay between the input and output signal, it is also called the envelop delay, which is mathematically defined as [2]

$$\tau_g = \frac{d\phi_{S_{21}}}{d\omega}, \quad (2.2)$$

where

$$\phi_{S_{21}} = \text{Arg}S_{21}(j\omega) \quad (2.3)$$

The locations of the poles and zeros at the complex s-plane are also considered to be important. To be able to find that, we have to define the rational transfer function, which for is defined linear time-invariant network, such as filters, as [2]

$$S_{21}(s) = \frac{N(s)}{D(s)}, \quad (2.4)$$

where $N(s)$ and $D(s)$ are polynomials in the complex frequency variable $s = \sigma + j\omega$. Where the roots of the numerator are usually the zeros of the transfer function, and the roots of the denominator are the poles.

2.1 Filter Types

The filters are classified into different types depending on their filtering function $F_n(\omega)$, which in turn affect the values of elements used in the filter structure to achieve a certain filter response.

2.1.1 Butterworth Response

The frequency response of the Butterworth filter is maximally flat (has no ripples) in the passband, and rolls off towards zero in the stopband. All poles are distributed on a unity circle on the complex s-plane. The amplitude-square transfer function of filter is given by [2]

$$|s_{21}(j\omega)|^2 = \frac{1}{1 + \omega^{2n}}, \quad (2.5)$$

where n is the degree (order) of the filter, which corresponds to the number of reactive elements required in the lowpass prototype. Its all stopband zeros (transmission zeros) located at infinity, and the poles are distributed in a circle.

2.1.2 Chebyshev Response

Chebyshev response has steeper cut-off than that of the maximally flat response, since it exhibits the equi-ripple in the passband. The amplitude-square transfer function of the filter is given by [2]

$$|s_{21}(j\omega)|^2 = \frac{1}{1 + \varepsilon^2 T_n^2(\omega)}, \quad (2.6)$$

where the ripple constant ε is related to a given passband ripple L_{Ar} in dB by

$$\varepsilon = \sqrt{10^{\frac{L_{Ar}}{10}} - 1} \quad (2.7)$$

$T_n(\omega)$ is the chebyshev function of order n and defined as

$$T_n(\omega) = \begin{cases} \cos(n \cos^{-1} \omega), & |\omega| \leq 1 \\ \cosh(n \cosh^{-1} \omega), & |\omega| \geq 1 \end{cases} \quad (2.8)$$

The same as in the case of butterworth, all transmission zeros are located at infinity, while all poles are distributed on an ellipse in the complex s-plane. Because of the passband ripple, the response of the filter has smoother response in the passband than in the case of Butterworth.

Another filter response related to Chebyshev function is called Chebyshev Type II Filter, also known as the Inverse Chebyshev Filter, the reason for naming it is called like this because its response is the inverse of the Chebyshev filter response. The amplitude-square transfer function is given as [53],

$$|s_{21}(j\omega)|^2 = \frac{1}{1 + \frac{1}{\varepsilon^2 T_n^2(\frac{j\omega}{\omega_c})}} \quad (2.9)$$

In contrary to the chebyshev filter, this response is maximally flat at passband and exhibits equi-ripple at the stopband.

2.1.3 Elliptic Response

It is also called Chebyshev-Cauer response. This kind of filters has equi-ripple at their passband and the stopband. The amplitude-squared transfer function is given in (2.1). Where $F_n(\omega)$ is the filtering function and it is given as [1]

$$F_n(\omega) = \begin{cases} M \frac{\prod_{i=1}^{\frac{n}{2}} (\omega_i^2 - \omega^2)}{\prod_{i=1}^{\frac{n}{2}} (\frac{\omega_s^2}{\omega_i^2} - \omega^2)}, & n = \text{even} \\ N \frac{\prod_{i=1}^{\frac{n-1}{2}} (\omega_i^2 - \omega^2)}{\prod_{i=1}^{\frac{n-1}{2}} (\frac{\omega_s^2}{\omega_i^2} - \omega^2)}, & n \geq 3 \quad (\text{odd}), \end{cases} \quad (2.10)$$

where ω_s is the stopband frequency, which is greater than one, M and N are constants.

2.2 Elements Realization for Lowpass Prototype Filters

The definition of the lowpass prototype filter is that filter whose elements are so normalized to make the source impedance equal to one, that is denoted as $g_o = 1$, and the cut-off frequency to be unity, which is denoted as $\omega_c = 1(\text{rad/s})$.

Fig. 2.1 shows two forms of lowpass prototype filter, each of the forms is dual to each other and give the same response, therefore, both structures can be used. It should be known that n is the order of the filter or the number of the reactive elements in the filter structure, thus, g_o, g_{n+1} represent the source and load impedances. This is also valid for even order filter form that is shown in Fig.2.2

These lowpass forms serve as a prototype for designing many practical filters with their cut-off frequency and element transformations. Therefore, it is important to study this prototype for the known filtering functions.

2.2.1 Butterworth Lowpass Prototype Filters

The values of electric elements of the butterworth response with cut-off frequency $\omega_c = 1$ at insertion loss $L_{Ar} = 3.01$, can be easily done by applying [1]

$$g_o = g_{n+1} = 1, \quad (2.11)$$

$$g_i = 2 \sin \left(\frac{\pi(2i-1)}{2n} \right), \quad \text{for } i = 1 \quad \text{to} \quad n, \quad (2.12)$$

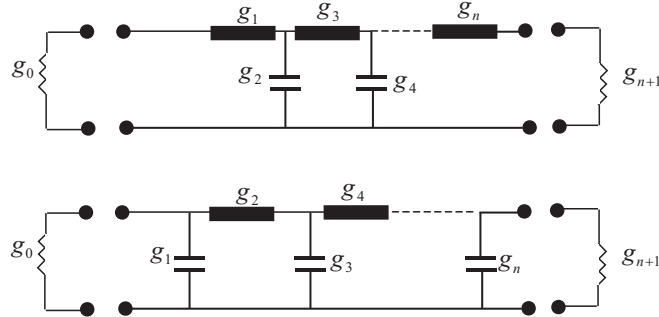


Figure 2.1: Two forms of odd order lowpass prototype filter, inductance as first element (up), capacitance as first element (down).

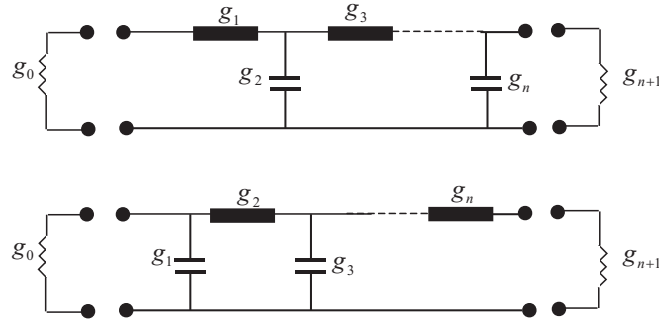


Figure 2.2: Two forms of even order lowpass prototype filter, inductance as first element (up), capacitance as first element (down).

From these two equations, we can notice that butterworth filter is always symmetrical network, which means that $g_1 = g_{n+1}, g_2 = g_n$ and so on. The higher the order of the filter is the higher the steepness of the cut-off slope, and the better the rejection at the stopband is. Thus, increasing the order of the filter or the user reactive elements would lead to better filter, the relation between n and the stopband attenuation can be written as

$$n \geq \frac{\log(10^{0.1L_{AS}} - 1)}{2 \log \omega_s}, \quad (2.13)$$

where L_{AS} is the stopband attenuation in dB at ω_s .

2.2.2 Chebyshev Lowpass Prototype Filters

Similarly, chebyshev response can be easily realized by reactive elements by applying the following equations [5].

$$g_o = 1, \quad (2.14)$$

$$g_1 = \frac{1}{\gamma} \sin\left(\frac{\pi}{2n}\right), \quad (2.15)$$

$$g_i = \frac{1}{g_{i-1}} \frac{4 \sin\left(\frac{\pi(2i-1)}{2n}\right) \sin\left(\frac{\pi(2i-3)}{2n}\right)}{\gamma^2 + \sin^2\left(\frac{\pi(2i-1)}{n}\right)}, \quad \text{for } i = 2 \text{ to } n, \quad (2.16)$$

$$g_{n+1} = \begin{cases} 1, & n \text{ odd} \\ \coth^2\left(\frac{\beta}{4}\right), & n \text{ even,} \end{cases} \quad (2.17)$$

where,

$$\beta = \ln\left(\coth\left(\frac{L_{Ar}}{17.37}\right)\right), \quad (2.18)$$

$$\gamma = \sinh\left(\frac{\beta}{2n}\right), \quad (2.19)$$

The order of the filter can be simply calculated by applying the following equation

$$n \geq \frac{\cosh^{-1} \sqrt{\frac{10^{0.1L_{As}} - 1}{10^{0.1L_{Ar}} - 1}}}{\cosh^{-1}(\omega_s)}, \quad (2.20)$$

where L_{As} , L_{Ar} are the minimum stopband rejection and the various ripple at the passband in dB, respectively.

2.2.3 Elliptic Lowpass Prototype Filters

Elliptic filters has equal-ripple at the passband and stopband, which means that this filter has similar response at the passband that chebyshev has, therefore it is called chebyshev-cauer filter. Elliptic lowpass prototype filter is realized by implementing either parallel resonator instead of series inductor as it is shown in Fig. 2.3, or by implementing series resonator instead of shunt capacitance as shown in Fig. 2.4. Unfortunately, there is no simple equation to realize the values of the elliptic lowpass filter elements as in the case of chebyshev and butterworth, but still there are some tables of the normalized filter element values [1],[2].

A simple realization for similar response can be realized by computing the elements of chebyshev prototype for the desired cut-off. Then replacing either parallel resonator instead of series resonator, or by implementing series resonator instead of shunt capacitance. This response is called quasi-elliptic filter response. Now, the values of the resonator elements can be calculated. For the first case where we have implemented parallel resonator instead of series inductance, at the cut-off frequency, the impedance of the resonator should be equal to the impedance of the original inductance. While, at attenuation pole (transmission zero), the admittance of the parallel resonator is equal to zero, which can be written as,

$$\frac{1}{j\omega_c C^e + \frac{1}{j\omega_c L^e}} = j\omega_c L, \quad (2.21)$$

$$j\omega_z C^e + \frac{1}{j\omega_z L^e} = 0, \quad (2.22)$$

where C^e and L^e are the capacitive and inductive values of the resonator, respectively, ω_z is the angular frequency at the desired transmission zero, ω_c is the angular cut-off frequency, and L is the inductive value of the original chebyshev element.

For the second case, where we have implemented a series resonator instead of the shunt capacitance in the original chebyshev lowpass filter, similar to the first realization the impedance of the resonator is equal to zero at the transmission zero frequency, and the impedance of the resonator should be equal to the impedance of the original shunt capacitance, which can be written as,

$$j\omega_z L^e + \frac{1}{j\omega_z C^e} = 0, \quad (2.23)$$

$$j\omega_c L^e + \frac{1}{j\omega_c C^e} = \frac{1}{j\omega_c C}, \quad (2.24)$$

where C^e and L^e are the capacitive and inductive values of the resonator, respectively, ω_z is the angular frequency at the desired transmission zero, ω_c is the angular cut-off frequency, and C is the capacitive value of the original Chebyshev element.

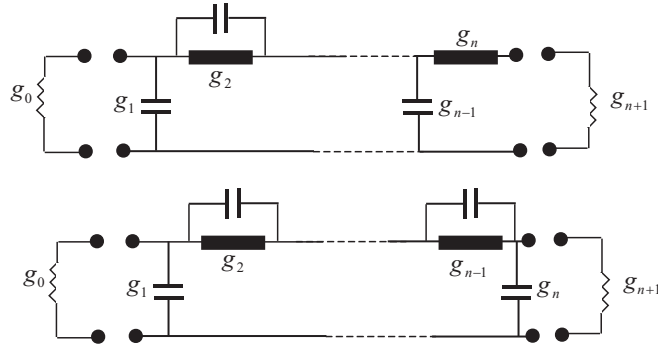


Figure 2.3: Elliptic lowpass prototype filter by using parallel resonators, even order (up), odd order (down).

2.2.4 Elements Transformations

The actual value of the lowpass filter elements are depending on the source impedance, cut-off frequency, and the normalized elements that have been described in this section. Having all these parameters, the actual element values can be formed as [1]

$$L_i = \frac{g_i Z_0}{\omega_c}, \quad (2.25)$$

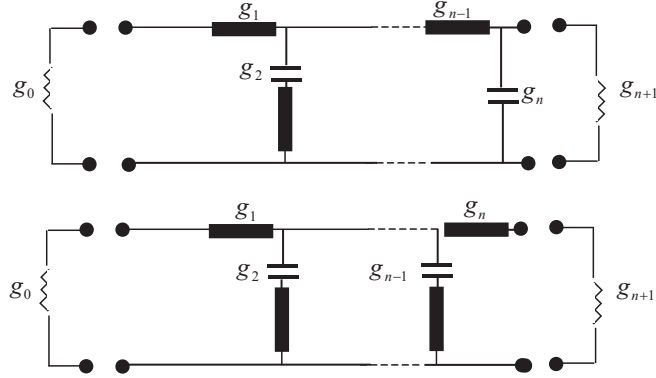


Figure 2.4: Elliptic lowpass prototype filter by using series resonators, even order (up), odd order (down).

$$C_i = \frac{g_i}{Z_0 \omega_c}, \quad (2.26)$$

where C_i and L_i are the capacitive and inductive values of the lowpass filter, respectively, Z_0 is the source impedance, and ω_c is the cut-off frequency.

For filters in microwave range the lumped elements are replaced by distributed elements, where their values can only be approximated. For this reason the achieved microwave filter responses do not fully agree with the prototype responses, therefore these filters are called quasi-chebyshev, quasi-butterworth or quasi-elliptic responses.

2.3 Bandpass Transformation

Lowpass to bandpass transformation can be achieved by transforming ω to ω' , where ω' is defined as [54]

$$\omega' = \alpha \left(\frac{\omega}{\omega_0} - \frac{\omega_0}{\omega} \right), \quad (2.27)$$

where

$$\alpha = \frac{1}{FBW} = \frac{\omega_0}{\omega_2 - \omega_1}, \quad (2.28)$$

where FBW is the fractional bandwidth of the bandpass filter, ω_2 , ω_1 are the upper and lower edges of the bandpass filter, respectively, and ω_0 is the center frequency of the filter that is mathematically defined as [54]

$$\omega_0 = \sqrt{\omega_1 \omega_2} \quad (2.29)$$

Applying this transformation to the impedance Z of the series inductance L we obtain [54]

$$Z = jL\omega \implies jL\alpha \left(\frac{\omega}{\omega_0} - \frac{\omega_0}{\omega} \right) = j \left(\frac{L\alpha}{\omega_0} \right) \omega - \frac{j}{\omega \left(\frac{1}{L\alpha\omega_0} \right)} \quad (2.30)$$

The resulting impedance is an impedance of a series resonator with inductive value

$$L' = \frac{L\alpha}{\omega_0}, \quad (2.31)$$

and capacitive value

$$C' = \frac{1}{L\alpha\omega_0} \quad (2.32)$$

Similarly, applying the same transformation for the admittance Y of shunt capacitance C , the resulting admittance is then an admittance of a parallel resonator with inductive value [54]

$$L' = \frac{1}{C\alpha\omega_0} \quad (2.33)$$

and capacitive value

$$C' = \frac{C\alpha}{\omega_0} \quad (2.34)$$

The resulting bandpass structure is shown in Fig. 2.5

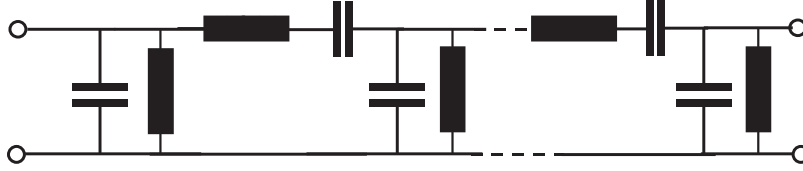


Figure 2.5: Bandpass filter prototype.

Due to the difficulty of achieving this bandpass filter prototype using the available technologies, immittance inverters may be used to overcome this problem. Immittance inverters are classified into either impedance or admittance inverter. An ideal immittance inverter is a two-port network having a unique property at all frequencies, so if an impedance Z_2 terminates one port, the impedance Z_1 seen looking at the other port as [2]

$$Z_1 = \frac{K^2}{Z_2}, \quad (2.35)$$

Where K is the characteristic impedance of the inverter.

The same is for the admittance inverter, so if an admittance Y_2 is connected to one port, the admittance Y_1 seen looking at the other port as

$$Y_1 = \frac{J^2}{Y_2}, \quad (2.36)$$

where J is the characteristic admittance of the inverter.

An important characteristic of the inverter is that it has a phase shift of ± 90 and its odd multiple [1].

To use these inverters in filter design we should know first that, a series inductance with an inverter on each side looks like a shunt capacitance from the output side as shown in Fig.2.6. Similarly, a shunt capacitance with an inverter on each side looks like series inductance as shown in Fig.2.7. It should also be known that the inverters have the ability to shift the impedance or the admittance depending on the value of the K , J parameters. Using the knowledge of these parameters enables us to convert a filter circuit to an equivalent form, which would be more convenient for implementation with microwave filters especially for bandpass filters, since both series and shunt resonators are not always available. A series resonator connected by impedance inverters from both sides looks like shunt resonator, and a shunt resonator connected by admittance inverters looks like series resonator

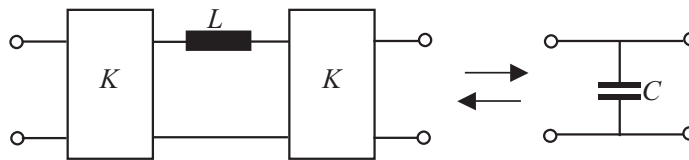


Figure 2.6: Admittance inverters used to convert a series inductance into its equivalent circuit with shunt capacitance.

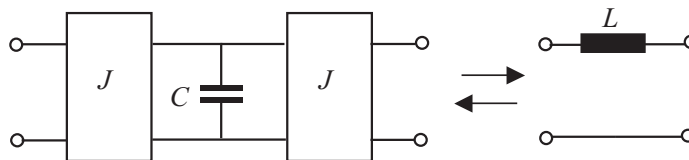


Figure 2.7: Admittance inverters used to convert a shunt capacitance into its equivalent circuit with series inductance.

To design a bandpass filter using the immittance inverters, it is effective to start from the lowpass filter. Fig.2.8 shows a lowpass filter using impedance inverters, similarly, Fig.2.9 shows a lowpass filter using admittance inverters. The values of the inductive and capacitive values of the filter can be arbitrary chosen, and then the K , J parameters are [2]

$$K_{0,1} = \sqrt{\frac{Z_0 L_{s1}}{g_0 g_1}}, \quad (2.37)$$

$$K_{i,i+1} = \sqrt{\frac{L_{si} L_{si+1}}{g_i g_{i+1}}}, \quad \text{for } i = 1 \text{ to } n - 1, \quad (2.38)$$

$$K_{n,n+1} = \sqrt{\frac{L_{sn}Z_{n+1}}{g_n g_{n+1}}}, \quad (2.39)$$

$$J_{0,1} = \sqrt{\frac{Y_0 C_{s1}}{g_0 g_1}}, \quad (2.40)$$

$$J_{i,i+1} = \sqrt{\frac{C_{si} C_{s_{i+1}}}{g_i g_{i+1}}}, \quad \text{for } i = 1 \text{ to } n-1, \quad (2.41)$$

$$J_{n,n+1} = \sqrt{\frac{C_{sn} Y_{n+1}}{g_n g_{n+1}}}, \quad (2.42)$$

where g_i are the values of the original prototype elements, Z_0, Y_0 are the generator impedance and admittance, respectively, and Z_{n+1}, Y_{n+1} are the load impedance and admittance, respectively.

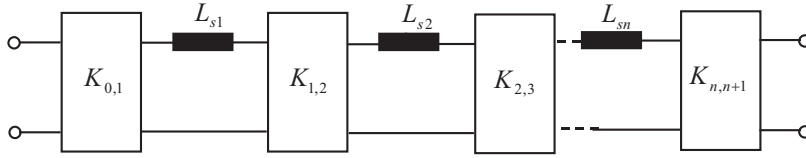


Figure 2.8: Low-pass filter structure using impedance inverters.

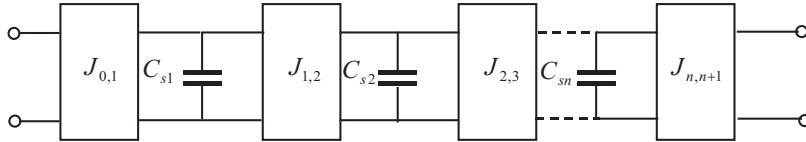


Figure 2.9: Low-pass filter structure using admittance inverters .

Since the inverters are frequency invariant, the lowpass to bandpass transformation can be easily done using the element transform that is discussed above. Fig. 2.10 shows bandpass filters using the impedance inverters connected to series resonators, while the filter shown in Fig. 2.11 consists of shunt resonators connected to admittance inverters. Since source impedances are the same for filters mentioned in both figures, there is no need for impedance scaling, the scaling factor is then $\gamma = 1$, and now the inductance of the lowpass filter will be transformed to a series resonator, then we obtain [54]:

$$L_{ai} = \left(\frac{\Omega_c}{FBW \omega_0} \right) L_{si}, \quad (2.43)$$

$$C_{ai} = \frac{1}{\omega_0^2 L_{si}} \quad (2.44)$$

Having transformed the series inductance into series resonator, we can easily transform the K parameter by substituting the value of L_s , then we get [2]

$$K_{0,1} = \sqrt{\frac{Z_0 FBW L_{a1} \omega_0}{\Omega_c g_0 g_1}}, \quad (2.45)$$

$$K_{i,i+1} = \frac{FBW \omega_0}{\Omega_c} \sqrt{\frac{L_{ai} L_{a(i+1)}}{g_i g_{i+1}}}, \quad \text{for } i = 1 \text{ to } n - 1, \quad (2.46)$$

$$K_{n,n+1} = \sqrt{\frac{Z_{n+1} FBW L_{an} \omega_0}{\Omega_c g_n g_{n+1}}}, \quad (2.47)$$

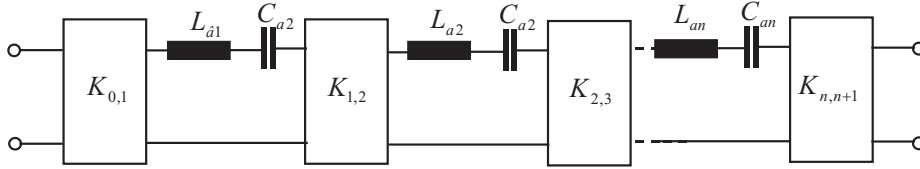


Figure 2.10: Bandpass filter built with impedance inverters and series resonators .

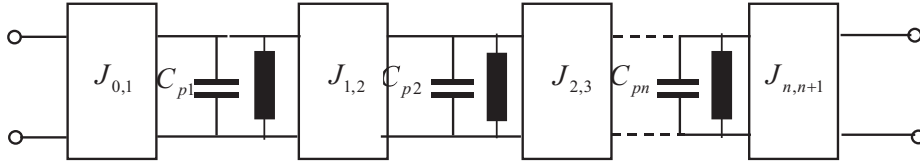


Figure 2.11: Bandpass filter built with admittance inverters and parallel resonators.

Similarly, transformation of the lowpass filter to a bandpass filter using parallel resonator connected to admittance inverters can be easily done in the same way, but in this case, the lowpass filter to be transformed is the one with shunt capacitances connected to admittance inverters, see Fig.2.9.

$$C_{pi} = \left(\frac{\Omega_c}{FBW \omega_0} \right) C_{si}, \quad (2.48)$$

$$L_{pi} = \frac{1}{\omega_0^2 C_{pi}} \quad (2.49)$$

Having transformed the shunt capacitance into parallel resonator, we can easily transform the J parameter by substituting the value of C_p , then we get

$$J_{0,1} = \sqrt{\frac{Y_0 FBW C_{p1} \omega_0}{\Omega_c g_0 g_1}}, \quad (2.50)$$

$$J_{i,i+1} = \frac{FBW \omega_0}{\Omega_c} \sqrt{\frac{C_{pi} C_{p(i+1)}}{g_i g_{i+1}}}, \quad \text{for } i = 1 \text{ to } n - 1, \quad (2.51)$$

$$J_{n,n+1} = \sqrt{\frac{Y_{n+1}FBWC_{pn}\omega_0}{\Omega_c g_n g_{n+1}}} \quad (2.52)$$

Since most of the microwave filters are waveguide and planar based it is important that these distributed elements or resonators have the same reactance or susceptance equal to that for LC resonators. Thus, it is important that the reactance/susceptance and the reactance/susceptance slope are equal to their corresponding lumped resonator value at the center frequency. This is however, convenient for narrow band filters. Fig. 2.12 shows a bandpass filter using distributed elements connected to impedance inverters, while, Fig. 2.13 shows a bandpass filter using distributed elements connected to admittance inverters. The reactance slope for a resonator having zero at the center frequency is

$$x = \frac{\omega_0}{2} \frac{dX}{d\omega}, \quad \omega = \omega_0, \quad (2.53)$$

where ω_0 is the center frequency, and $X(\omega)$ is the reactance of the distributed resonator. It is known that in the ideal case, the reactive slop parameters of a series resonator is $\omega_0 L_{ai}$, so by replacing this value by the x_i parameters, we can define the impedance inverter as [2]

$$K_{0,1} = \sqrt{\frac{Z_0 FBW x_1 \omega_0}{\Omega_c g_0 g_1}}, \quad (2.54)$$

$$K_{i,i+1} = \frac{FBW}{\Omega_c} \sqrt{\frac{x_i x_{i+1}}{g_i g_{i+1}}}, \quad \text{for } i = 1 \text{ to } n - 1, \quad (2.55)$$

$$K_{n,n+1} = \sqrt{\frac{Z_{n+1} FBW x_n \omega_0}{\Omega_c g_n g_{n+1}}}, \quad (2.56)$$

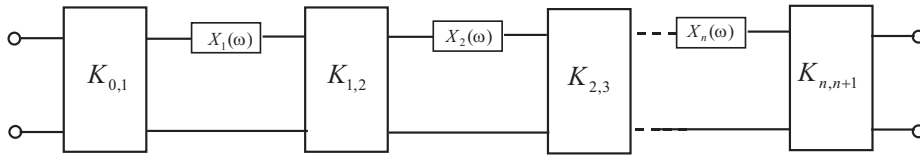


Figure 2.12: Bandpass filter using distributed elements connected to impedance inverters.

The same is valid for the second structure (see Fig.2.13), the susceptance slope parameters for a resonator having zero at the center frequency is

$$b = \frac{\omega_0}{2} \frac{dB(\omega)}{d\omega}, \quad \omega = \omega_0, \quad (2.57)$$

where ω_0 is the center frequency, and $B(\omega)$ is the susceptance of the distributed resonator. It is known that in the ideal case, the susceptance slope parameters of a

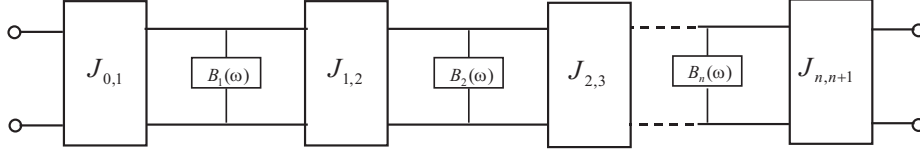


Figure 2.13: Bandpass filter using distributed elements connected to admittance inverters.

parallel resonator is $\omega_0 C_p$, so by replacing this value by b_i , the admittance inverter parameters we can define the as

$$J_{0,1} = \sqrt{\frac{Y_0 FBW b_1 \omega_0}{\Omega_c g_0 g_1}}, \quad (2.58)$$

$$J_{i,i+1} = \frac{FBW}{\Omega_c} \sqrt{\frac{b_i b_{i+1}}{g_i g_{i+1}}}, \quad \text{for } i = 1 \text{ to } n - 1, \quad (2.59)$$

$$J_{n,n+1} = \sqrt{\frac{Y_{n+1} FBW b_n}{\Omega_c g_n g_{n+1}}}. \quad (2.60)$$

2.4 Coupling Matrix and Cross Coupled Resonators

Coupling matrix is a representation of the filter that describes the coupling between the resonators of a certain filter with certain bandwidth and center frequency, regardless of the nature of the coupling between the resonators. Fig. 2.14 shows the bandpass filter with n -coupled resonators, where R , C , and L are resistance capacitance and inductance, respectively. i is the current and e_s is the voltage source. The coupling between one resonator and all other resonators is allowed.



Figure 2.14: n -coupled resonators [2].

Using the voltage law, that is the sum of the voltage around any closed circuit must be zero. This law is called Kirchhoff's second law. Applying it for our case will

results with [2]

$$\begin{aligned}
(R_1 + jL_1\omega + \frac{1}{jC_1\omega})i_1 - jL_{12}i_2 \dots - jL_{1n}i_n &= e_s \\
-jL_{21}i_1 + (jL_2\omega + \frac{1}{jC_2\omega})i_2 \dots - jL_{2n}i_n &= 0 \\
&\vdots \\
-jL_{n1}i_1 - jL_{n2}i_2 + \dots (jL_n\omega + \frac{1}{jC_n\omega} + R_n)i_n &= 0,
\end{aligned} \tag{2.61}$$

where L_{ij} is the mutual coupling between the resonators. The resulting equations can be written in matrix form as [2],

$$[\mathbf{z}][\mathbf{i}] = [\mathbf{e}], \tag{2.62}$$

where $[\mathbf{z}]$ is $(N \times N)$ impedance matrix, $[\mathbf{i}]$ is the current vector, and $[\mathbf{e}]$ is the voltage vector. For this case, let us assume that all resonators have the same resonance frequency, which means that the inductive and capacitive values of all resonators have the same values, let it be L for the inductance and C for the capacitance. Now the impedance matrix can be written as [2],

$$[\mathbf{z}] = \omega_0 LFBW \overline{[\mathbf{Z}]}, \tag{2.63}$$

where FBW is the fractional bandwidth and $\overline{[\mathbf{Z}]}$ is the normalized impedance matrix, which can be written as [2]

$$\overline{[\mathbf{Z}]} = \begin{pmatrix} \frac{R_1}{\omega_0 LFBW} + p & -j \frac{\omega L_{12}}{\omega_0 L} \frac{1}{FBW} & \dots & -j \frac{\omega L_{1n}}{\omega_0 L} \frac{1}{FBW} \\ -j \frac{\omega L_{21}}{\omega_0 L} \frac{1}{FBW} & p & \dots & -j \frac{\omega L_{2n}}{\omega_0 L} \frac{1}{FBW} \\ \vdots & \vdots & \ddots & \vdots \\ -j \frac{\omega L_{n1}}{\omega_0 L} \frac{1}{FBW} & -j \frac{\omega L_{n2}}{\omega_0 L} \frac{1}{FBW} & \dots & \frac{R_n}{\omega_0 LFBW} + p \end{pmatrix}, \tag{2.64}$$

where,

$$p = j \frac{1}{FBW} \left(\frac{\omega}{\omega_0} - \frac{\omega_0}{\omega} \right), \tag{2.65}$$

the external quality factor is defined as

$$Q_{ei} = \frac{\omega_0 L}{R_i}, \tag{2.66}$$

where $i = 1, \dots, n$, Defining the coupling coefficient as

$$M_{ij} = \frac{L_{ij}}{L}, \tag{2.67}$$

and assuming $\omega/\omega_0 \approx 1$ for narrow band, we get

$$\overline{[\mathbf{Z}]} = \begin{pmatrix} \frac{1}{q_{e1}} + p & -jm_{12} & \dots & -jm_{1n} \\ -jm_{21} & p & \dots & -jm_{2n} \\ \vdots & \vdots & \ddots & \vdots \\ -jm_{n1} & -jm_{n2} & \dots & \frac{1}{q_{en}} + p \end{pmatrix}, \tag{2.68}$$

where q_{e1} and q_{en} are the scaled external quality factors and defined as

$$q_{ei} = Q_{ei}FBW, \quad (2.69)$$

and m_{ij} is the normalized coupling coefficient which is defined as

$$m_{ij} = \frac{M_{ij}}{FBW}, \quad (2.70)$$

$$S_{21} = \frac{b_2}{a_1} \Big|_{a_2=0} = \frac{2\sqrt{R_1 R_n} i_n}{e_s}, \quad (2.71)$$

$$S_{11} = \frac{b_1}{a_1} \Big|_{a_2=0} = 1 - \frac{2R_1 i_1}{e_s}, \quad (2.72)$$

where

$$i_1 = \frac{e_s}{\omega_0 L FBW} [\bar{\mathbf{Z}}]_{11}^{-1}, \quad (2.73)$$

$$i_n = \frac{e_s}{\omega_0 L FBW} [\bar{\mathbf{Z}}]_{n1}^{-1}, \quad (2.74)$$

substituting (2.73) in (2.71) and (2.74) in (2.72) then

$$S_{21} = \frac{2}{\sqrt{q_{e1} q_{en}}} [\bar{\mathbf{Z}}]_{n1}^{-1} \quad (2.75)$$

and

$$S_{11} = 1 - \frac{2}{q_{e1}} [\bar{\mathbf{Z}}]_{11}^{-1} \quad (2.76)$$

the coupling coefficients for coupling structure with resonators having different resonant frequency are

$$M_{ij} = \frac{L_{ij}}{\sqrt{L_i L_j}}, \quad i \neq j, \quad (2.77)$$

which leads to

$$[\bar{\mathbf{Z}}] = \begin{pmatrix} \frac{1}{q_{e1}} + p - m_{11} & -jm_{12} & \dots & -jm_{1n} \\ -jm_{21} & p - m_{22} & \dots & -jm_{2n} \\ \cdot & \cdot & \cdot & \cdot \\ \cdot & \cdot & \cdot & \cdot \\ -jm_{n1} & -jm_{n2} & \dots & \frac{1}{q_{en}} + p - m_{nn} \end{pmatrix} \quad (2.78)$$

The same can be applied for the case of capacitive coupling between the resonators, but instead of using the impedance matrix $[\mathbf{Z}]$, the admittance matrix $[\mathbf{Y}]$ is used, we will not go through the derivations, nevertheless, the transfer function and the return loss can be written as

$$S_{21} = \frac{2}{\sqrt{q_{e1} q_{en}}} [\bar{\mathbf{Y}}]_{n1}^{-1}, \quad (2.79)$$

and

$$S_{11} = \frac{2}{q_{e1}} [\bar{\mathbf{Y}}]_{11}^{-1} - 1 \quad (2.80)$$

The most important point needed is that the formulation of the normalized impedance matrix $[\bar{Z}]$ to that of the normalized $[\bar{Y}]$. So we can generalize coupling between the resonators no matter what the coupling nature is, by

$$S_{21} = \frac{2}{\sqrt{q_{e1}q_{en}}} [A]_{n1}^{-1}, \quad (2.81)$$

and

$$S_{11} = \pm \left(\frac{2}{q_{e1}} [A]_{11}^{-1} - 1 \right), \quad (2.82)$$

where $[A]$ is $N \times N$ matrix and formed as

$$[A] = [q] + p[U] - j[m], \quad (2.83)$$

where $[q]$ is $(N \times N)$ matrix with all entries zeros except $q_{11} = 1/q_{e1}$ and $q_{nn} = 1/q_{en}$, $[U]$ is $(N \times N)$ unit matrix, and $[m]$ is $(N \times N)$ coupling matrix

2.5 Planar Transmission Lines

A planar transmission line is a transmission line with multiple conducting metal strips lying in parallel planes. These planes are mostly placed on dielectric material. The most widely used transmission lines are microstrip line, coplanar waveguide, and suspended stripline.

2.5.1 Microstrip Line

Microstrip line is a transmission line which consists of a conducting strip separated from a ground plane by a dielectric layer. Fig.2.15 shows the cross section of the microstrip line. The main advantages of microstrip line are that it is suitable technique for MICs, and the radiation that it provides can be used for antenna design. The main disadvantage of this type of transmission lines is that via holes are necessary in the case of shunt connections which is complex especially in the case of MMICs.

The characteristic impedance of the microstrip line is depending on the width of the guided wave line, substrate thickness, and the effective dielectric constant of the substrate ϵ_r . The effective dielectric constant is given in the following form [55–57]

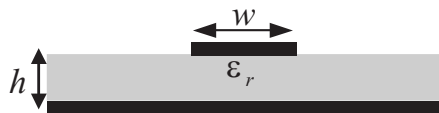


Figure 2.15: Microstrip line cross section.

$$\varepsilon_{eff} = \frac{\varepsilon_r + 1}{2} + \frac{\varepsilon_r - 1}{2\sqrt{1 + \frac{10h}{w}}}, \quad (2.84)$$

where ε_r and h are the permittivity and thickness of the substrate, respectively, and w is the strip width, the characteristic impedance of the microstrip is given as

$$Z_c = \frac{\eta}{2\pi\sqrt{\varepsilon_{eff}}} \ln \left(\frac{Fw}{h} + \sqrt{1 + \left(\frac{2w}{h}\right)^2} \right), \quad (2.85)$$

where $\eta = 120\pi\Omega$, and

$$F = 6 + (2\pi + 6) \exp \left(- \left(\frac{30.666w}{h} \right)^{0.7528} \right) \quad (2.86)$$

2.5.2 Coplanar Waveguide

Coplanar waveguide (CPW) is basically a single strip located between two ground planes on the same side of the substrate, see Fig. 2.16. The main advantages for this type of transmission lines is thae fact that it can be easily integrates with the MIC's. Furthermore shunt connections can be easily realized without the need of via holes. in addition it is less sensitive to the substrate thickness than in the case of microstrip [58]. However the losses in this transmission line are higher than that in the case of microstrip lines. Both ground planes must be at the same potential, to avoid the asymmetric, which may excites the slot mode. Therefore air bridges are used to keep symmetrical potential at both ground planes.



Figure 2.16: Coplanar waveguide cross section.

The characteristic impedance of the coplanar waveguide with finite substrate thickness is given by [58],

$$Z_c = \frac{f(K)}{4} \sqrt{\frac{\mu_0}{\varepsilon_0 \varepsilon_{eff}}}, \quad (2.87)$$

where,

$$\varepsilon_{eff} \approx 1 + \frac{\varepsilon_r - 1}{2} f(K_1) f(K), \quad (2.88)$$

$$K = \frac{w}{w + 2s}, \quad (2.89)$$

$$K_1 = \sqrt{\frac{1}{1 + q}}, \quad (2.90)$$

$$q = \frac{\left[\sinh \left(\frac{w\pi}{4h} \right) \right]^2}{\sinh \left(\frac{s\pi}{2h} \right) \sinh \left(\frac{\pi(w+s)}{2h} \right)}, \quad (2.91)$$

$$f(K) = \begin{cases} \frac{1}{4} \ln \left(\frac{2}{\sqrt{K}} \right), & K \leq 0.173 \\ \frac{\pi}{\ln \left(2 \frac{1+\sqrt{K}}{1-\sqrt{K}} \right)}, & K \geq 0.173, \end{cases} \quad (2.92)$$

where h is the substrate thickness, w is the width of the transmission line, and s is the spacing between the transmission line and the ground planes.

2.5.3 Suspended Stripline

Suspended stripline (SSL) has been introduced as an alternative to coaxial line in [59]. It is basically a substrate that is shielded inside a housing mount, as it is shown in Fig. 2.17. Suspended stripline is also possible with multiple substrates [60–64]. The ground plane of this transmission line is the mount itself. Due to the existence of the mount around the guided wave line, there is no radiation loss introduced by this transmission line. SSL has another main advantage, which is due to the ability of building the resonators on both sides of the substrate, it is the most suitable technique for broadband circuits [24, 40, 65]. Due to the larger cross section with a considerable amount of electromagnetic field in the air, the effective dielectric constant of the SSL is rather low, and therefore the dielectric loss is very low in this transmission line.

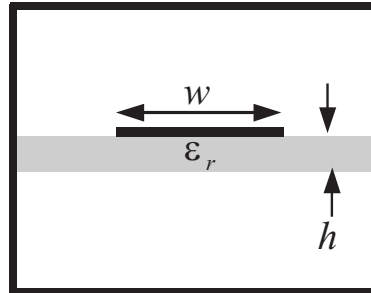


Figure 2.17: Suspended stripline cross section.

Since most MICs are microstrip based, there might be a need to integrate the SSL filters with microstrip components. That can be realized by having a groove under the portion of the filter in the carrier block of the circuit and fixing a small cap over the SSL filter to build the channel of the filter, see [66]. The characteristic impedance, and the effective dielectric constant of the SSL are given as [67], [68],

- When $0 < w < a/2$

$$Z_c = \frac{\eta_0}{2\pi} \left[V + R \ln \left(\frac{6}{w/b} + \sqrt{1 + \frac{4}{w/b}} \right) \right], \quad (2.93)$$

$$\varepsilon_{eff} = \frac{1}{\left(E - F \ln \frac{w}{b} \frac{1}{\sqrt{\varepsilon_r}}\right)^2}, \quad (2.94)$$

where w is the width of the transmission line, a is the width of the mount, b is the height of the mount,

$$V = 1.7866 + 0.2035 \frac{h}{b} + 0.4750 \frac{a}{b}, \quad (2.95)$$

$$R = 1.0835 + 0.1007 \frac{h}{b} - 0.09457 \frac{a}{b}, \quad (2.96)$$

$$E = 0.2077 + 1.2177 \frac{h}{b} - 0.08364 \frac{a}{b}, \quad (2.97)$$

$$F = 0.03451 - 0.1031 \frac{h}{b} + 0.01742 \frac{a}{b}, \quad (2.98)$$

- $\frac{a}{2} < w < a$

$$Z_c = \eta_0 \left(V + \frac{R}{\frac{w}{b} + 1.393 + 0.6670 \ln \left(\frac{w}{b} + 1.444 \right)} \right), \quad (2.99)$$

$$\varepsilon_{eff} = \frac{1}{\left(E - F \ln \frac{w}{b} \frac{1}{\sqrt{\varepsilon_r}}\right)^2}, \quad (2.100)$$

where,

$$V = -0.6301 - 0.07083 \frac{h}{b} + 0.247 \frac{a}{b}, \quad (2.101)$$

$$R = 1.9492 + 0.1553 \frac{h}{b} - 0.5123 \frac{a}{b}, \quad (2.102)$$

$$E = 0.464 + 0.9647 \frac{h}{b} - 0.2063 \frac{a}{b}, \quad (2.103)$$

$$F = -0.1424 + 0.3017 \frac{h}{b} - 0.02411 \frac{a}{b} \quad (2.104)$$

2.5.4 Multilayer Transmission Lines

Multilayer transmission lines are mainly introduced for MMIC's. It is basically a combination of CPW and microstrip line, this structure is built on a thin film placed on a thick substrate, fabrication, however, is very expensive since Si, Ge, or GaAs is used. The main advantage of this techniques is that it can be easily integrated with CPW and microstrip components. It also provide high coupling between the resonators, which makes it useful for broadband components [40], [69–72].

Chapter 3

Multilayer Structures and Filter Applications

Multilayer structures represent a potential technology for MMIC and MIC circuits [69–72] and [73]. These structures were introduced as a good candidate for filter applications in [70]. They offer a wider range for nearly constant characteristic impedance and provide more effective capacitive coupling between the resonators by locating them on the two sides of the substrate [70], [72].

Multilayer structures are normally used for coplanar waveguide (CPW), Microstrip line (ML), and suspended stripline (SSL) techniques. They give the designer extra degree of freedom in designing the microwave and millimeter wave components. The multilayer structures for CPW are normally built on a thin film structure, where the metallization strips and ground planes are etched [72]. In case of high frequency components, the material that is used for the thin film is silicon dioxide SiO_2 [74], [75]. The thin film is then built over high resistivity silicon substrate. This process is, however, a complicated process rather expensive.

This chapter investigates the cross section of multilayer structure and introduces different filters using this technology. Compact lowpass and bandpass filters are designed using this technology showing the ability of these filters to be integrated with ML, CPW, or both. The filter are designed using quasi-lumped elements. In the last section an ultra-wideband suspended stripline filter is presented. The filter has very wide stopband which is much wider than that for the other available structures, in addition the filter has low group delay variation with the passband.

3.1 Multilayer Coplanar Line Cross Section

The multilayer coplanar line (MCL) of a modified cross section is investigated in this section. Fig. 3.1 shows the cross section of the proposed MCL. Only one substrate is used and the filter is built on both sides of it. Fig. 3.1a shows the MCL cross section which is used in the case of broadside coupling, by this configuration high capacitive

coupling can be achieved, since it allows the overlapping between the metallization on both sides of the substrate. This structure can be easily integrated with both CPW- and microstrip-based circuits, depending on which side of the substrate these circuits are built. This is not the case with the standard microstrip and CPW lines, as these technologies need transition networks to be integrated together. Fig. 3.1b shows the cross section of the MCL, which is designed to be integrated with the standard CPW. Fig. 3.1c shows the cross section of the line that is compatible with the microstrip line.

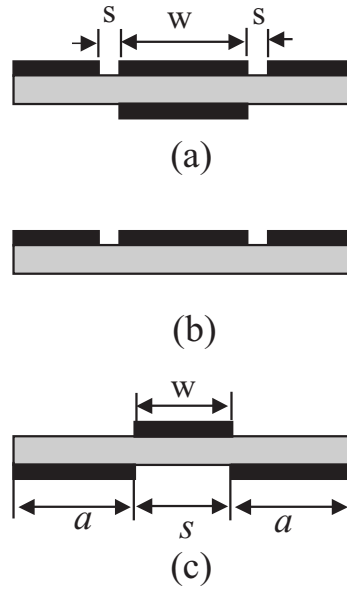


Figure 3.1: (a) Cross section of MCL , (b) the MCL compatible with CPW , (c) the MCL compatible with microstrip line .

A comparison is made on the capacitive coupling between 50Ω microstrip line, CPW, and MCL broadside coupling. The 50Ω lines were built on a AR600 substrate 0.787 mm in thickness with relative permittivity ϵ_r of 6, as shown in Fig. 3.2. The study is done on frequency band of 6 GHz . The capacitive values of these structures are calculated in two steps. First, the reflection coefficient of the coupling structure S_{11} were computed at certain frequencies. In the second step, the coupling structure is considered equivalent to a series capacitance, whose reactance X_i can be calculated from

$$S_{11} = \frac{jX_i - Z_0}{jX_i + Z_0}, \quad (3.1)$$

where z_i is the input impedance - here the load is series capacitance- and Z_0 is the source impedance which is 50Ω in our case. Having calculated the load impedance, the capacitive value of the coupling structure can be easily calculated from

$$C = \frac{-1}{X_i \omega}, \quad (3.2)$$

where w is the angular frequency.

Fig. 3.3 shows a comparison between the capacitive values of ML-ML, CPW-CPW and broadside coupling structure as a function of the distance. As it can be clearly seen, the broadside coupling structure provides higher capacitive coupling between the two 50Ω lines since it allows the overlapping between the metallization on both sides of the substrate. These coupling structure can be used for broadband circuits and filters.

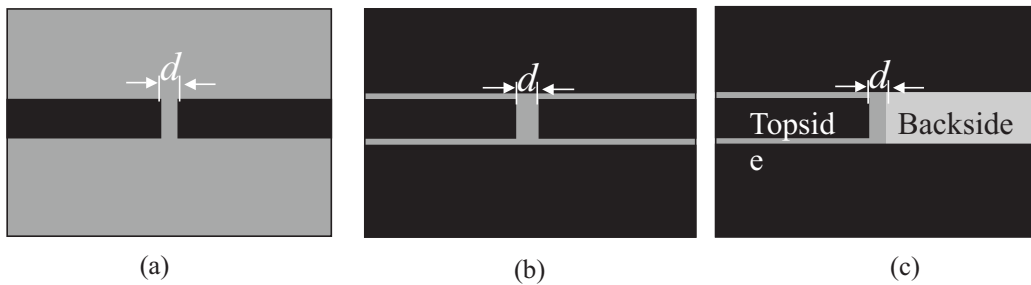


Figure 3.2: coupling two 50Ω lines structure (a) microstrip-microstrip, (b) CPW-CPW, and (c) CPW-slotted microstrip line.

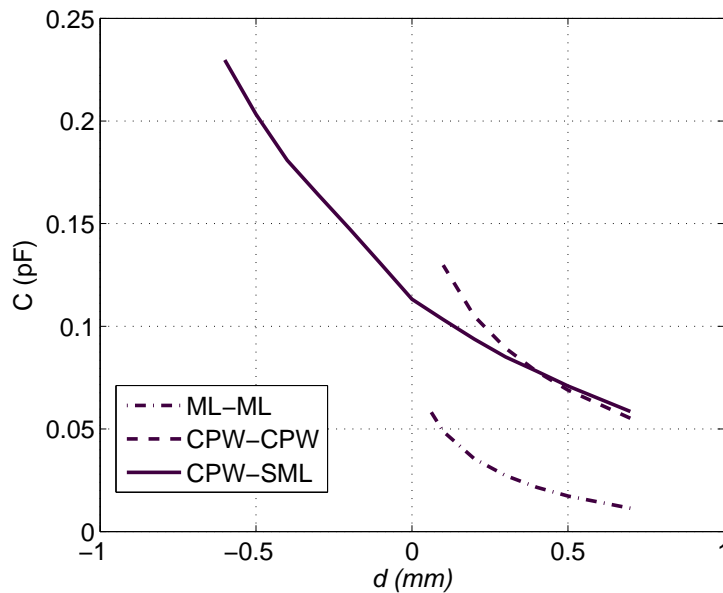


Figure 3.3: Calculated capacitive coupling values between the two ends of 50Ω strips of particular lines: CPW-CPW, microstrip-microstrip (ML-ML), and broadside coupling CPW-slotted microstrip line.

In addition to the high capacitive coupling that the MCL offers, it also provides wide characteristic impedance range at the same frequency band. To show that, a simple analysis is done by using the same substrate. The study has been done on

the slotted microstrip line (see Fig. 3.1c). Fig. 3.4 shows the relation between the characteristic impedance Z_0 of the transmission line and the width of the transmission line w for different slot widths s . As it is shown in the same Figure the impedance Z_0 can reach 135Ω with transmission line width equals 0.5 mm and slot width of 4 mm , and 16.2Ω with transmission line width of 6 mm and slot width of 1 mm .

Another study has been done on the impedance of the transmission line by changing the width of the ground planes a , and fixing both the width of the transmission line w and the slot width s at 2.7 mm and 2.8 mm , respectively, (see Fig. 3.1c). Fig. 3.5 shows the relation between the impedance of the transmission line and the width of the ground planes. From the figure, one can see that the width of the ground plane has almost no effect on the characteristic impedance unless it is less than 2 mm . The characteristic impedance of the transmission line starts increasing by decreasing the width of the ground planes.

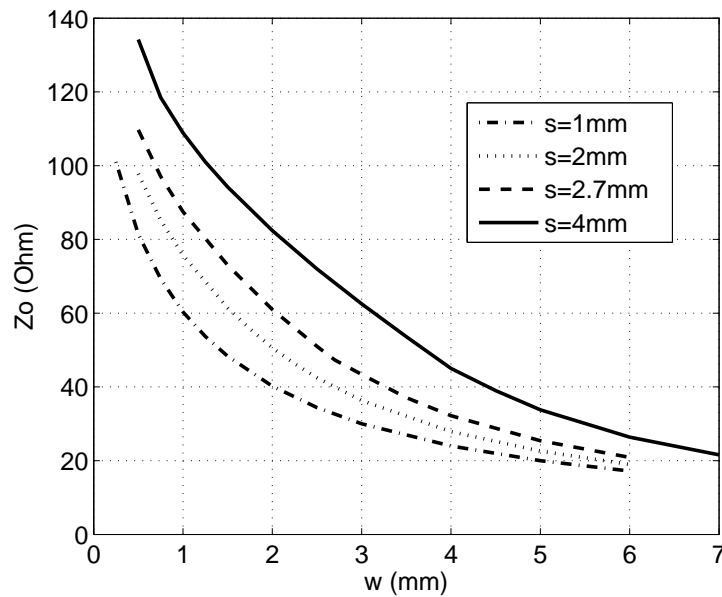


Figure 3.4: Characteristic impedance of slotted microstrip line as function of w for different slot width s .

3.2 Quasi-Lumped Elements

The quasi-lumped elements are used in the microwave filters due to the advantages they offer. Due to the short transmission line length that is used for quasi-lumped elements, which must be much shorter than quarter-wavelength, the filters designed using these elements have compact size, low losses, and wide stopband [24],[26], [27], and [76–78].

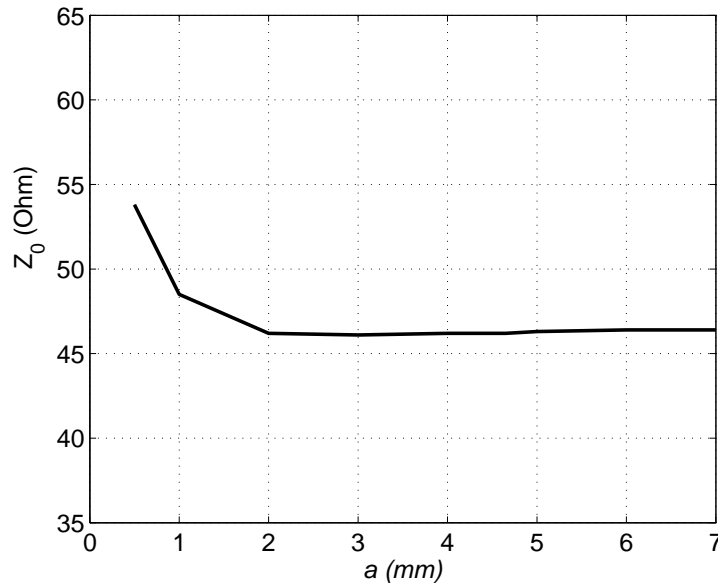


Figure 3.5: Characteristic impedance of slotted microstrip line as function of the width of the ground plane a .

Since microwave filters require both series and shunt inductances and capacitances and their combination to form either series or parallel resonators, it is necessary to understand how to realize each element for the available transmission lines.

Wide microstrip line and wide CPW line sections with low characteristic impedance already form shunt capacitances. Fig. 3.6 shows layouts of shunt CPW microstrip line capacitances. In the case of suspended stripline, shunt capacitance is realized by having additional metallization at the backside of the substrate which is connected to the walls of the housing mount from both sides, in addition to the wide transmission line that lies on the topside of the substrate. Fig. 3.7 shows 3D view for shunt suspended stripline capacitance.

Shunt inductor is realized by connecting a narrow stripline with circuit from one side and to the ground from the other side. In the case of CPW, the ground planes are located near the guided wave line, so realizing shunt inductance can be easily done. It is the same in the case of suspended stripline, the narrow stripline can be shunted by connecting it to the side wall of the housing mount. For microstrip and since the ground plane and guided waveline are built on the opposite sides of the substrate, the narrow stripline is shunted by using via hole, this process is more complicated than in the case of CPW and suspended stripline. Fig. 3.8a, and Fig. 3.8b show the CPW and microstrip shunt inductance, respectively, while Fig. 3.9 shows 3D view of suspended stripline shunt inductance.

A narrow transmission line that is connected from both sides to the input and output represents series inductance, this applies to CPW, microstrip, and suspended

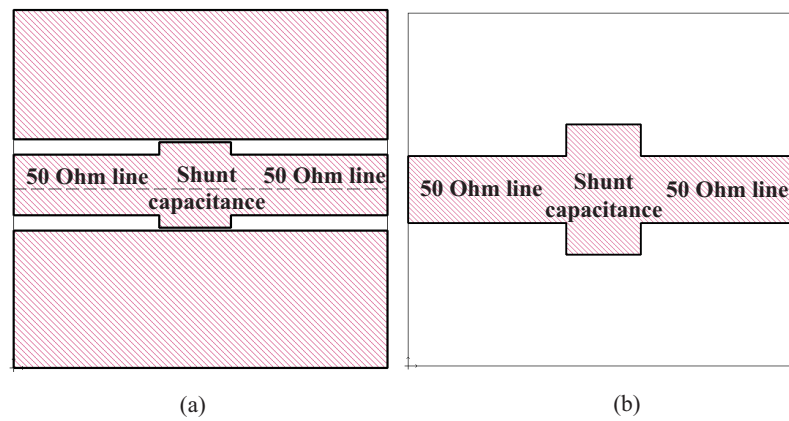


Figure 3.6: Layouts of shunt capacitance for (a) CPW , (b) microstrip.

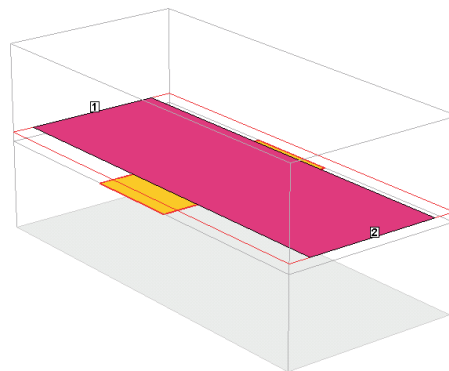


Figure 3.7: 3D view of suspended stripline shunt capacitance.

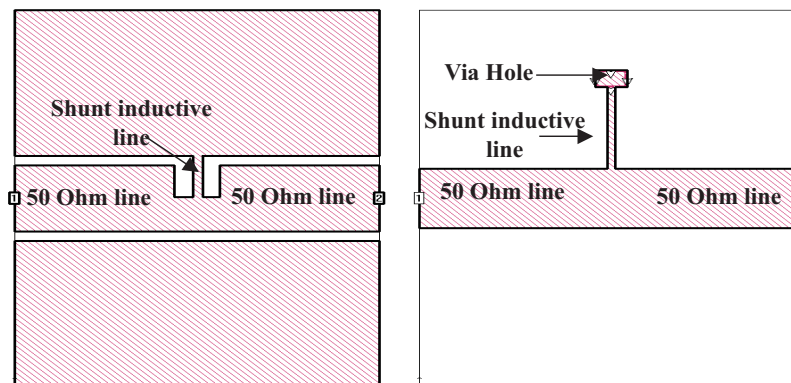


Figure 3.8: Layouts of shunt inductance for (a) CPW , (b) microstrip.

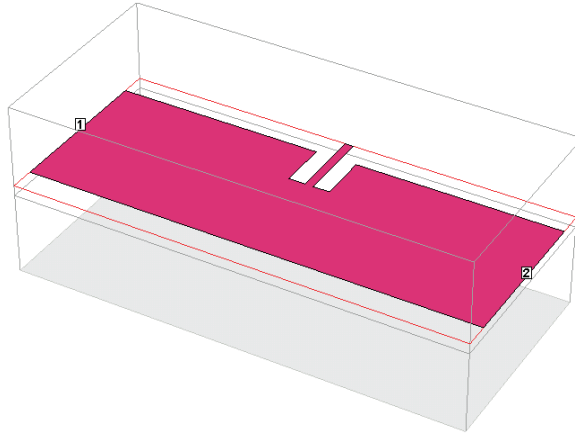


Figure 3.9: 3D view of suspended stripline shunt inductance.

stripline. The inductive value of this line is depending on the characteristic impedance of the transmission line, the length of the transmission line, and the effective dielectric constant.

Series capacitance is realized by different coupling structures, the first structure is end to end coupling structure [2]. However, the capacitive value that this structure provides is very low for all transmission line techniques, (see Fig. 3.3, and [24]). Another coupling structure that is used mainly for CPW, and microstrip line is the interdigital coupling structure as shown in Fig. 3.10, [79], [80]. This structure consists

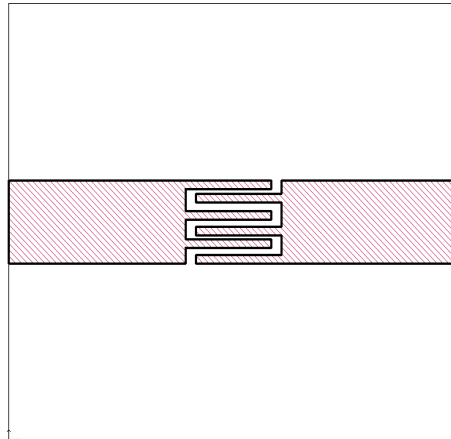


Figure 3.10: Layout of microstrip interdigital capacitance.

of metallic fingers intersect with each other. This structure provides tight capacitive value, however, the losses of this structure are much higher than the first structure due to the narrow strips used in realizing this structure. For suspended stripline and for multilayer coplanar line, where it is allowed to build the resonators on both sides of the substrate, broadside coupling structures are used. These structures allow overlapping between the resonators, which increases the capacitive coupling between

the resonators without increasing the losses on the structure.

3.3 Lowpass Filters

Microstrip lowpass filter using multilayer technique has been introduced earlier [73]. The filter was realized by opening apertures under the narrow transmission lines to increase the inductive values of these transmission line sections. This section deals with CPW lowpass filter built on the same technique, Fig. 3.1. The filter shows a great advantage in minimizing the size of the filter, particularly the size of the capacitive line sections. The filter is realized by implementing patches under the capacitive transmission line sections of the classical CPW lowpass filter structure. Since the wide patches increase the capacitive value of the capacitive transmission line sections, shorter capacitive transmission line sections are used. To design a CPW lowpass filter we have to go through two steps:

First, designing a lumped chebyshev lowpass filter, that requires knowing the order, the cut-off frequency, and passband ripple of the filter as described in sec. 2.2. Having the order, the cut-off frequency, and passband ripple, the lumped elements of the chebyshev can be simply calculated. As an example, a fifth order chebyshev filter with cut-off frequency of 4 GHz, and passband ripple of 0.1 dB. The normalized elements for this filter are $g_0 = g_6 = 1$, $g_1 = g_5 = 1.1468$, $g_2 = g_4 = 1.3712$, and $g_3 = 1.975$. Where g_0 , and g_6 represent the source and load impedances, respectively, that is considered for our filter to be $Z_0 = 50\Omega$. Substituting these values in (2.25), and (2.26), the actual filter element values can be calculated, which is for our filter $C_1 = C_5 = 0.92$ pF, $L_2 = C_4 = 2.73$ nH, and $C_3 = 1.57$ pF.

The second step is to realize the desired capacitive and inductive values of the filter elements by the stubs of the high/low-impedance transmission line, the characteristic impedance Z_0 and the effective dielectric constant ε_{eff} of the used transmission lines have to be determined. To determine this, a commercial MoM simulator [81] is used. By assuming the transmission line lengths of the filter elements are much shorter than the wavelength, the transmission line length can be calculated from

$$C_k = \frac{l_k}{Z_{0k}v_{ph,k}}, \quad (3.3)$$

$$L_j = \frac{l_j Z_{0j}}{v_{ph,j}}, \quad (3.4)$$

where the indices k and j correspond to elements with capacitive and inductive character, respectively. C_k and L_j are the capacitance and inductance of the equivalent circuit of the filter, respectively. The phase velocity v_{ph} is calculated by

$$v_{ph,j} = \frac{c}{\sqrt{\varepsilon_{eff}}}, \quad (3.5)$$

where c is the speed of light in the free space.

Having determined all transmission line lengths, these transmission line sections can be combined to build the desired lowpass filter, however, some optimization is needed to take into account the involved discontinuities and to achieve good matching in the passband. The dimensions of the lowpass filter portion are given as part of the overall filter in Fig. 3.11.

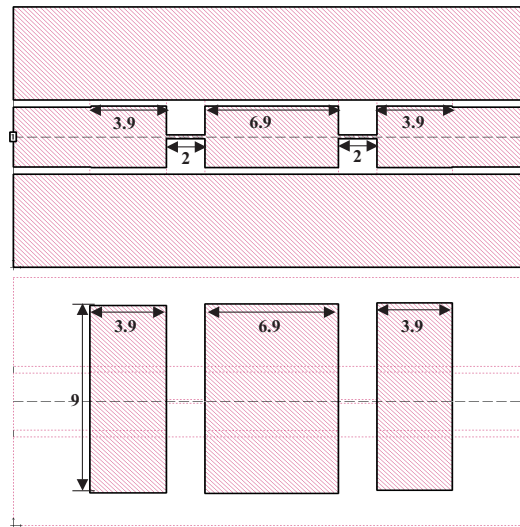


Figure 3.11: Top (up) and backside (down) layouts of a CPW lowpass filter, all dimensions are in mm .

A comparison between two filters with the same dimensions is made. The first one is built on one side of the substrate, and the second one having wide patches at the backside of the substrate, as it is shown Fig. 3.12 the cut-off frequency of the CPW lowpass filter using MCL (with patches at the backside of the substrate) is much lower than that for the CPW classical lowpass filter. That means that adding patches under the capacitive transmission line sections decreases the size of the lowpass filter.

Fig. 3.13 shows the measured and insertion loss of the lowpass filter, the filter has insertion loss at the passband is better than 0.7 dB, and group delay variation within the passband is about 0.11 ns.

As it is shown in Fig. 3.13, the filter has flat cut-off and the rejection at the stopband is about 23.4 dB, which is not sufficient for some applications. Therefore, transmission zeros are needed to increase the rejection at the stopband and to enhance the cut-off sharpness. In order to introduce transmission zeros, the side patches were loaded by two half-wavelength stubs. These stubs are coupled capacitively to the topside of the substrate. Since each of the additional stubs introduces a transmission zero to the filter response at the corresponding frequency, two transmission zeros were introduced by this configuration. Fig. 3.14 shows the top and backside layouts of the CPW lowpass filter with the additional stubs. Fig. 3.15 shows the measured and

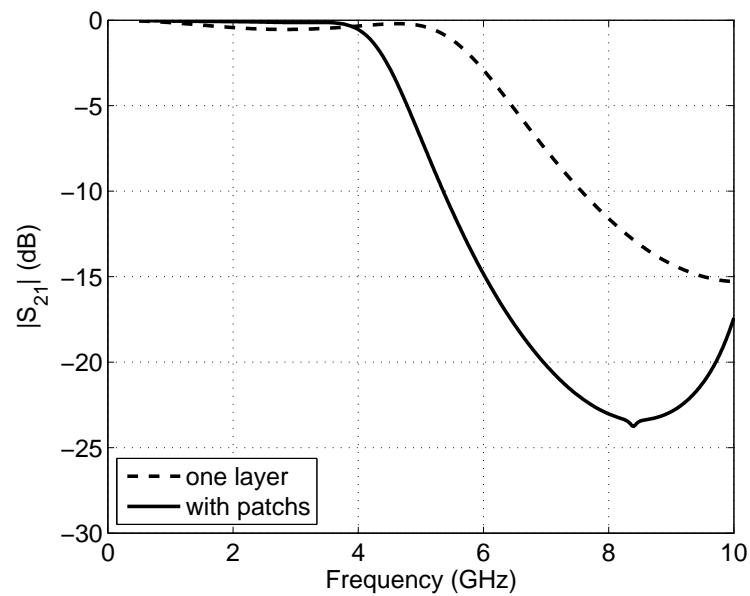


Figure 3.12: Insertion loss of CPW lowpass filter built on one layer of the substrate and Insertion loss of CPW lowpass filter with wide patches under the capacitive transmission line.

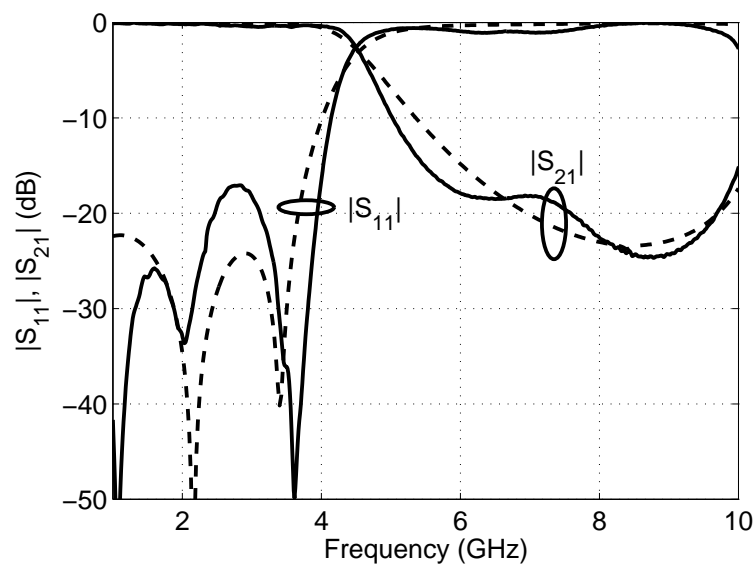


Figure 3.13: Measured (solid) and simulated (dashed) insertion and return loss of a CPW lowpass filter with patches.

simulated insertion and return loss of the filter. The measured insertion loss at the passband is better than 0.5 dB. The measured transmission zeros are located at 5.7 and 6.7 GHz. Good agreement is achieved between the measured and the simulated results except small shift is the location of the transmission zeros, this probably occurs due to fabrication errors.

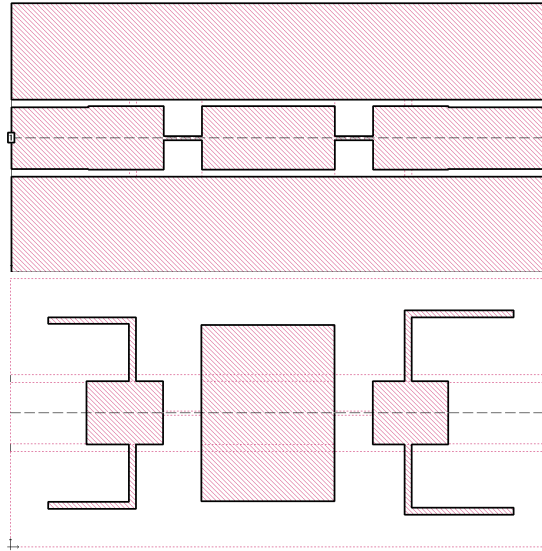


Figure 3.14: Top (up) and backside (down) layout of the CPW lowpass filter with additional stubs.

3.4 Microstrip Bandpass Filters Using Multilayer Line

Using MCL technology and quasi-lumped elements, a bandpass filter compatible with the microstrip line has been designed. The resonators were placed on the backside of the substrate. Fig. 3.16 shows the layout of the filter. The equivalent circuit model for the proposed structure is shown in Fig. 3.17. Each of the two resonant circuits consists of a wide patch capacitively coupled through the substrate to a $50\ \Omega$ microstrip line. This coupling is provided by capacitor C_1 , as shown in Fig. 3.17. The narrow strips that are mutually connecting the two patches, (see Fig. 3.17), are represented by the series inductor L_3 . This resonant structure is connected to the ground by another narrow strip represented by the shunt inductor L_4 . Since the slot between the patch and the ground metallization is narrow, it provides a capacitive coupling between the patch and the ground, which is represented by capacitor C_2 .

The bandwidth of this filter can easily be widened by either narrowing the shunt inductive strips, or by increasing the coupling between the patches and the input/output lines. The center frequency of the filter can be controlled namely by inductive strip

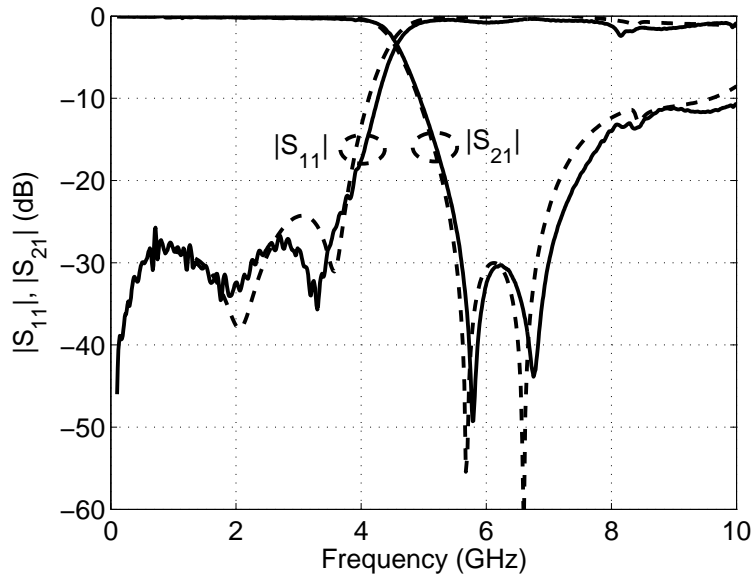


Figure 3.15: Measured (solid) and simulated (dashed) insertion and return loss of a CPW lowpass filter with two transmission zeros.

length l , see Fig.3.16. This is documented by the results of a parametric study in Fig.3.18, where the return loss of the filter for different l is plotted. Increasing l shifts the center frequency of the filter to a lower frequency band, consequently, the bandwidth of the filter is reduced. The structure has been simulated and optimized by the commercial MoM simulator [81], and the circuit simulation has been performed on the equivalent circuit using Microwave Office [82]. Using the circuit topology shown in Fig.3.17 and the scattering parameters calculated by the EM simulator for the filter with dimensions shown in Fig.3.16, the circuit parameters were tuned till a sufficient match between the circuit and the EM analyses was achieved. The resulting circuit parameters are $C_1 = 0.119$ pF, $C_2 = 0.105$ pF, $L_1 = 2.72$ nH, and $L_2 = 0.407$ nH. Fig.3.19 shows the EM and circuit simulations of the filter with dimension shown in Fig.3.16. Fig.3.20 shows the simulated and measured insertion and return loss of the filter. The filter has insertion loss at the passband better than 0.9 dB. Very good agreement has been achieved between the EM, circuit simulations and measurement.

A transmission zero was introduced to the filter response by inserting a strong capacitive coupling between the patches. Fig. 3.21 shows the layout of the filter with the transmission zero, while Fig. 3.22 shows the equivalent circuit model of this filter. The capacitive coupling between the patches is due to an additional patch located between the 50 Ω lines on the topside. The slot in this patch is etched to keep the inductances of the strips on the backside at their original value. The patches on the backside were simultaneously widened as it can be observed from a comparison of Fig. 3.16 with Fig. 3.21. This coupling is represented in the equivalent circuit by capacitor C_3 , Fig. 3.22. The structure was simulated, optimized and measured.

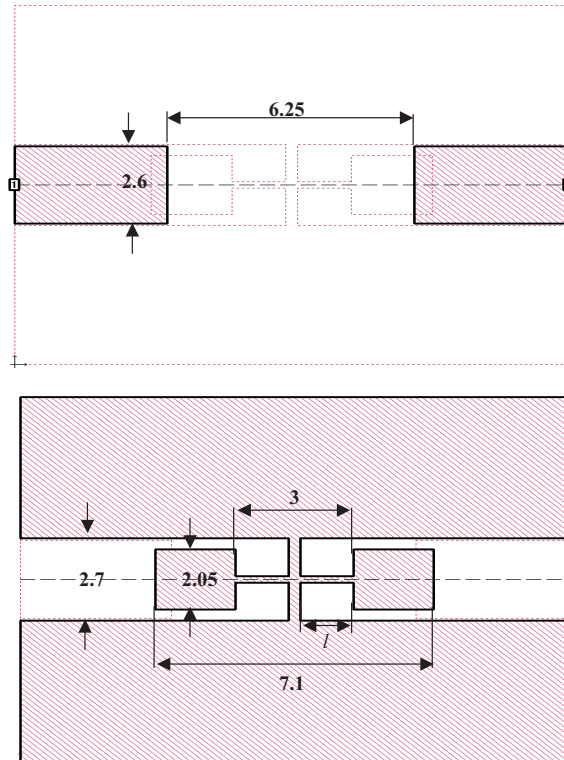


Figure 3.16: Topside (up), and backside (down) layout of an MCL bandpass filter compatible with the microstrip line.

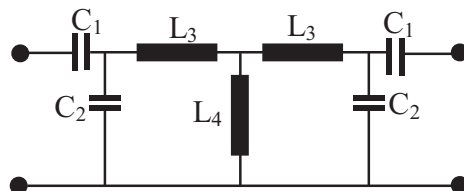


Figure 3.17: Equivalent circuit model of the bandpass filter.

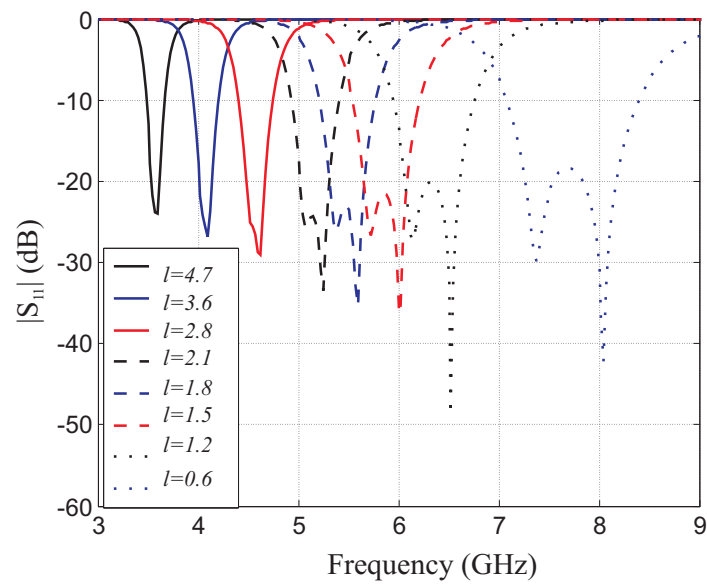


Figure 3.18: Simulated return loss of the filter with inductive strip length l vary from 4.7 to 0.6 mm.

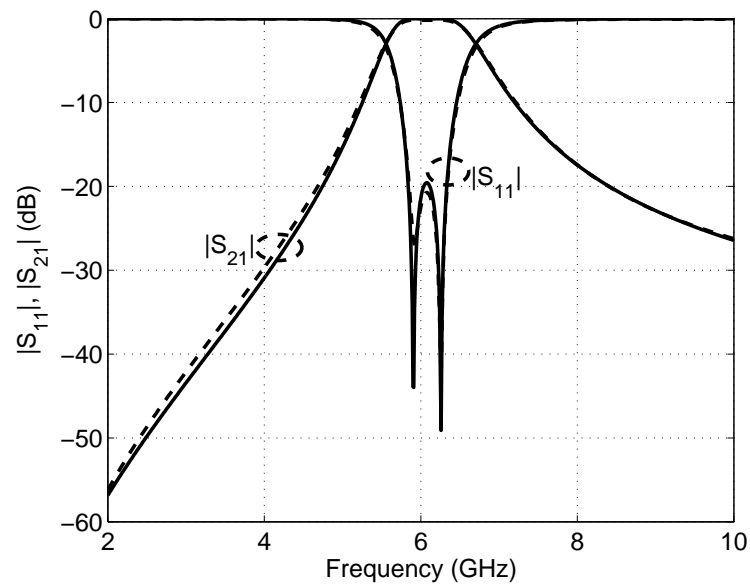


Figure 3.19: EM (solid) and Circuit (dashed) simulation of the insertion and return loss of the filter and its equivalent circuit.

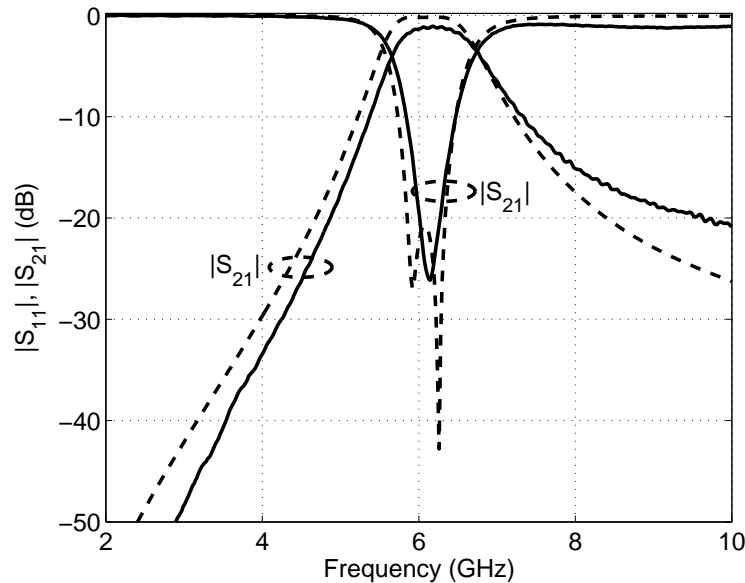


Figure 3.20: Simulated and measured insertion and return loss of the ML bandpass filter.

The insertion and return losses for the filter are demonstrated in Fig. 3.23. The transmission zero is introduced at about 7 GHz. The frequency shift between the simulated and measured data is caused by the discrepancies between the dimensions of the designed and fabricated filter layouts.

3.5 CPW Bandpass Filters Using Multilayer Line

In the previous section we have introduced microstrip bandpass filter using the MCL technology. In this section we will introduce the same filter for CPW. To get such a filter, the ground metallization was etched on the topside instead of the backside. By this configuration the filter is now fed by the $50\ \Omega$ CPW. The structure of the resonators was taken from the filter shown in Fig. 3.16. The shunt inductor is now connected to the ground via additional patches, which are capacitively coupled through the substrate with the ground planes, as shown in Fig. 3.24. These patches are represented in the equivalent circuit of Fig. 3.25 by capacitor C_4 . Since a shunted series resonator is used instead of the parallel inductance, the transmission zero is generated.

The filter was optimized, fabricated and measured. The area occupied by this filter is nearly the same as the area occupied by the filter shown in Fig.3.16. Fig.3.26 shows the simulated and measured insertion and return loss of the filter. The insertion loss at the passband is better than 0.9 dB and the upper stopband rejection better than 26 dB that reaches to higher than 14 GHz. Good agreement has been achieved

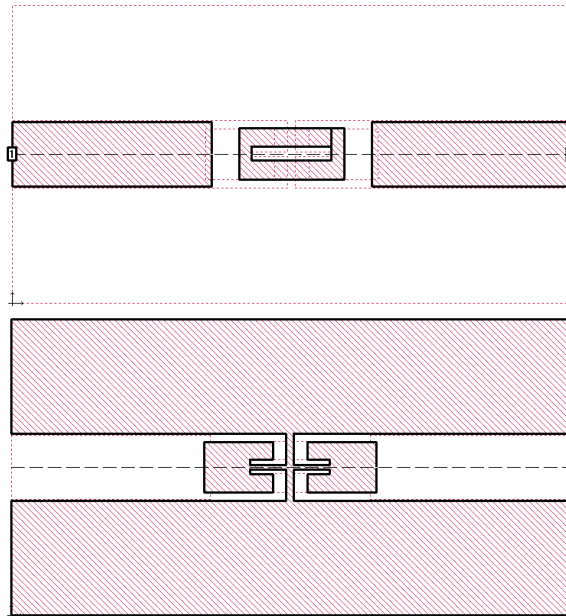


Figure 3.21: Topside (up), and backside (down) layout of an MCL bandpass filter with additional capacitive coupling between the resonators.

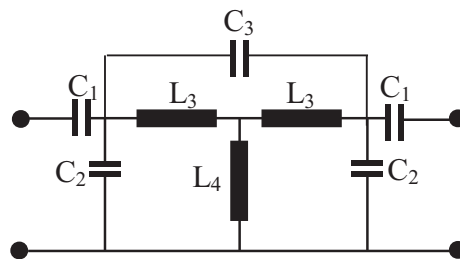


Figure 3.22: Equivalent circuit model of the bandpass filter with additional capacitive coupling between the resonators.

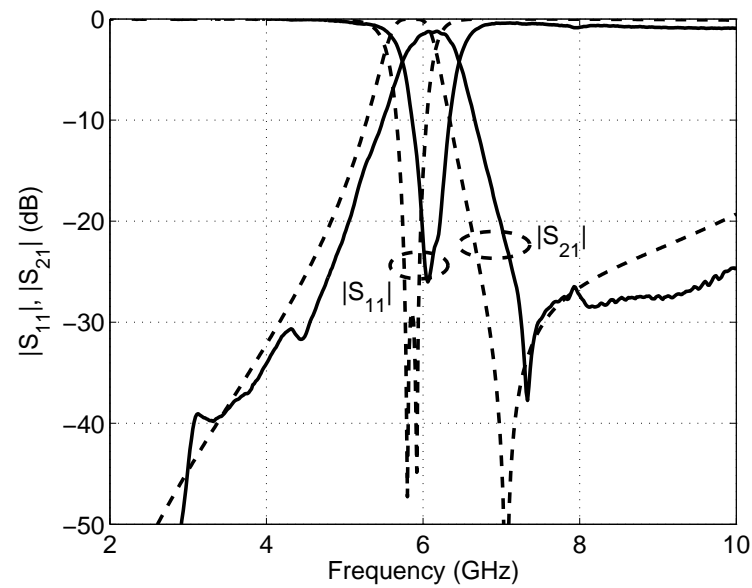


Figure 3.23: Measured (solid) and simulated (dashed) insertion and return loss of the microstrip filter with additional transmission zero.

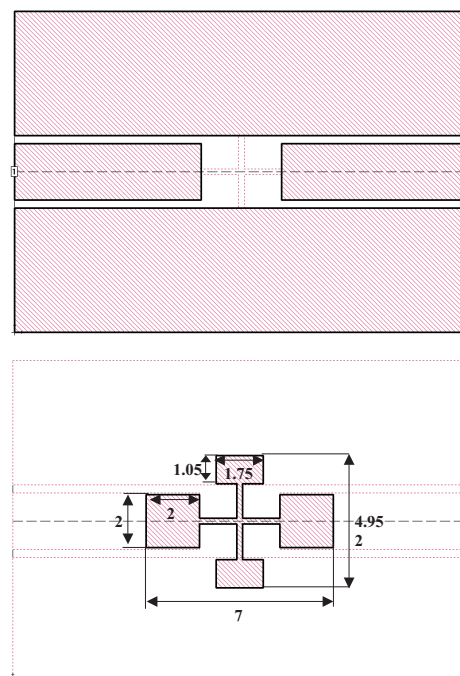


Figure 3.24: Top (up) and backside layouts (down) of an MCL bandpass filter with CPW feed lines, (all dimensions are in mm).

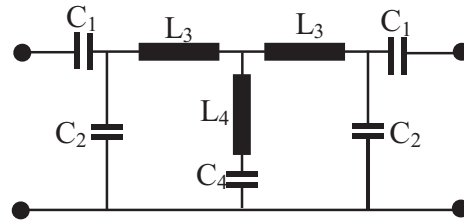


Figure 3.25: The equivalent circuit of the CPW bandpass filter.

between the simulated and measured results.

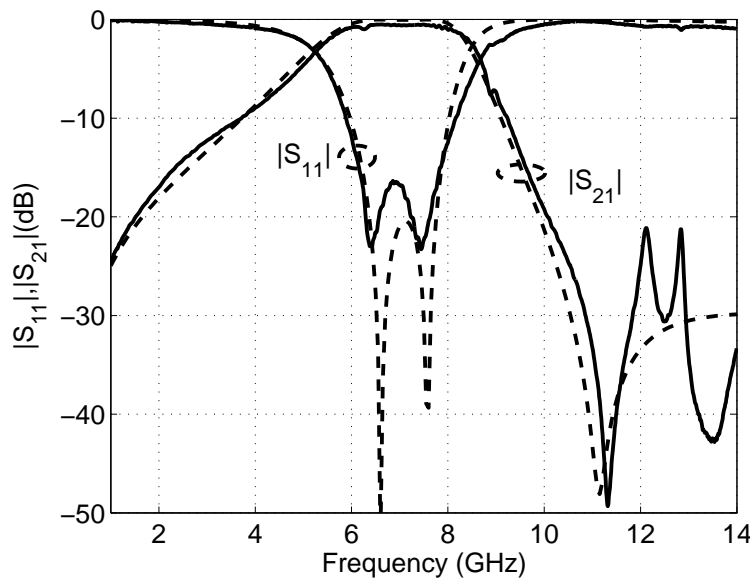


Figure 3.26: Measured (solid) and simulated (dashed) insertion and return loss of the CPW bandpass filter with transmission zero.

3.6 Bandpass Filter with Microstrip-CPW Feed Lines

The bandpass filter introduced in sec.3.4 and shown in Fig.3.16 has been reconstructed again to achieve a bandpass filter compatible with both CPW and microstrip feed lines. The original filter consists of two wide patches coupled to the input/output 50Ω slotted microstrip feed lines. The patches are interconnected by narrow inductive strip, which is grounded at its center by shunt inductive strips. This filter reconstructed to obtain the microstrip-CPW feeding lines. So the ground planes under the original 50Ω slotted microstrip feeding line were closed, so the slotted microstrip line was thus replaced by a 50Ω microstrip line coupled via a patch. The slotted microstrip line from the other side of the filter was replaced by 50Ω CPW line, and

a small patch was added on the topside of the substrate to increase the capacitive coupling between the CPW line and the filter itself. The layout of the modified filter is shown in Fig. 3.27, while the simulated insertion and return loss of the filter over wide frequency range are shown in Fig. 3.28. the filter has center frequency of 3.55 GHz.

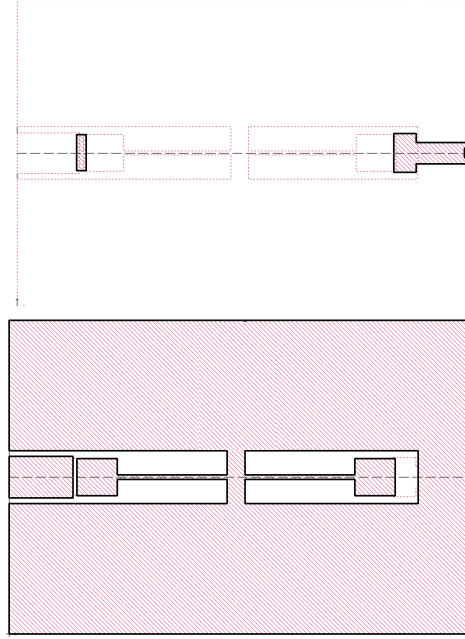


Figure 3.27: Top (up) and backside (down) layouts of a bandpass filter with microstrip-CPW feeding lines.

The filter is designed as a microstrip-CPW transition in addition to its filtering function. As an application to such structure, the filter can be attached to a microstrip antenna that radiates at 3.55 GHz from the microstrip feeding line side. A simple antenna was chosen for this work which is a rectangular patch antenna. The antenna width is chosen to be 15 mm, the length of the antenna can be calculated from [83], and [84]

$$L = L_{eff} - 2\Delta L \quad (3.6)$$

where L_{eff} is the effective patch length and formed as

$$L_{eff} = \frac{c}{2f_0\sqrt{\epsilon_{eff}}} \quad (3.7)$$

where c is the speed of light in the free space and ϵ_{eff} is the effective dielectric constant that can be calculated from (2.84). ΔL is the fringing patch length which formed as [85]

$$\Delta L = 0.412h \left(\frac{(\epsilon_{eff} + 0.3)(\frac{W}{h} + 0.264)}{(\epsilon_{eff} - 0.258)(\frac{W}{h} + 0.8)} \right) \quad (3.8)$$

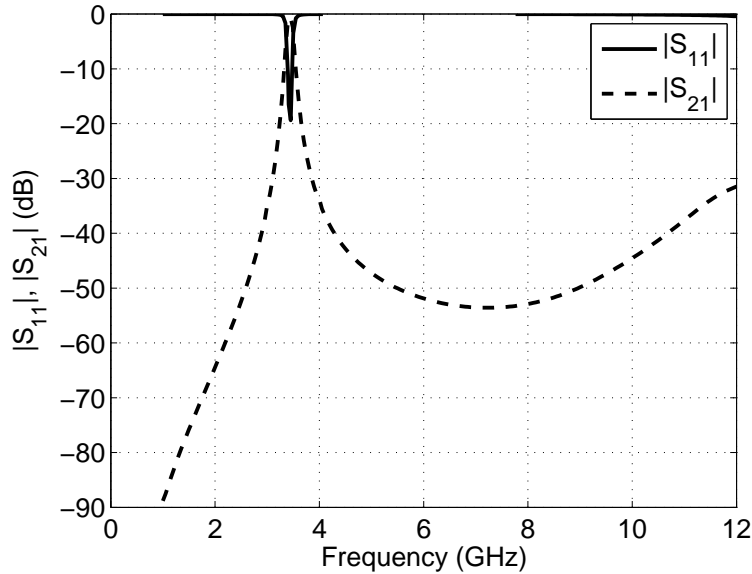


Figure 3.28: Simulated insertion and return loss of the Microstrip- CPW filter.

where h is the thickness of the substrate and W is the width of the antenna.

The antenna was connected to a microstrip feed line. The feeding line was extended inside the patch to archive the best matching. Finally, the antenna was attached to the filter, however, some optimization took place to take in account the involved discontinuity and to achieve best matching. The layout of the filter attached to the antenna is shown in Fig. 3.29. The simulated return loss of the antenna, antenna connected to the bandpass filter, and the measured return loss of the antenna with the filter together are shown in Fig. 3.30. As it is shown in the figure, the antenna has resonances at about 6.7, 7.9, and 10.1 GHz, which has been blocked by the filter, in addition to that, the antenna can be now integrated with CPW system. Good agreement has been achieved between the simulated and measured results except a small frequency shift has occurred in measured return loss, this is normally happens in the fabrication of narrow band filters and circuits especially when they have small geometry.

3.7 Suspended Stripline Ultra-Wideband Bandpass Filter

Suspended stripline (SSL) is considered as a multilayer structure [59], [69], [86], since it is consisting of a substrate shielded by waveguide housing. over and below the substrate there are two layers of air. The air layers are normally having the same dimensions. Fig. 3.31 shows the cross-section of the suspended stripline with the dimensions used in this section. Multi-substrates have also been proposed for such

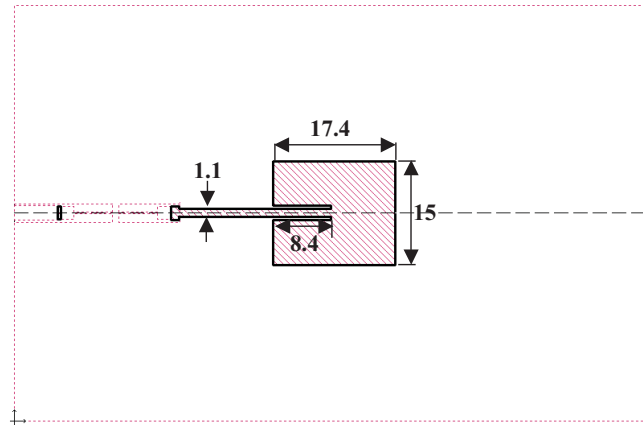


Figure 3.29: Top layer CPW-microstrip filter connected to patch antenna.

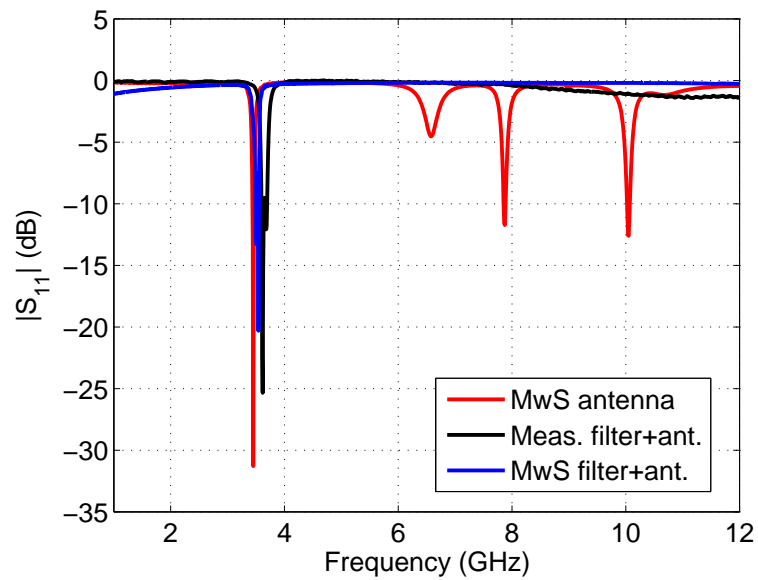


Figure 3.30: Return loss of the patch antenna itself and the patch antenna with the filter.

structures in [87], and [88]. Due to the existence of the mount, the electromagnetic field in SSL is concentrated in the air, therefore, the effective dielectric constant is low compared to the other planar techniques, furthermore, due to same reason no radiation loss, and the dielectric loss is very low in the SSL structure. On the other

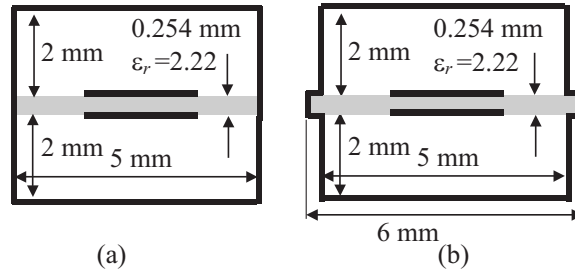


Figure 3.31: Cross-section of SSL (a) used in simulation process, (b) realized in practice.

hand the Federal Communications Commission (FCC) has released the unlicensed use of ultra-wideband (UWB: 3.1 to 10.6 GHz) wireless systems in February 2002 [42]. Since then, the ultra-wideband wireless communication systems with such frequency band have gained an increased interest, since they transmit higher data rates with lower transmitted power. Various filter structures have been proposed in the literature, e.g. [15], [43], and [89–92]. The combination of a lowpass filter with a high-pass filter is a classical structure for such kind of filters [89], [90]. It occupies, however, a large area, which may increase the losses, and the group delay variation of the filter. In [91], an UWB filter was built by cascading various ring filters, while, in [15], and [43], UWB filters were designed using multi-mode resonators. However, due to the long transmission line sections used in these structures, higher order resonances do not allow a wide stop band. An UWB filter introduced in [92] was designed by employing quasi-lumped microstrip resonators built on both sides of the substrate. The fabrication of this filter, however, is difficult due to the via holes necessary to increase the stopband up to 16 GHz.

In this section, a simple ultra-wideband bandpass filter is presented, showing a great simplicity of the design concept compared to earlier known structures. The filter is realized by coupling an SSL quasi-lumped lowpass filter capacitively to the I/O ports. A very wide stopband is obtained due to the short transmission line sections used in the filter structure. The filter is built on an RT Duroid substrate with a thickness of 0.254 mm and a relative dielectric constant ϵ_r of 2.22. The substrate is shielded in a split-block mount with dimensions of 5 mm width and 2 mm height over and below the substrate. The substrate is suspended in the mount by extending it 0.5 mm inside the mount from both edges (Fig.3.31). The additional substrate portion within the clamping region is fully metallized to provide good connection between the mount and the substrate. This is particularly important in case of shunt connections.

Due to the small dimensions of the housing mount, the waveguide cut-off frequency is slightly above 20 GHz.

To design the ultra-wideband bandpass filter with a frequency range from 3.1 to 10.6 GHz using a lowpass filter, two steps are necessary:

We firstly design a lowpass filter with a cut-off frequency of 10.6 GHz. In general, the cut-off frequency of the lowpass filter can be adjusted by setting proper values of the lumped elements of the filter. The capacitive and inductive elements of the filter are realized by short sections of high/low-impedance transmission lines. The low impedance sections are implemented by adding a ground metallization at the backside of the substrate [64], as it is described in sec. 3.3.

Having determined all transmission line lengths the lowpass filter can be combined, however, some optimization can be done to take into account the involved discontinuities and to achieve good matching in the passband. Fig. 3.32 shows the top and backside layouts of the SSL lowpass filter. Fig. 3.33 shows the simulated insertion and return loss of the filter. The filter has a cut-off frequency of 10.6 GHz, with very good matching at the passband. At about 16.5 GHz a transmission zero occurred due to the short inductive transmission line sections that allow capacitive coupling between the wide patches, and in parallel to inductances.

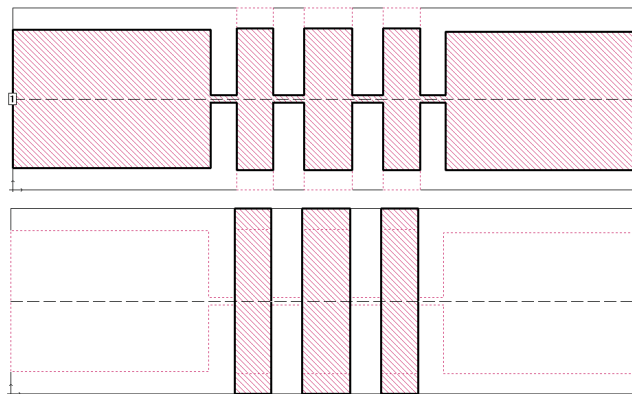


Figure 3.32: Top (up), and backside (down) layouts of an SSL lowpass filter.

Next, we must suppress transmission in the frequency band below 3.1 GHz. The SSL technology provides strong broadside coupling between transmission lines on the opposite sides of the substrate [40], [24]. By overlapping a section of the original input and output lines of the lowpass filter with new input and output lines on the other side of the substrate, capacitive highpass sections [64] are formed to shape the lower filter edge. Fig. 3.34 shows the top and backside layouts of the filter, while Fig. 3.35 shows the equivalent circuit of the structure.

The proposed filter was optimized, fabricated, clamped into the mount, and soldered to coaxial connectors fixed at the ends of the mount, see Fig. 3.36. Measurements were done using a coaxial calibration, the transitions from SSL to coaxial line

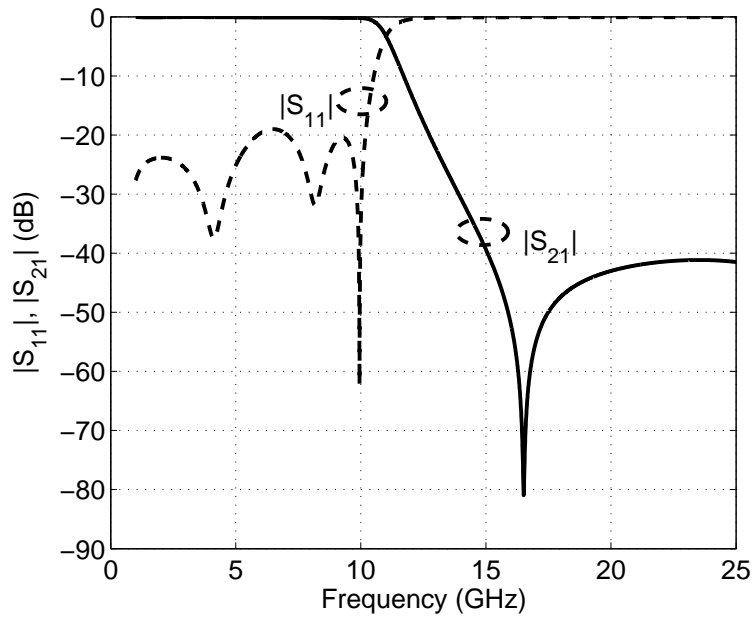


Figure 3.33: Simulated insertion and return loss of a SSL lowpass filter.

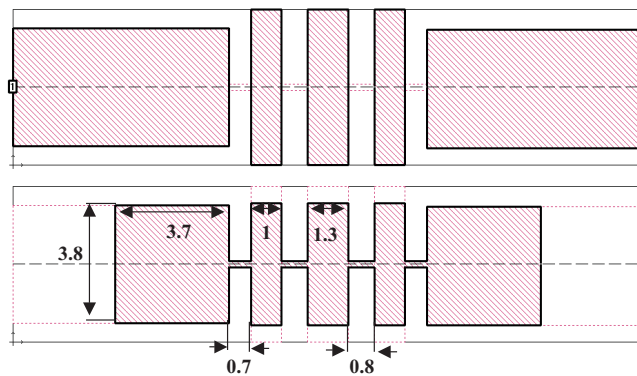


Figure 3.34: Top (up) and backside (down) layouts of the SSL UWB filter using a coupled lowpass filter.

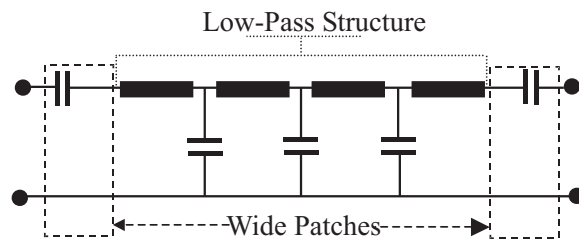


Figure 3.35: Equivalent circuit of the ultra-wideband bandpass filter using a coupled lowpass filter structure.

as well as some portion of SSL transmission line are included into the experimental results. Fig. 3.37 shows the simulated and measured return and insertion loss of the filter. As expected, the filter has a very wide stopband with a good rejection of better than 40 dB up to 25 GHz. The insertion loss of the filter in the passband is better than 0.5 dB as shown in Fig. 3.38. The group delay variation in the passband is smaller than 0.19 ns.

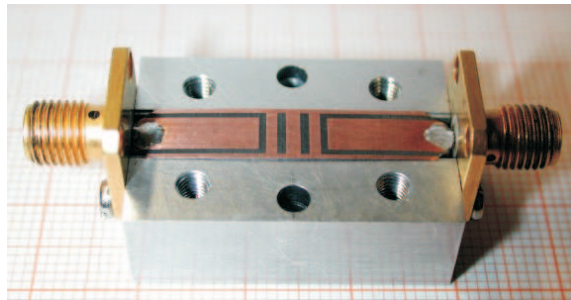


Figure 3.36: Photograph of the ultra-wideband bandpass filter with opened mount.

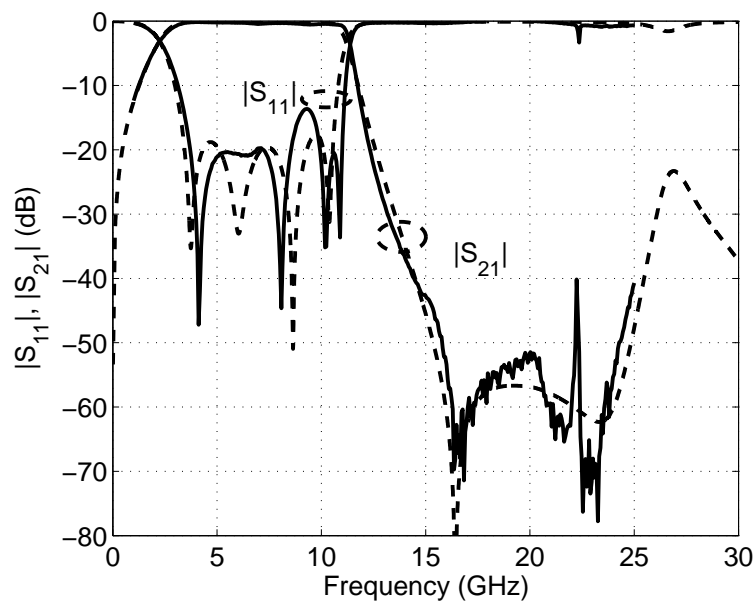


Figure 3.37: Simulated (dashed) and measured (solid) insertion and return loss of the UWB filter.

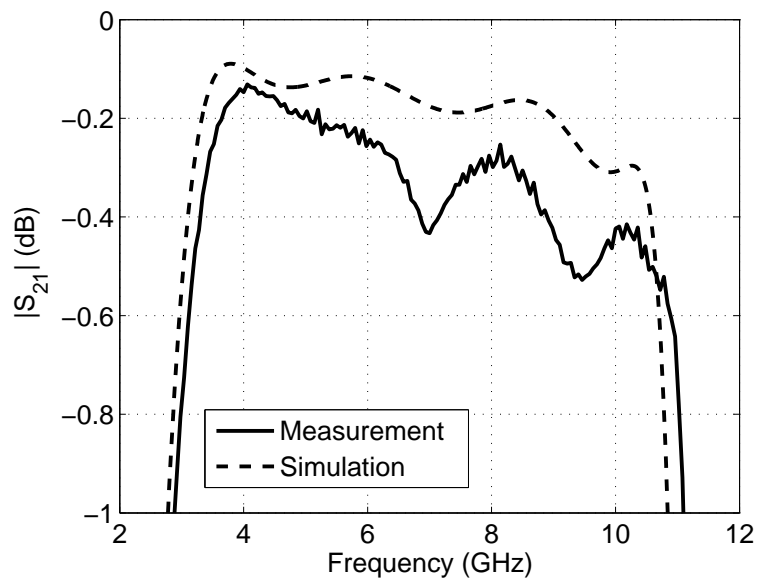


Figure 3.38: Simulated and measured insertion loss at the passband of the UWB filter.

Chapter 4

Defected Ground Structures

Defected ground structures have been introduced first in [16], they are known in the literature as DGS. This technique is realized by etching slots in ground plane of the microwave circuit and is namely applied for the microwave filters. This technique is used for microstrip and coplanar waveguide transmission lines. These slots are designed to achieve better performance for the microwave filters, such as increasing steepness of the cut-off slop, and to increase the stopband range of the microwave filters, moreover, compact filter can also be achieved using this technique. Many slot shapes have been introduced for microstrip technology [16–23]. Increasing the stopband of microstrip lowpass filter by introducing transmission zeroes have been obtained by different slot shapes, e.g. [16],[17], [22], and [34–37]. Periodic structures, e.g.[18], [21] and [93]. Even bandpass filters have been presented using this technique, e.g. [19], [20],[22], and [94]. Fig 4.1 shows the backside of the substrate of three different slots that have been introduced in [16–18].

A simple study is done on the square head dumbbell slot with dimensions $a= 4$ mm, $S=0.25$ mm and $d=5$ mm etched under 50Ω line to show how this structure behave over wide frequency band [16]. The insertion and return loss of the structure are shown in Fig.4.2. It can be clearly seen that at 6.5 GHz a transmission zero occurred. Basically, the reason behind this behavior is the increase of the inductance of the transmission line and it introduces series capacitance which is in parallel to the original inductance. Thus, the equivalent circuit of a 50Ω line over a DGS slot can be represented as a parallel resonator [18], see Fig. 4.3. The current density distribution at the slot metallization is shown in Fig. 4.4. At frequencies lower than the resonant frequency of the slot, the current density is concentrated around the slot metallization as shown in Fig. 4.4a. At frequencies higher than the resonant frequency of the slot (Fig.4.4b) one can see that the current density is concentrated at the slot center. Fig. 4.5 shows a representation of the wave propagating at frequencies lower and higher than the resonant frequency.

To control the resonant frequency of the DGS slot, it is required to change the dimensions of the area occupied by the slot [16–23],[34–37]. For example, to set the

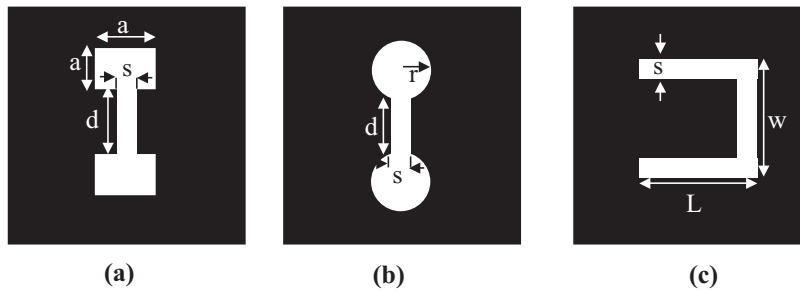


Figure 4.1: Layouts of defected ground slots, (a) dumb bell structure with square head, (b) dumb bell structure with circular head, (c) U shape DGS structure.

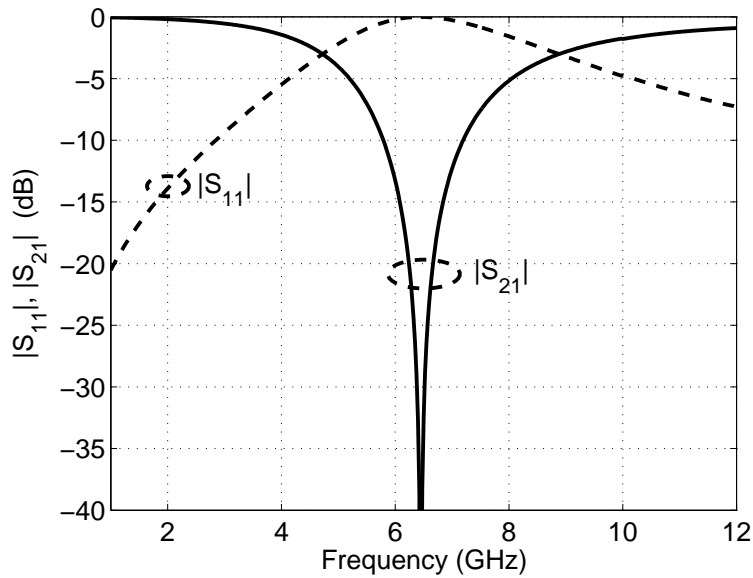


Figure 4.2: Simulated insertion and return loss of a dumb-bell slot etched under 50-ohm transmission line.

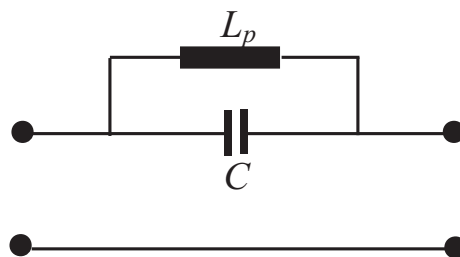


Figure 4.3: equivalent circuit of a DGS slot etched under 50 Ω transmission line.

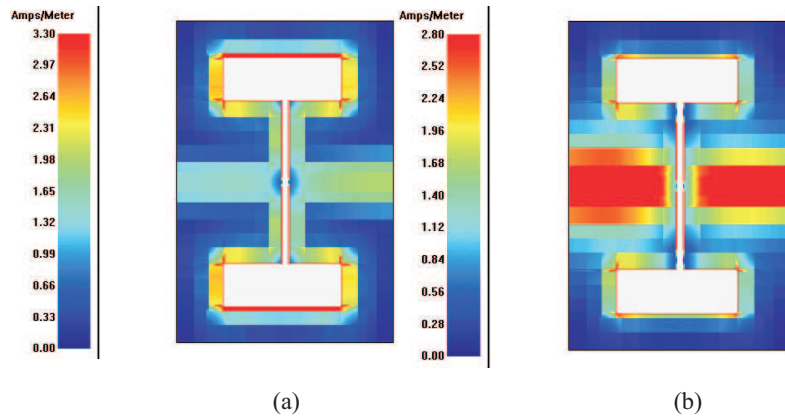


Figure 4.4: Current density distribution on the slot metallization (a) at 2.5 GHz, (b) at 9 GHz.



Figure 4.5: Representation for the wave propagating on the slot metallization (a) at frequency lower than the resonant frequency, (b) at frequency higher than the resonant frequency.

resonant frequency of the square head dumbbell slot at low frequency it is required to increase either the dimensions of square head (a), the length of the slot (d), or both in most of the cases. Another parameter that can be set, is the spacing between the both ends of the slots [19], see Fig. 4.1.

This chapter demonstrates a compact slot in form of interdigital microstrip capacitance. The resonant frequency of the line that is under-etched with this slot can be controlled by adjusting the distance between the fingers of the slot without enlarging the size of the slot. Using this slot two quasi-elliptic lowpass filters are designed. All of these filters have been design and fabricated on a RO4003c substrate that has a thickness of 0.831 and relative dielectric constant of 3.38. In addition, this chapter demonstrates a solution for the packaging problem that may occur due to the defected ground structure.

4.1 Interdigital DGS Slot

In this section, an interdigital DGS slot is proposed. The slot is shown in Fig. 4.6. It is etched in the ground metallization under the microstrip line. This slot has a major advantage in providing higher capacitive coupling to the line in comparison to known microstrip DGS structures. Moreover, the resonant frequency of the structure can be controlled by changing the distance between the metal fingers. The resonant frequency of the slot can also be modified by changing the number of metal fingers, so there is, in most cases, no need to enlarge the overall slot size.

The equivalent circuit of the proposed structure assuming lossless metal, illustrated in Fig. 4.7, is a combination of the interdigital capacitance equivalent circuit [1] and the equivalent circuit of the DGS [16]. The series $C L_s$ circuit represents an equivalent circuit of the interdigital capacitance [1]. In the case of lossy metal, a resistance R is replaced in the equivalent circuit instead of the series inductance L_s .

Fig. 4.8 shows the insertion loss of an interdigital slot in comparison with dumbbell slot. The interdigital slot has a length of 3.75 mm and a width of 4.9 mm. The slot consists of six interdigital fingers each has 3.5 mm length and 0.3 mm width. The dumb-bell slot has rectangular head with the dimensions $a=4$ mm and $d= 5$ mm. both slots have resonance at the same frequency. this shows how much is the interdigital slot smaller than the earlier presented slot.

The current density distribution is calculated on the slot metallization at frequencies lower and higher than the resonant frequency of the slot. The current density is concentrated at the edges of the slot at frequencies lower than resonant frequency, where, at frequencies higher than the resonant frequency of the slot it is concentrated at the metallic fingers , as shown in Fig. 4.9.

Controlling the bandwidth of this slot can be done in three different ways:

1. Changing the length of the metallic fingers: The resonant frequency of the slot strongly depends on the length of the metallic fingers. Basically, by changing the

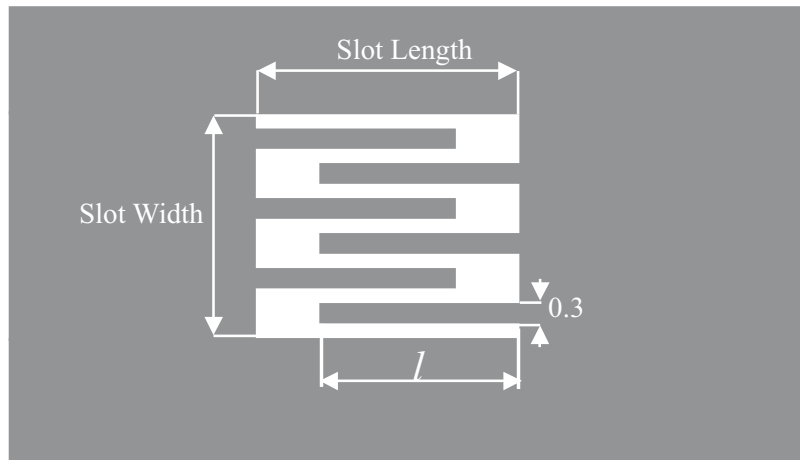


Figure 4.6: Backside layout of the interdigital slot.

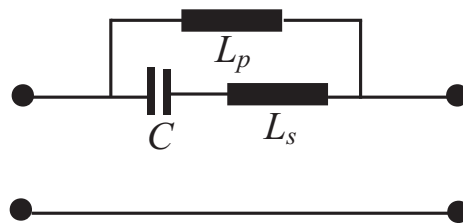
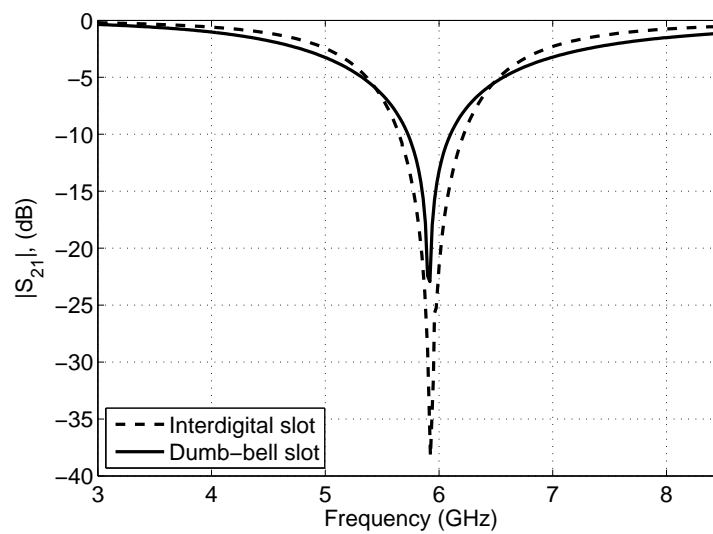
Figure 4.7: Equivalent circuit of the interdigital DGS slot etched under $50\ \Omega$ transmission line.

Figure 4.8: Simulated insertion and return loss of the interdigital slot.

length of the fingers, the series capacitive value of the slot is changed. So increasing the length of the fingers means increasing the capacitive value of the slot and vice versa. A simple study is done on the relation between the length of the metallic fingers and the resonant frequency of the slot. The dimensions of the used slot are 3.5 mm in length and 4.9 mm in width. The spacing between metallic fingers is 0.3 mm and the number of fingers is 6. Fig. 4.10 shows the relation between the length of the fingers and the resonant frequency of the slot.

2. Number of fingers: It is the second parameter that is not less important than the first one. Increasing the number of metallic fingers increases the series capacitive value that the slot provides, which shifts the resonant frequency of the slot to the lower band. Decreasing the number of metallic fingers is responsible for shifting the resonance frequency of the slot to a higher frequency band. A simple parametric study was done to show the relation between the number of the fingers and the resonance frequency of the slot. The slot used in the last study is used here, the length of the used fingers is kept 3.5 mm. Fig. 4.11 shows the relation between the number of the used metallic fingers and the resonant frequency of the slot. As shown in the fingers, the resonant frequency of the slot varies between 6 GHz with 6 metallic fingers and 11 GHz with one finger.

3. Spacing between fingers: As it is well known, the spacing between the interdigital fingers is an important parameter that the capacitive value of the interdigital capacitance depends on. To show that, a slot with three fingers was chosen. The length of each of the fingers was chosen to be 3.5 mm. The distance between the fingers varies between 0.2 to 1.4 mm, the other slot dimensions were kept as in the last two studies. Fig. 4.12 shows the relation between the spacing between the fingers and the resonant frequency of the slot.

The inductive and the capacitive values of the slot with the transmission line above that is represented by the equivalent circuit shown in Fig. 4.7 can be approximated as follows:

At the resonant frequency, the admittance of the equivalent circuit Y_{total} is equal to zero, where Y_{total} can be written as

$$Y_{total} = \frac{1}{j\omega L_p} + \frac{1}{j\omega L_s + \frac{1}{j\omega C}} \quad (4.1)$$

At the resonant frequency

$$\frac{1}{j\omega L_p} = \frac{-1}{j\omega L_s + \frac{1}{j\omega C}} \quad (4.2)$$

where L_p , L_s , C are defined in Fig. 4.7.

The transmission coefficient of the of any tow-port network is given by [1]

$$s_{21} = \frac{2Z_0}{2Z_0 + Z_{total}} \quad (4.3)$$

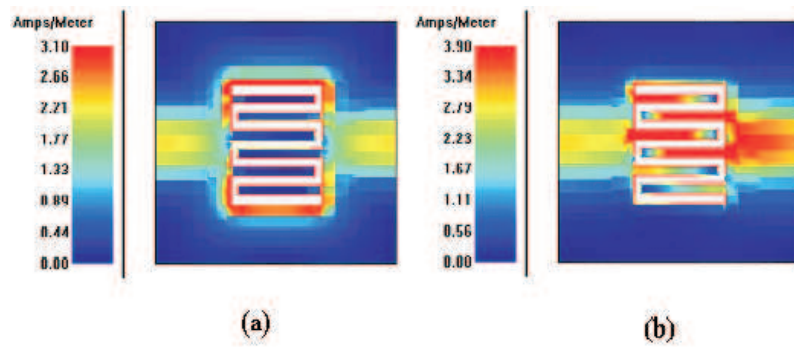


Figure 4.9: Current density distribution (a) at 1 GHz, (b) 9.5 GHz.

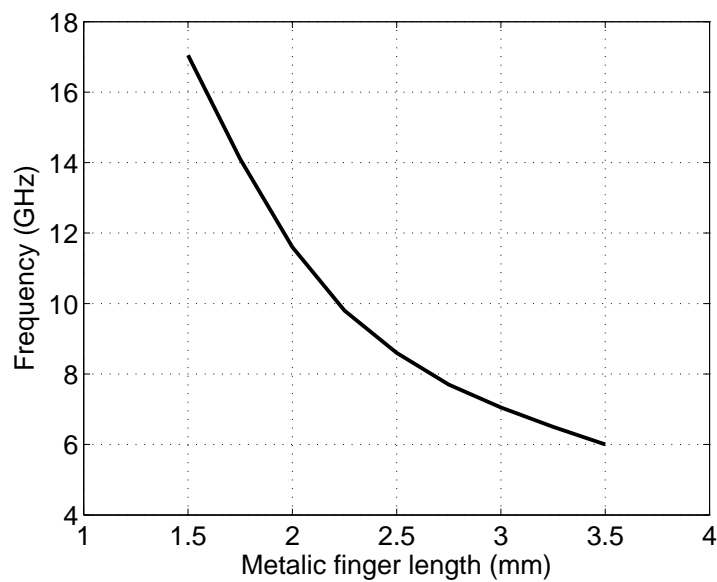


Figure 4.10: Relation between the interdigital slot resonant frequency and the length of the metallic fingers.

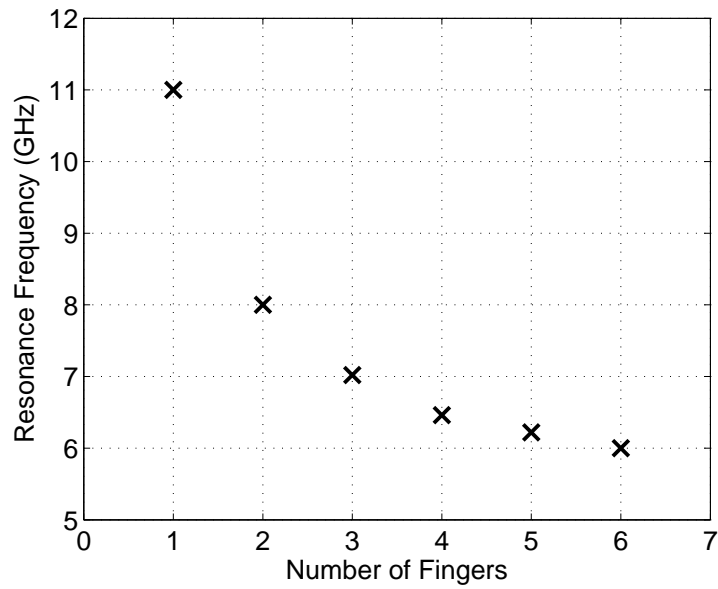


Figure 4.11: Relation between the interdigital slot resonant frequency and the number of the metallic fingers.

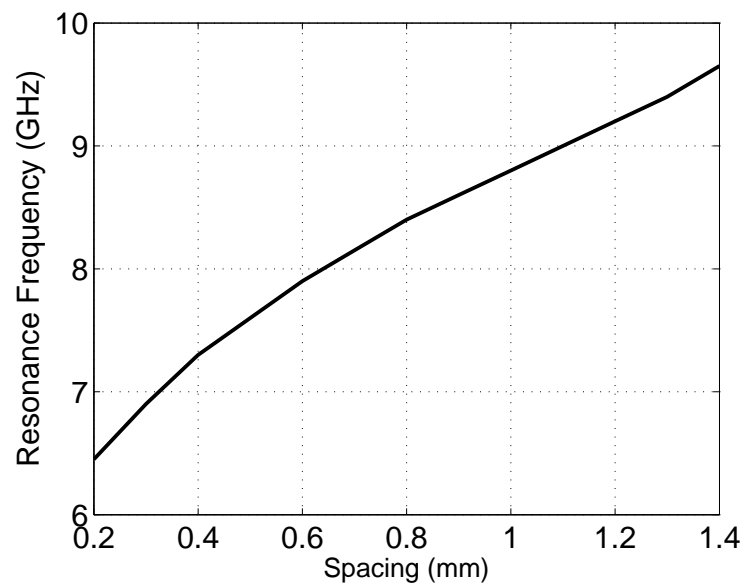


Figure 4.12: Relation between the interdigital slot resonant frequency and the spacing between metallic fingers.

Where Z_0 is the input impedance and Z_{total} is given as

$$Z_{total} = \frac{j\omega L_p \left(\frac{1}{j\omega C} + j\omega L_s \right)}{\frac{1}{j\omega C} + j\omega L_s + j\omega L_p} \quad (4.4)$$

at the 3dB cut-off frequency the transmission coefficient equal to $\frac{1}{\sqrt{2}}$ this leads to

$$\frac{1}{\sqrt{2}} = \frac{2Z_0}{2Z_0 + \frac{j\omega L_p \left(\frac{1}{j\omega C} + j\omega L_s \right)}{\frac{1}{j\omega C} + j\omega L_s + j\omega L_p}} \quad (4.5)$$

Since the major changes in the interdigital slot is on the finger lengths, the parallel inductance L_p remains unaffected. The inductive value of the inductance L_p can be simply calculated by approximating the effective dielectric constant ϵ_{eff} and the characteristic impedance Z_0 of the transmission line with aperture under etched, which can be easily done using [81]. having calculated ϵ_{eff} and Z_0 , the inductive value of of the line can be calculated using (3.4).

4.2 Quasi Elliptic Microstrip Lowpass Filters

Quasi-elliptic filter responses are achieved by realizing equal-ripple in the passband and transmission zeros in the stopband, which leads to sharper cutoff frequency than in case of chebyshev and Butterworth filter responses, and higher rejection at the stop band. Quasi-elliptic lowpass filters are normally realized by going through two steps.

First, designing a lumped chebyshev lowpass filter, that requires the order and the cut-off frequency of the filter. Having the order, the cut-off frequency, and passband ripple, the lumped elements of the chebyshev can be simply calculated. As an example a fifth order chebyshev filter with cut-off frequency of 3 GHz and passband ripple of 0.1 dB. The normalized elements for this filter are $g_0 = g_6 = 1$, $g_1 = g_5 = 1.1468$, $g_2 = g_4 = 1.3712$, and $g_3 = 1.975$ [1]. g_0 and g_6 represent the source and load impedances, respectively, that is considered for our filters to be $Z_0 = 50 \Omega$. The proper lumped elements of the filter can be calculated by using equations (2.25), and (2.26). Realizing these elements in microstrip transmission line can be easily done in the same way described in sec. 3.3.

Using this way, a microstrip lowpass filter has been designed by opening apertures under the high impedance transmission line, to increase the impedances of these lines, which lead to higher inductive values for these lines that is for the classical inductive microstrip line [73]. Fig. 4.13 shows the layout of a microstrip lowpass filter with apertures under the high impedance transmission lines [73].

The response of this filter is however a chebyshev response. In other words, the filter response has no resonance at the stopband, which may introduce a transmission zero. Replacing the interdigital slot instead of the rectangular apertures will introduce

transmission zeros for the filter response. Since each slot introduces one transmission zero, thus, the number of the introduced transmission zeros is equal to the number of the replaced slots.

One transmission zero is introduced into the filter response by replacing the central aperture by the interdigital slot structure. This slot, however, shifts the cut-off frequency of the filter to a lower frequency band. To shift the cut-off frequency back, it is necessary to reduce the inductance of the narrow stripline that is located over the slot. This can be easily done by increasing the width of the strip. Fig. 4.14 shows the backside layouts of the designed filter, where the top side is remained as shown in Fig. 4.13. Fig. 4.15 shows the measured and simulated return and insertion loss of the filter. A transmission zero, which improves the behavior of the filter stop band, is observed at 6.32 GHz. The maximum insertion loss of the filter in the passband is better than 0.4 dB. The measured group delay variation within the passband is less than 0.275 ns.

Using two interdigital slots with different finger lengths inserted in the positions of the side apertures instead of the central one introduce two transmission zeroes. Fig. 4.16 shows the top and backside layouts of the filter. Fig. 4.17 shows the simulated and measured insertion and return loss of the filter. Two transmission zeros are introduced to the filter response at about 6.45 GHz and 8.6 GHz. Consequently a wide stopband was achieved. The maximum insertion loss in the passband is better than 0.5 dB. The maximum group delay variation within the passband of this filter is less than 0.26 ns.

4.3 Defected Ground Structure and Packaging

The defected ground structures for microstrip need much effort in packaging and in integrating it with deferent elements that are printed on one side of the substrate. Since it needs either to suspend the whole substrate by holders, such as screws , see Fig. 4.18, or drilling channel inside the carrier block of the whole system. However, the distance between the carrier block and the slot should be carefully calculated. Since it has a significant effect on the resonant frequency of the slot, which may affect the response of the filter. It may not have a large effect on the response of the lowpass filter, but the effect will be significant on the narrow bandpass filter response.

To find the relation between the dimensions of the recessed region under the DGS slot and its resonant frequency, a simple study has been done using an interdigital slot that was introduced and studied in sec. 4.1. The DGS slot has dimensions of 3.75 mm in length, 4.9 mm in width, see Fig.4.6. The dimensions of the fingers are 3.55 mm length and 0.3 mm width, and six fingers have been used. The resonant frequency of the slot is 5.95 GHz in case of free the space used under the slot. The free space has been replaced by a metallic box with dimension of 10 mm length and 10 mm width. Fig.4.19 shows the relation between the resonant frequency of the slot

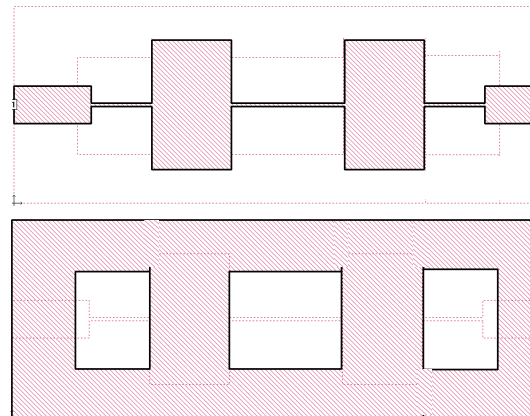


Figure 4.13: Top (above) and rear (below) layouts of a fifth order lowpass filter with apertures under the high-impedance transmission lines.

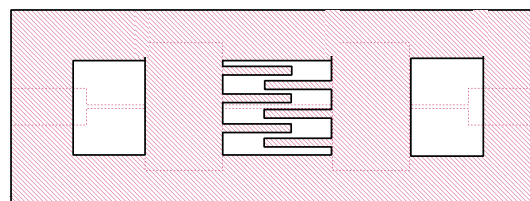


Figure 4.14: backside Layout of a fifth order lowpass filter with one interdigital DGS slot.

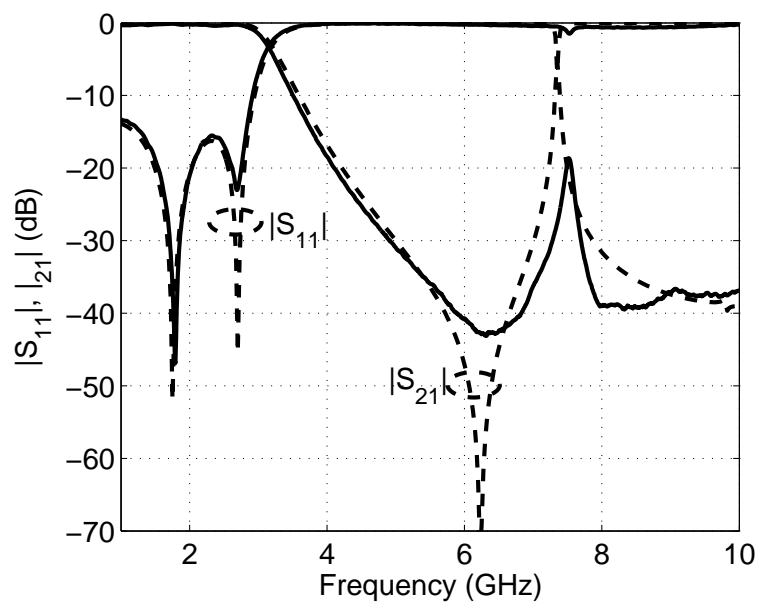


Figure 4.15: Simulated (dashed) and measured (solid) return and insertion loss of a fifth order lowpass filter with one transmission zero.

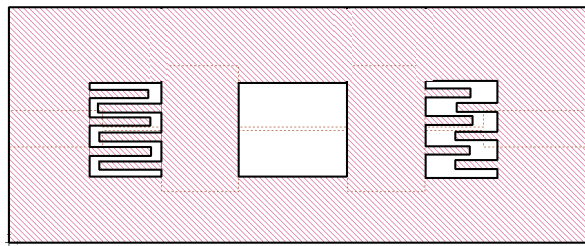


Figure 4.16: backside Layout of a fifth order lowpass filter with two interdigital DGS slots.

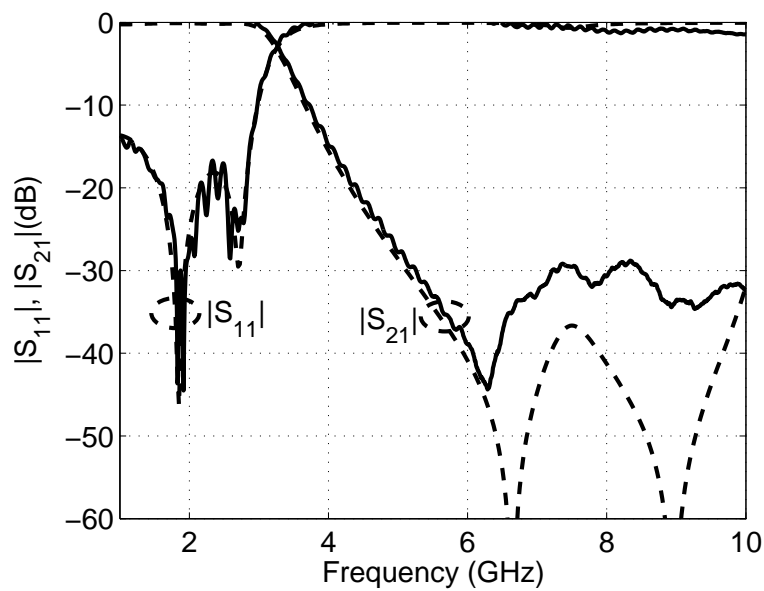


Figure 4.17: Simulated (dashed) and measured (solid) return and insertion loss of a fifth order lowpass filter with two transmission zeroes.

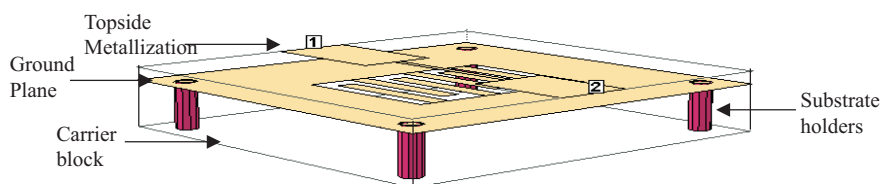


Figure 4.18: 3D view of suspended DGS structure.

and the height of the metallic box. As it can be clearly seen from the figure, the slot resonance changes dramatically by changing the height of the metallic box.

To reduce the packaging difficulties such as using a recessed area in the carrier block, the original ground plane of the circuit is kept fully metallized, and the interdigital slot is etched on a superstrate, which is placed on the top of the substrate. The ground plane of the substrate is connected with the metal on superstrate by via holes. Fig. 4.20 shows a 3D view of the proposed structure. This structure has higher quality factor than that for the classical DGS structures, since it has narrower stopband. Fig. 4.21 shows the simulated response of the proposed structure in comparison with the standard structure described in sec. 4.1. The interdigital slot dimensions are defined in Fig. 4.6. The resonant frequency of the proposed structure is located around 5.65 GHz which is lower than the resonant frequency of the standard DGS slot that is located at about 5.95 GHz. Moreover, the proposed structure has narrower stopband than the standard DGS.

Using this structure, a quasi-elliptic lowpass filter is designed by using two interdigital DGS slots. The filter is etched on two substrates. The dielectric constant of both substrates is 3.38, and each substrate has thickness of 0.813 mm. Since the two substrates are placed over each other, and both of them have a fully metallized ground plane, the effective dielectric constant increases, which decreases the characteristic impedance of both high and low impedance transmission lines. Thus, the high impedance line sections needed to design a lowpass filter with 3 GHz cut-off are longer than those needed to design a lowpass filter with the same cut-off frequency using the standard structure. While the opposite is correct in the case of low impedance line sections, i.e., shorter low impedance line sections are needed to design a filter for the same cut-off frequency, which compensates the increasing length of the inductive transmission line. Fig. 4.22 shows the filter layout that is built on the top side of the substrate, the backside of this substrate is fully metallized. Fig. 4.22 shows the metallization layout on the superstrate consisting of two interdigital slots and one aperture. The backside of the superstrate is non-metallized. The slots that are etched on the second substrate are connected with the ground plane of the first substrate by vias with diameter of 0.3 mm. After optimization the filter has been fabricated and measured. Fig. 4.24 shows a photograph of the measured structure. Fig. 4.25 shows measured and simulated insertion and return loss of the filter. The filter has rejection at the stopband better than 23 dB up to 8 GHz, and has insertion loss within the passband better than 0.4 dB. A good agreement between the measured and simulated results is achieved.

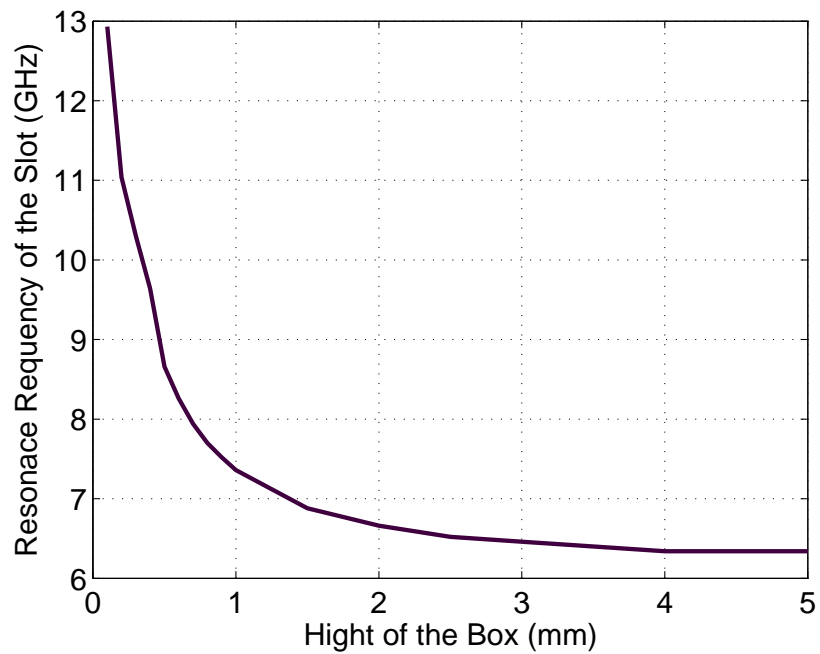


Figure 4.19: Calculated relation between the resonance frequency of the interdigital slot and the depth of the recessed region under DGS.

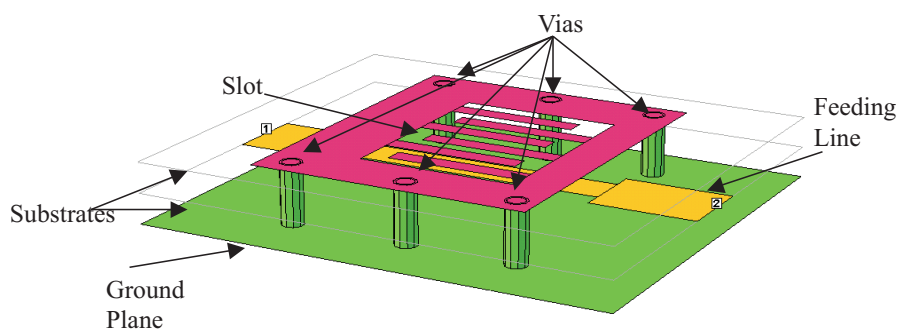


Figure 4.20: 3D view of the proposed structure with an interdigital slot.

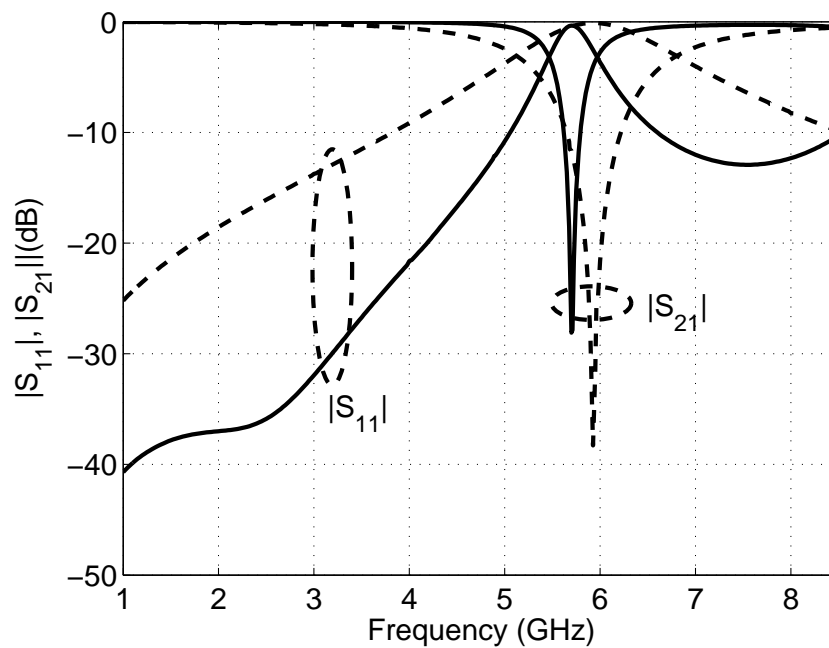


Figure 4.21: Simulated insertion and return loss of the proposed structure (solid) in comparison with the standard DGS structure (dashed).

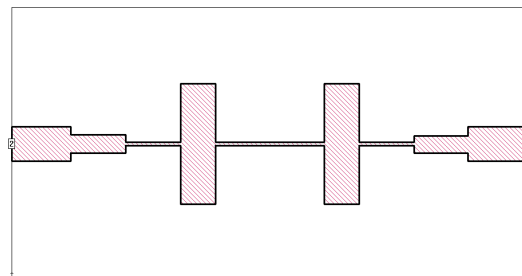


Figure 4.22: Top layout of a fifth order lowpass filter, the rear of the substrate is fully metallized.

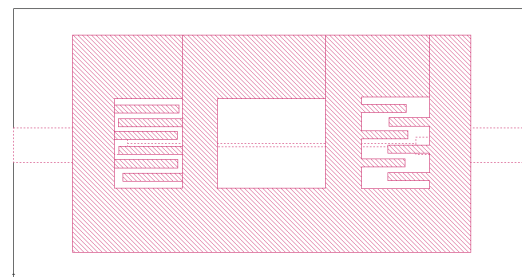


Figure 4.23: 2 Metallization of the additional substrate, which contains two slots with finger lengths 3.55, and 2.45 mm, and one aperture.

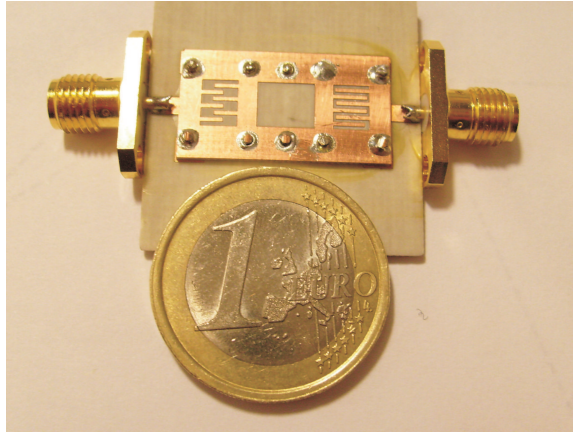


Figure 4.24: Photograph of the fabricated lowpass filter.

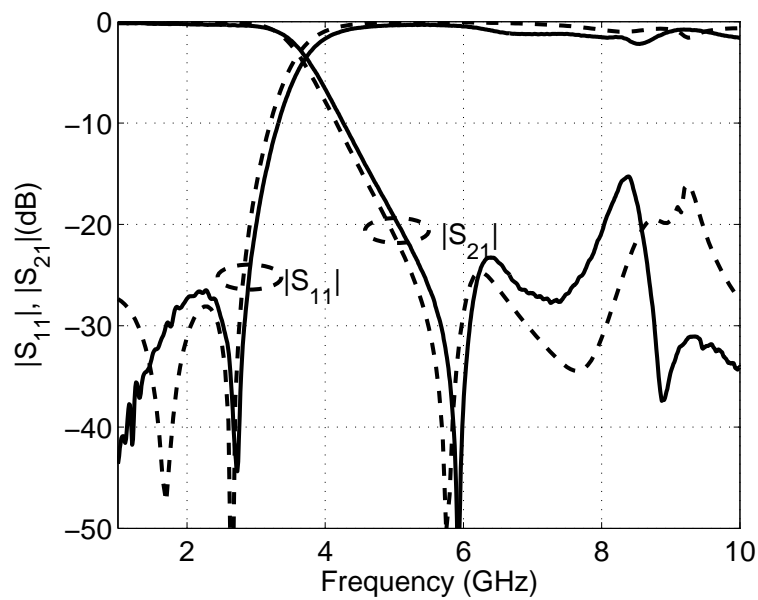


Figure 4.25: Simulated (dashed) and measured (solid) insertion and return loss of a lowpass filter with the proposed DGS structure.

Chapter 5

Dual and Triple-Mode Resonators and Filters

The classical planar filters are mostly designed using single mode resonators. In the recent years, dual-mode resonators have been increasingly used in wireless communication systems and other RF applications, since they can offer low-losses with compact size, and high selectivity. In general, the dual-mode resonator must be built in such a way that the fields are distributed symmetrically between the resonator and the ground plane. Therefore most of the known dual-mode resonator structures are built using microstrip technique. Many dual-mode resonators have been introduced using this technique. Among these resonators are the square-loop dual mode resonators, meander loop, triangular closed loop, and the hexagonal loop [9–11], and [95, 96]. The two resonance modes of the circular ring, square-loop, and hexagonal resonators are excited and coupled to each other by perpendicular feed line and attaching a small square patch at the corner of the resonator [9–11], Fig. 5.1 shows the topologies of dual-mode resonators fed by perpendicular feeding lines. The closed loop resonators have smaller size than the patch resonators. Therefore most of the research activities nowadays are done on the loop resonators. Moreover, size reduction has been already done for such resonators by extending the loop inside the resonator [97], or by connecting the original resonator by identical open-loop from the corner sides [98] and [99]. Another class of this kind of resonators is fed by using parallel feed lines [95], [100] and [101]. Fig. 5.2 shows dual mode triangular resonators as well as a meander closed loop resonator.

The main advantage of the dual-mode patches and loops is that the degenerate modes can be splitted by having a small patch attached to the resonator corner or by having a square cut (perturbation element) in one of the resonator corners. Moreover, the strength of the coupling between the degenerate modes depends on the size of the perturbation element [102]. The nature of the coupling between the modes depends on the shape of the perturbation element [3], so by having a cut at one corner of the resonator, (see Fig. 5.3a), an inductive coupling between the modes is induced,

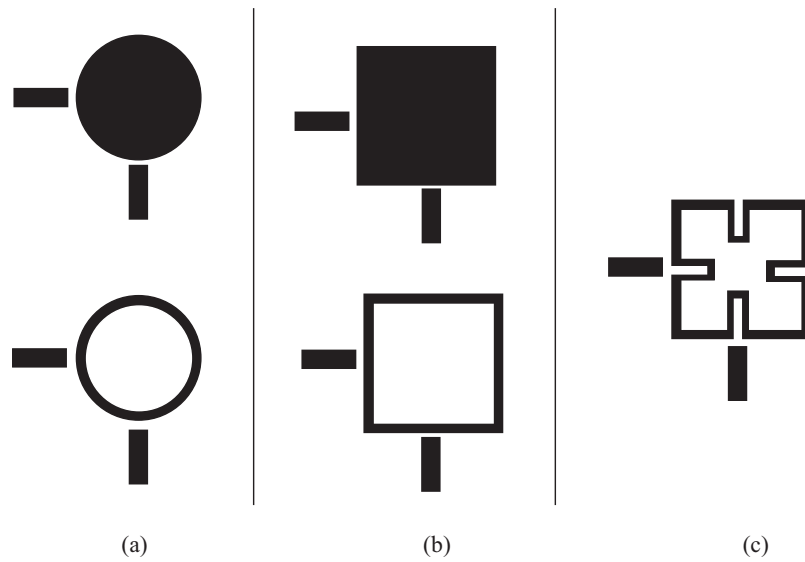


Figure 5.1: Dual-mode circular loop, patch resonator (a), square loop, patch resonator (b), square meander loop resonator (c).

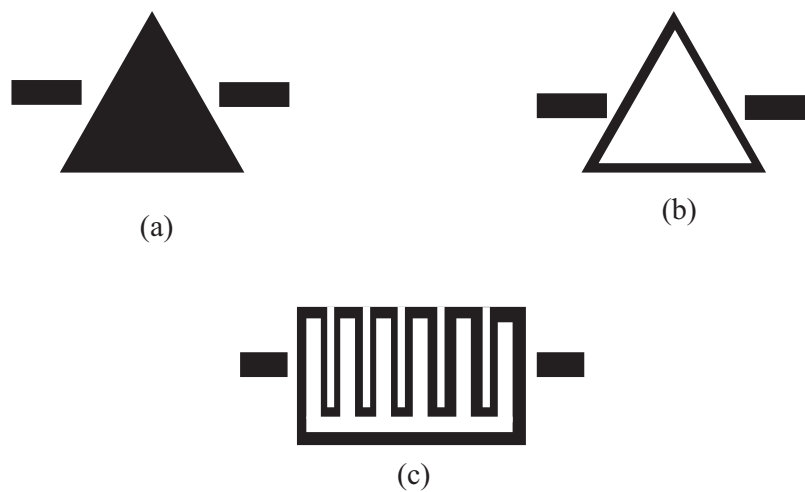


Figure 5.2: Dual-mode triangular patch resonator (a), triangular closed loop (b), meander loop resonator (c).

while attaching a small patch at the one corner will induce an capacitive coupling between the modes, (see Fig. 5.3b, and Fig. 5.3c). Furthermore, the position of the attenuation poles can also be adjusted by coupling the dual-mode resonator with feed line location not at the center of the arms of the resonator [103].

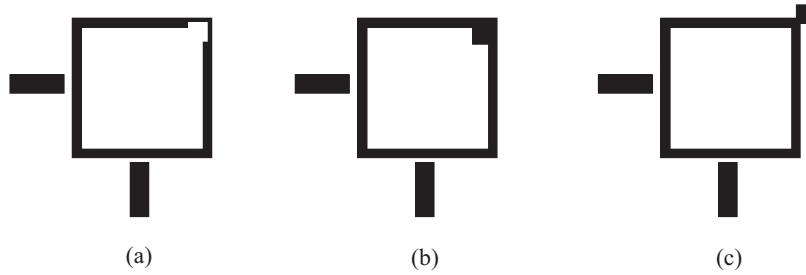


Figure 5.3: (a) Dual-mode filter with inner corner cut perturbation, (b) dual-mode filter with inner corner patch perturbation, (c) dual-mode filter with outer corner patch perturbation[3].

The triple-mode resonators are those resonators that provide three resonances in the passband. These resonators are efficient for bandpass filter applications. Such resonators have been introduced in the past using dielectric filled waveguide of rectangular or cylindrical shape. For most part, triple-mode operation is achieved by dielectric filled structure inside a resonant metal cavity. Then the cavity is perturbed using tuning and coupling elements such as metal rods or screws [104–106]. However, such structures are huge rather expensive. A triple-mode microstrip filter has been reported in [107]. It was realized by placing a microstrip square-loop dual mode resonator inside a cavity that provides the third resonance [107]. The walls of the cavity were realized by periodic metal vias that connect the top and the bottom ground plane. The fabrication of such structure may not be easily done due to the via hole needed to generate the third mode.

This chapter is divided into two parts, the first part of the chapter is introducing a simple microstrip triple-mode resonator, some parametric study is also done. The resonator is used for designing third order quasi-elliptic bandpass filters. The second part of the chapter is introducing a dual-mode suspended stripline resonator, this resonator is used for bandpass filter design, where second and fourth order bandpass filter are designed.

5.1 Triple-Mode Microstrip Resonator

5.1.1 Resonator Topology

A pure microstrip triple-mode resonator is introduced in this section. The resonator is realized by adding an additional path to the traditional square-loop dual-mode

resonator. The additional path is realized by a meander half wavelength strip that is connected to two opposite corners of the square-loop resonator. Fig. 5.4 shows the layout of the triple-mode and dual-mode resonators coupled by perpendicular feeding lines, and perturbed from one corner by an outer patch. Fig. 5.4a shows a second

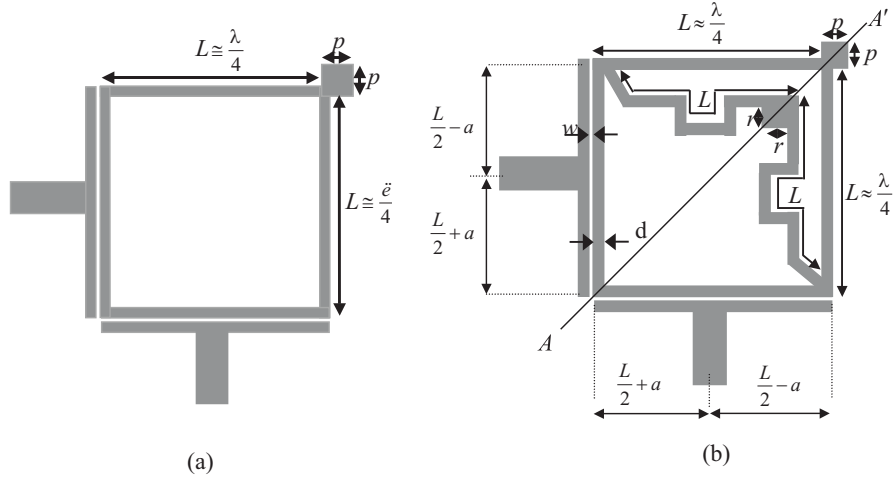


Figure 5.4: Layout of a microstrip (a) dual-mode resonator, (b) triple-mode resonator coupled by perpendicular feeding lines and perturbed by outer patch.

order bandpass filter which consists of a square-loop dual-mode resonator [10]. It consists of four identical arms of length L . To couple the two modes, a small square is attached to the corner of the loop. The structure is coupled to the input and output ports by two perpendicular lines. The fundamental resonances occur when L is approximately equal to a quarter of a wavelength. The position and geometry of the corner patch determine the nature of the coupling between the two modes [108].

A microstrip triple-mode resonator is created by adding an additional path to the square-loop dual-mode resonator shown in Fig. 5.4a. This path is realized by etching a meander stripline that is connected to two opposite corners of the main resonator. The length of this stripline is one half of a wavelength. Fig. 5.4b shows the layout of the resulting structure. The resonator resonates when the length of the arms is equal to one quarter of a wavelength. This additional line is again loaded by a square patch as a perturbation element with edges of length r .

5.1.2 Modes and Perturbations p , r

In the case of dual-mode resonators, the resonances are generated by a single even mode and one odd mode. In the case of triple-mode resonator (see Fig. 5.4b) we have two even mode and one odd mode. To justify that, we have placed a perfect magnetic wall at the symmetry plane ($A - A'$), i.e. the symmetry plane acts as an open circuit. Fig. 5.5 shows the reflection coefficient of the un-perturbed resonator.

It is obvious that there are two resonances at 5.12 GHz, and 5.28 GHz, which gives an indication that this resonator has two even mode resonances.

For the odd mode calculation, a perfect electric wall was placed at the symmetry plane ($A - A'$), now the symmetry plane operates as short circuit. Fig. 5.6 shows the reflection coefficient of the shorted un-perturbed resonator. From the Figure, it can be clearly seen that the resonator has a single mode resonance at 4.95 GHz.

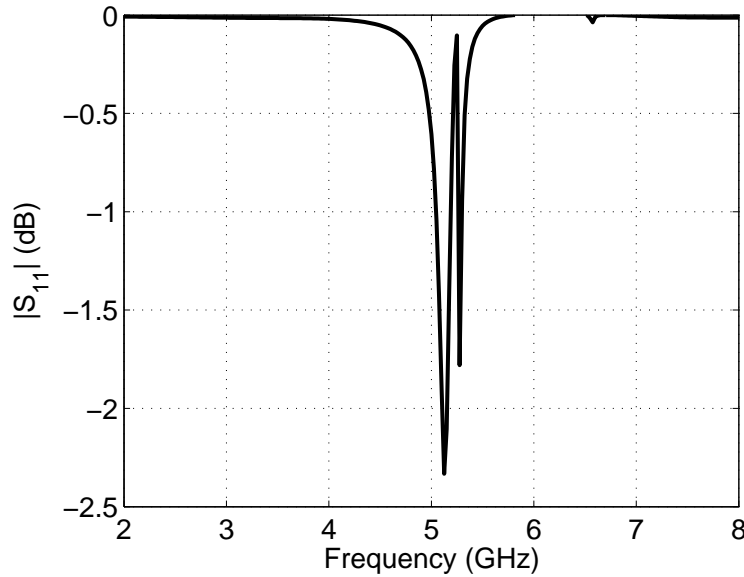


Figure 5.5: Reflection coefficient of un-perturbed resonator using perfect magnetic wall at the symmetry plane.

For un-perturbed resonator coupled to two perpendicular feeding lines, the filter response shows two un-split mode resonances, while the third mode resonance is located on a different frequency band, furthermore, the filter is not well matched by using un-perturbed resonator. Fig. 5.7 shows the reflection coefficient of the un-perturbed resonator fed by two perpendicular feeding lines.

In order to split the modes, two square patches are attached to two corners of the triple-mode resonator, (see 5.4b), the dimensions of the resonator chosen for the analysis are as the following, the length of each arm of the resonator $L = 10$ mm, and the width of the arm strips are $d = 0.3$ mm. Fig. 5.8 shows the dependence of mode resonances on the perturbation elements on p , where p is the length of the square patch that is located at the outer side of the resonator, while keeping $r = 0$ mm, where r is the length of the inner square patch. From the figure it is clearly seen that the resonance mode f_{03} is not affected by the perturbation element p , while the modes f_{01} , f_{02} start splitting when the dimension $p > 0.2$ mm.

Keeping the perturbation element un-presented ($p = 0$), and increasing the dimensions of the inner perturbation element r , see Fig.5.4b, the third-mode resonant frequency f_{03} decreases, while the other two modes remain un-split. When the

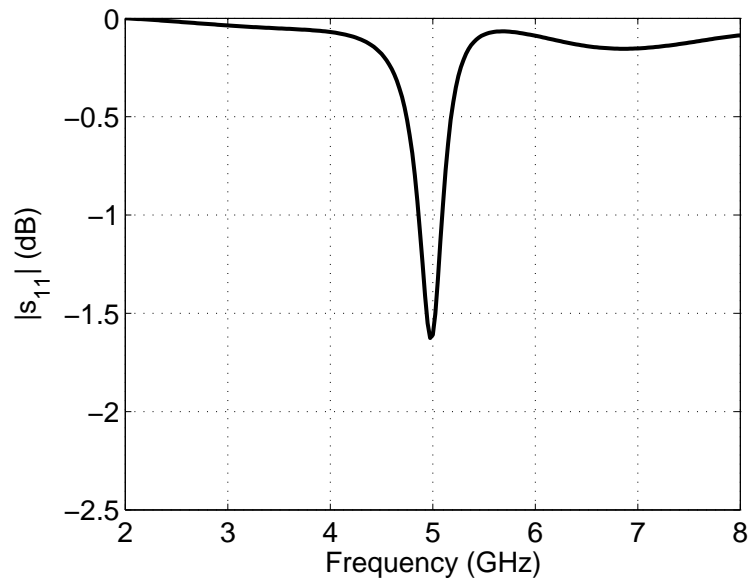


Figure 5.6: Reflection coefficient of un-perturbed resonator using perfect electric wall at the symmetry plane.

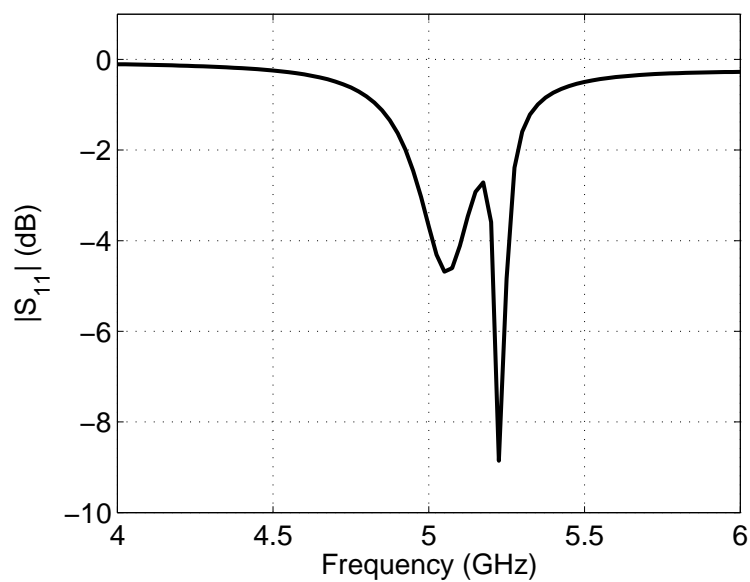


Figure 5.7: Reflection coefficient of un-perturbed resonator fed by two perpendicular feeding lines.

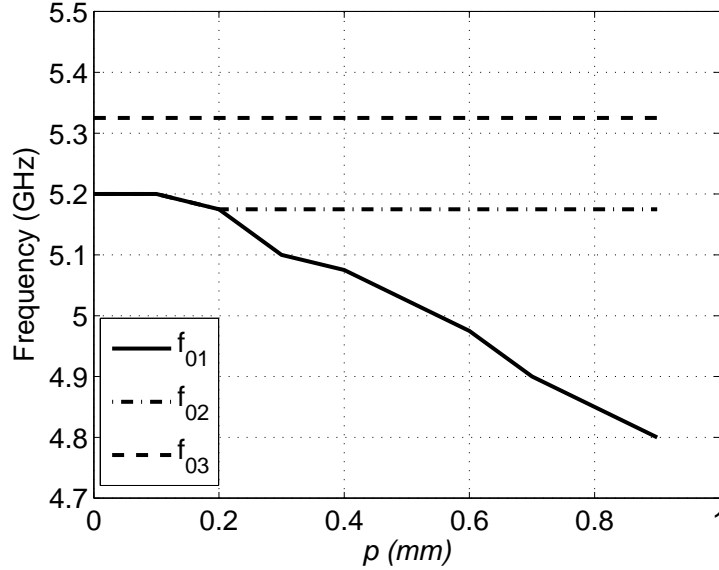


Figure 5.8: Relation between the size of the perturbation element p and the triple-mode resonance frequencies, perturbation r is not presented ($r=0$).

dimension $r > 0.7$ mm, all the modes share the same resonant frequency. Fig.5.9 shows the relation between the resonant frequencies and the size of the perturbation element r .

5.1.3 Triple-Mode Resonator and Filter Realization

Based on the above information, a third order bandpass filter has been designed. The dimensions of the filter were chosen as follows, $L = 10$ mm, $d = 0.3$ mm, $p = 0.9$ mm, $r = 0.2$ mm, the spacing between the resonator and the stubs that are connected to the feed lines is 0.2 mm. The filter has bandwidth of 0.3 GHz and centre frequency about 5.06 GHz. The coupling coefficient between the modes should be computed according to the theory of the coupled asynchronously tuned resonators as [2]

$$k_{nm} = \left(\frac{f_{sm}}{f_{sn}} + \frac{f_{sn}}{f_{sm}} \right) \sqrt{\left(\frac{f_{om}^2 - f_{on}^2}{f_{om}^2 + f_{on}^2} \right)^2 - \left(\frac{f_{sm}^2 - f_{sn}^2}{f_{sm}^2 + f_{sn}^2} \right)^2} \quad (5.1)$$

where f_{sm} and f_{sn} are the self-resonant frequencies of the resonator and f_{om} , f_{on} are the mode splitting frequencies. From the simulated results, we denote that the self-resonant frequencies are equal to the mode splitting frequencies. That leads to $k=0$. Therefore, the filter has a transversal coupling scheme [109], This means that each resonator is coupled with the source and the load in addition to the coupling between the source and the load, Fig. 5.10 shows the transversal coupling scheme of the our third order filter. The used coupling matrix for this analysis is $(N + 2) \times (N + 2)$, which supports analysis of fully canonical filtering function, i.e. the number of the

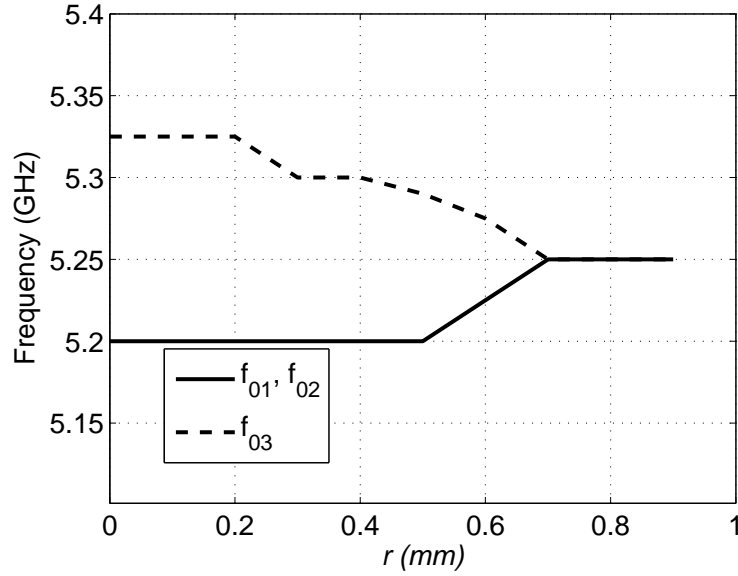


Figure 5.9: Relation between the size of the perturbation element r and the triple-mode resonance frequencies, perturbation p is not presented ($p=0$).

finite transmission zeros equal to the order of the filter.

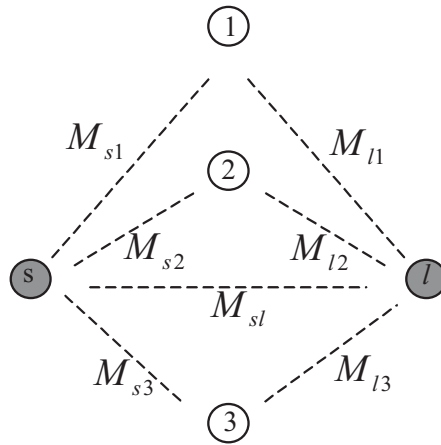


Figure 5.10: Coupling and routing scheme of the triple-mode filter.

The filtering function that characterizes the filter can be written as a rational function

$$F(\omega') = \frac{P(\omega')}{D(\omega')} \quad (5.2)$$

Where ω' is the low-pass prototype frequency related to the actual frequency ω by

$$\omega' = \frac{\omega_0}{\Delta\omega} \left(\frac{\omega}{\omega_0} - \frac{\omega_0}{\omega} \right) \quad (5.3)$$

The polynomial $P(\omega')$ is computed from a recursion method introduced in [110] which is given as

$$P_{N+1}(\omega') = -P_{N-1}(\omega') \left(1 - \frac{\omega'}{\omega'_N}\right)^2 \frac{\left(1 - \frac{1}{\omega'^2_{N+1}}\right)^{0.5}}{\left(1 - \frac{1}{\omega'^2_N}\right)^{0.5}} + P_N(\omega') \left[\omega' - \frac{1}{\omega'_{N+1}} + \left(\omega' - \frac{1}{\omega'_N}\right) \frac{\left(1 - \frac{1}{\omega'^2_{N+1}}\right)^{0.5}}{\left(1 - \frac{1}{\omega'^2_N}\right)^{0.5}}\right] \quad (5.4)$$

where ω'_N is the position of the pre-defined attenuation pole, $P_0(\omega') = 1$ and $P_1(\omega') = \omega' - \frac{1}{\omega'_1}$.

The Polynomial $D(\omega')$ can be given as

$$D(\omega') = \prod_{N=1}^K \left(1 - \left(\frac{\omega'}{\omega'_N}\right)\right), \quad (5.5)$$

where ω_N represents the N^{th} attenuation pole. The transmission coefficient can be expressed as

$$|S_{21}(\omega')|^2 = \frac{1}{1 + \epsilon^2 F^2(\omega')}, \quad (5.6)$$

where the parameter ϵ is a constant related to the passband return loss RL , it is expressed by the following formula

$$\epsilon = \left[10^{\frac{RL}{10}} - 1\right]^{-0.5} \quad (5.7)$$

The loop currents through the filter resonators can be grouped in a vector I and given by the following matrix form [111]

$$[-jR + \omega'W + M]I = AI = -jE, \quad (5.8)$$

where R is an $(N+2) \times (N+2)$ matrix with zeros entries except $R_{1,1} = R_{N+2,N+2} = 1$, W is an $(N+2) \times (N+2)$ diagonal matrix whose main diagonal elements are ones except $W_{1,1} = W_{N+2,N+2} = 0$, M is the normalized coupling matrix, and $E = [1, 0, \dots, 0]$ is the excitation vector. The transmission and reflection coefficients S_{11} and S_{21} are given by

$$S_{12} = -2j[A^{-1}]_{N+2,1} \quad (5.9)$$

$$S_{11} = 1 + 2j[A^{-1}]_{1,1} \quad (5.10)$$

The synthesis problem can be formulated as follows. Looking for the suitable coupling matrix M that minimizes a certain cost function C , so that the entries of the optimization function are the non-zero elements of the coupling matrix with initial guess. The cost function to be minimized can be expressed as

$$C = \sum_{i=1}^K |S_{11}(\omega'_{p_i})|^2 + \sum_{i=1}^H |S_{12}(\omega'_{tz_i})|^2 + \left(|S_{11}(\omega'_{\mp 1})| - \frac{\epsilon}{\sqrt{1+\epsilon^2}} \right)^2 \quad (5.11)$$

where p_i , tz_i , and H are the positions of the poles (roots of $P(\omega')$), the positions of the attenuation poles, and the number of the attenuation poles, respectively. The flow chart shown in Fig. 5.11 explains the optimization procedure used to synthesize the filter response. The scheme starts by an initial guess of the coupling coefficients, then calculates the matrices $[A]$ and $[A]^{-1}$ at the roots of the polynomials $P(\omega')$ and $P(\omega)$. After that the const function is calculated and checked whether it satisfies a predefined value, if not the scheme changes the initial values and calculates C again until achieving the satisfied value.

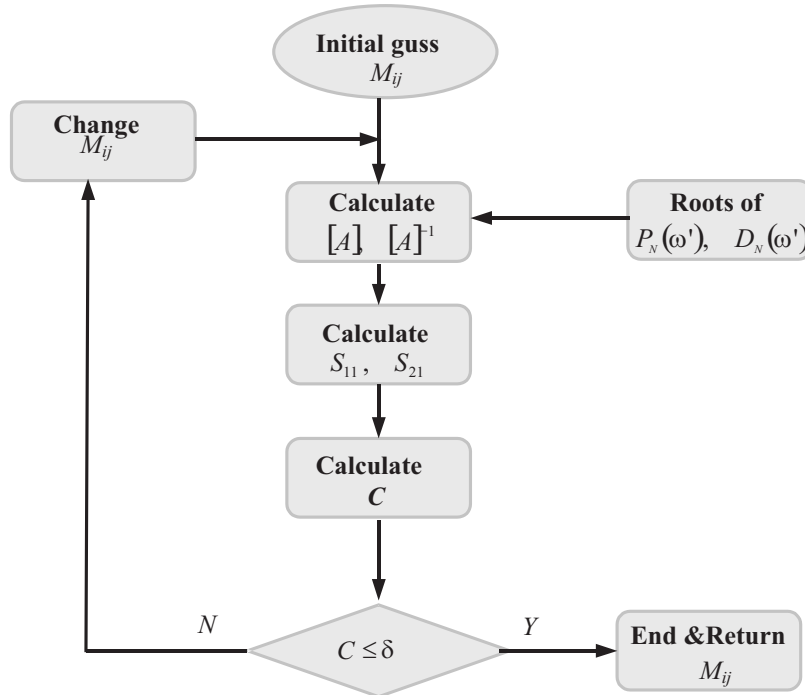


Figure 5.11: flow chart of the used optimization method.

Due to the symmetry of the structure its modes exhibit either a magnetic wall or an electric wall along the main diagonal. It is important to keep in mind that these modes are determined with reference planes placed right at the coupling stubs at the input and output. Under the lossless assumption, these modes are not coupled to each other but are all coupled to the input and the output. Higher order modes, including surface modes, contribute to a small direct coupling between the input and the output. A narrowband equivalent circuit based on this coupling scheme is shown in Fig. 5.10, which is a transversal coupling matrix [105]. The narrowband response of this filter is, therefore, described by a coupling matrix of the form

$$M = \begin{pmatrix} 0 & M_{s1} & M_{s2} & M_{s3} & M_{sl} \\ M_{s1} & M_{l1} & 0 & 0 & M_{l1} \\ M_{s2} & 0 & M_{22} & 0 & M_{l2} \\ M_{s3} & 0 & 0 & M_{33} & M_{l3} \\ M_{sl} & M_{l1} & M_{l2} & M_{l3} & 0 \end{pmatrix} \quad (5.12)$$

Since there are two even modes and one odd mode in this third order structure with a symmetry plane along the main diagonal. At the coupling matrix level, this implies that one of the coupling coefficients to the ports is negative. This is taken as the third resonance leading to the choice

$$M_{s1} = M_{l1}, \quad M_{s2} = M_{l2}, \quad M_{s3} = -M_{l3} \quad (5.13)$$

The filter response is compared with a third order chebyshev response. However, a disagreement between EM and the synthesized filter indicates that complex attenuation poles exist at the upper stopband. Therefore a filter has been synthesized as transversal, assuming two attenuation poles on the real axis of the s-plane addition to one transmission zero located at the lower stopband, which is laying on the imaginary axis of the s-plane. For given specifications, the entries of the coupling matrix can be extracted analytically by following the presentation in [109]. For example, for a third order filter with an in-band return loss of 20 dB, one attenuation pole at $s=-6.471j$ and a pair of complex transmission zeros at $s=\pm 2.25$, we get the following coupling matrix

$$M = \begin{pmatrix} 0.0000 & 0.6441 & -0.5648 & 0.7152 & -0.0307 \\ 0.64411 & -1.4992 & 0.0000 & 0.0000 & 0.64411 \\ -0.5648 & 0.0000 & 1.4756 & 0.0000 & -0.5648 \\ 0.7152 & 0.0000 & 0.0000 & 0.1061 & -0.7152 \\ -0.0307 & 0.7152 & -0.5648 & -0.7152 & 0.0000 \end{pmatrix}$$

A filter was designed to implement this coupling matrix. Its response is shown in Fig. 5.12 along with that of this coupling matrix. Good agreement is achieved between The EM simulation and the coupling matrix synthesized results .

Changes to the dimensions of perturbation elements p and r lead to changes in the positions of the transmission zeros. These zeros can even be migrated in the complex plane from the real axis to the imaginary axis, and vice versa [3], and [108]. The positions of the transmission zeros can also be controlled by adjusting the electrical length between the I/O feeding lines [103], [112]. Fig. 5.13 shows the insertion loss of the filter with different feed line positions a , where a is the distance between the feeding lines and the centre of the resonator arms, as shown in Fig. 5.4b. As can be clearly seen, with the I/O feeding lines connected at the centre of the feeding stub $a = 0$, the transmission zeros at the higher stopband disappear (i.e., the transmission zeros are located on the real axis of the complex s-plane), and the attenuation pole that is in the lower stopband is located at $s = -6.346j$. By increasing a , see Fig. 5.4b,

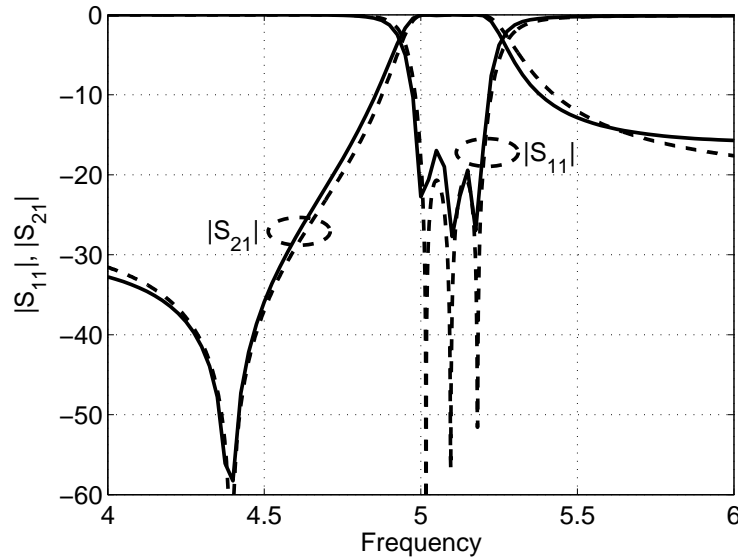


Figure 5.12: EM simulation (solid) synthesized (dashed) reflection and transmission coefficients of a triple-mode bandpass filter.

the positions of the transmission zeros are moved, and are possibly transferred on to the imaginary axis of the complex s -plane.

A triple-mode filter with the feed line located at $a=1.35$ mm was designed as shown in the previous section. It has a centre frequency of 5.06 GHz, a bandwidth of 220 MHz, and three attenuation poles at $s = -1.497j$, $3.317j$, and $7.86j$, respectively. The resulting coupling matrix of the coupling scheme shown in Fig. 5.10 is

$$M = \begin{pmatrix} 0.0000 & 0.4820 & -0.3377 & -0.7599 & -0.0235 \\ 0.4820 & -1.2827 & 0.0000 & 0.0000 & 0.4820 \\ -0.3377 & 0.0000 & 1.2083 & 0.0000 & -0.3377 \\ -0.7599 & 0.0000 & 0.0000 & 0.2281 & 0.7599 \\ -0.0235 & 0.3377 & -0.3377 & 0.7599 & 0.0000 \end{pmatrix}$$

The filter response based on this coupling matrix and compared with the EM simulation is shown in Fig.5.14. Good agreement between the two results is achieved, except at the stopbands, as the coupling matrix can only be applied in a narrowband range.

5.1.4 Broadband Equivalent Circuit

The coupling matrix describes the filter behavior properly only in the close vicinity of the passband, see Fig. 5.14. Consequently, some design tools working in a wider frequency band are required. For this purpose, an equivalent circuit has been found as a very effective way to analyze the filter. This circuit is shown in Fig. 5.15. It is simply derived from the filter layout in Fig. 5.4b. This equivalent circuit is based on

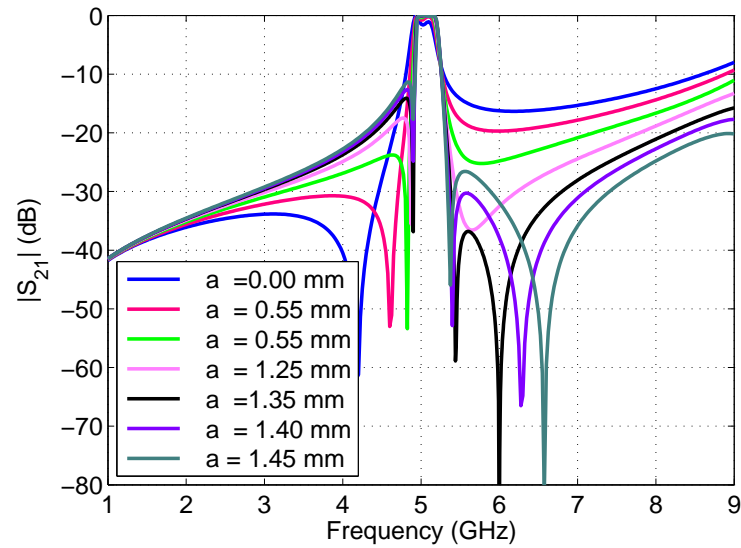


Figure 5.13: Transmission coefficient of a triple-mode bandpass filter with various a values.

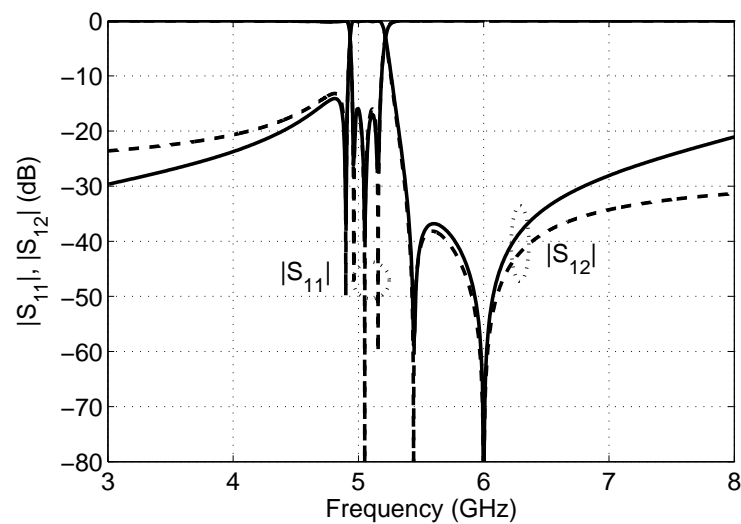


Figure 5.14: EM simulation (solid) synthesized (dashed) reflection and transmission coefficients of triple-mode bandpass filter with three transmission zeros.

the representation of the microstrip line. The effective dielectric constant ε_{eff} , and the characteristic impedance of this line is well defined in (2.84), (2.85).

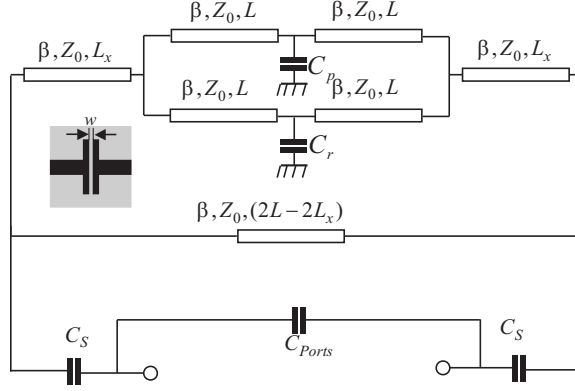


Figure 5.15: Broadband equivalent circuit of the triple- mode microstrip filter. The inset shows the circuit used to determine C_s .

Having calculated ε_{eff} and Z_c , the electrical length of each transmission line can easily be calculated by

$$\Theta = L\beta \quad (5.14)$$

where L is the physical transmission line length and β is the propagation constant, which is defined as

$$\beta = \frac{2\pi}{\lambda_g} \quad (5.15)$$

where

$$\lambda_g = \frac{\lambda}{\sqrt{\varepsilon_{eff}}} \quad (5.16)$$

For our filter, which has dimensions $L=10$ mm and $L_x = 3.4$ mm, where $L_x = L - a$, we obtained $\theta = 90^\circ$, 29° , respectively. The capacitances of the perturbation elements can be approximated as in [3]

$$C_i = \sqrt{2}C_0, \quad i = p, r \quad (5.17)$$

where

$$C_0 = \varepsilon_0 \varepsilon_r \frac{A_i}{h}, \quad i = p, r \quad (5.18)$$

where A_i is the area of the perturbation elements, h is the thickness of the substrate, ε_r is the relative dielectric constant of the substrate, and ε_0 is the free-space dielectric constant.

Capacitance C_S that is between the resonator and the stubs connected to the feeding lines was determined by calculating the capacitance between the feeding line terminated by the stub and its mirror image, as shown in the inset of Fig. 5.15.

Capacitance C_{Ports} representing the direct coupling between the filter ports cannot be simply and directly determined. Fig. 5.16 shows the transmission characteristics of the equivalent circuit from Fig. 5.15 calculated for selected values of C_{Ports} , this calculation has been done using a circuit simulator [113]. This capacitance is finally determined by fitting these results to the characteristic obtained by the EM simulation. The final fit using $C_{Ports} = 0.01$ pF is shown in Fig. 5.17.

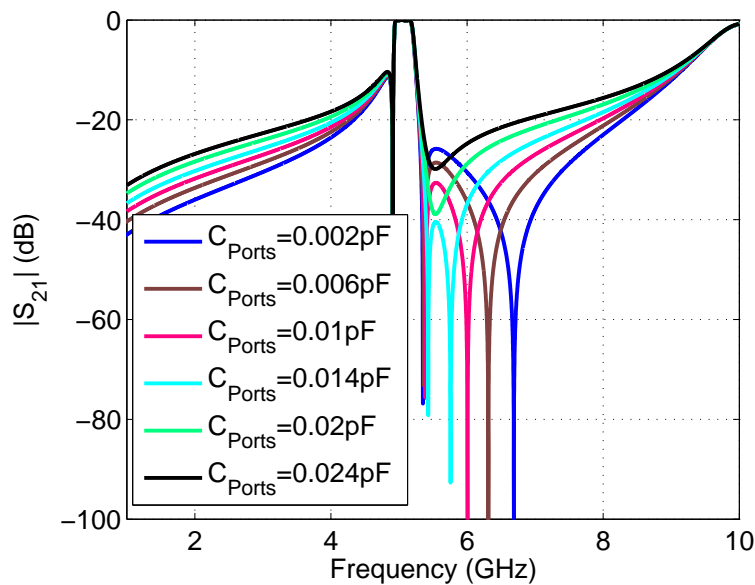


Figure 5.16: Transmission coefficient of the Broad-band equivalent circuit for different values of C_{Ports} .

5.1.5 Experimental Results

The two triple-mode filters were designed using the proposed resonator. The first filter has dimensions of $L = 10$ mm, $d = 0.3$ mm, $p = 0.9$ mm, $r = 0.2$ mm, and the spacing between the resonator and the stubs connected to the feed lines is $w = 0.2$ mm. This filter has one transmission zero in its lower stop band and two complex attenuation poles. A photograph of the fabricated structure is shown in Fig. 5.18. The simulated and measured return and insertion loss of the filter are shown in Fig. 5.19. There is good agreement between the two results, apart from a small shift at the lower cut-off frequency. The maximum return loss at the pass band is about 11 dB, which can be attributed to fabrication errors. The insertion loss at the passband is better than 2.9 dB; this relatively high magnitude of the insertion loss corresponds

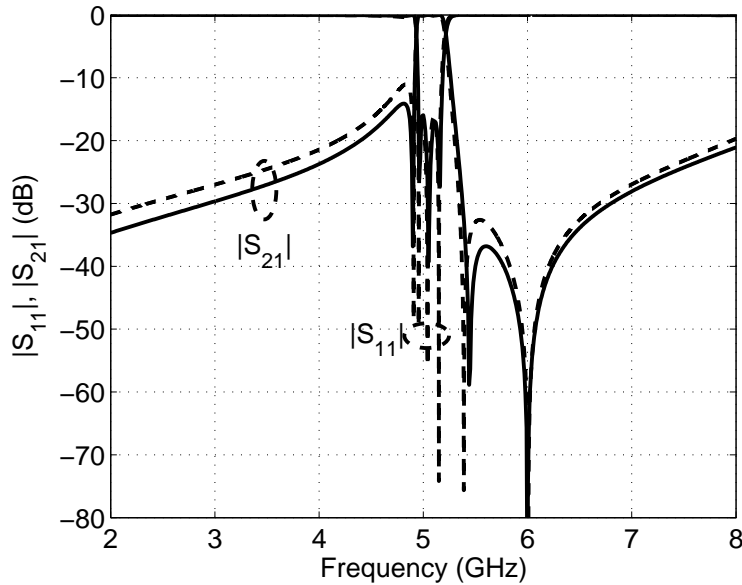


Figure 5.17: EM simulation (solid) and equivalent circuit simulation (dashed) when $C_{Ports}=0.01$ pF.

to the high return loss at the passband. The group delay variation in the passband is smaller than 0.51 ns.

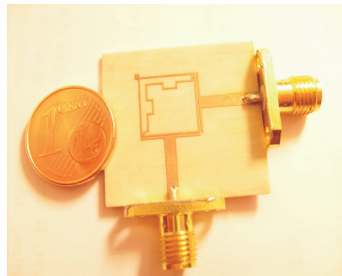


Figure 5.18: Photograph of a third order bandpass filter using the proposed triple-mode resonator.

The second filter is designed to have the same resonator dimensions; the only change concerns the locations of the feeding lines. The feeding lines are located off-center at $a=1.35$ mm, see Fig. 5.4b. The filter has three transmission zeros, one in the lower stopband, and two in its upper stopband. Fig. 5.20 shows the simulated and measured insertion and return loss of the filter. The two transmission zeros in the upper stopband considerably improve the filter behavior in this stopband, in comparison with the characteristics of the first filter version. The in-band insertion loss is better than 2.3 dB. The group delay variation in the passband is smaller than 1.5 ns.

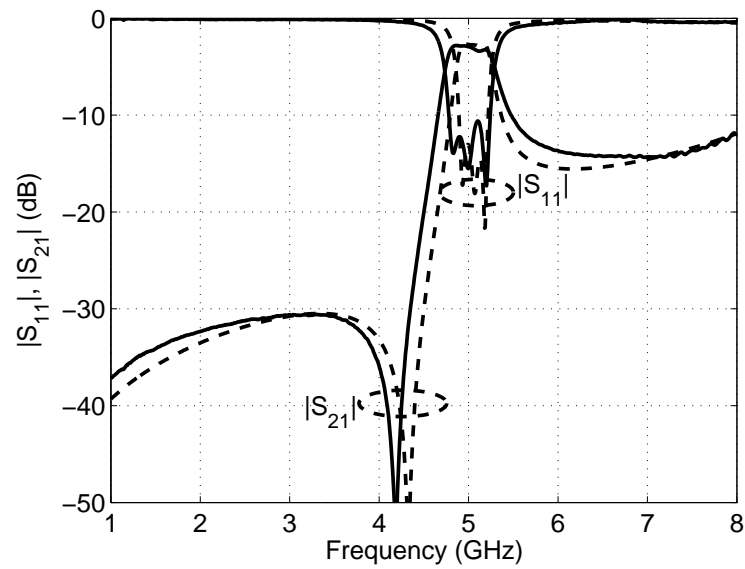


Figure 5.19: Simulated(dashed) and measured (solid) insertion and return loss of trip-mode bandpass filter with one transmission zero.

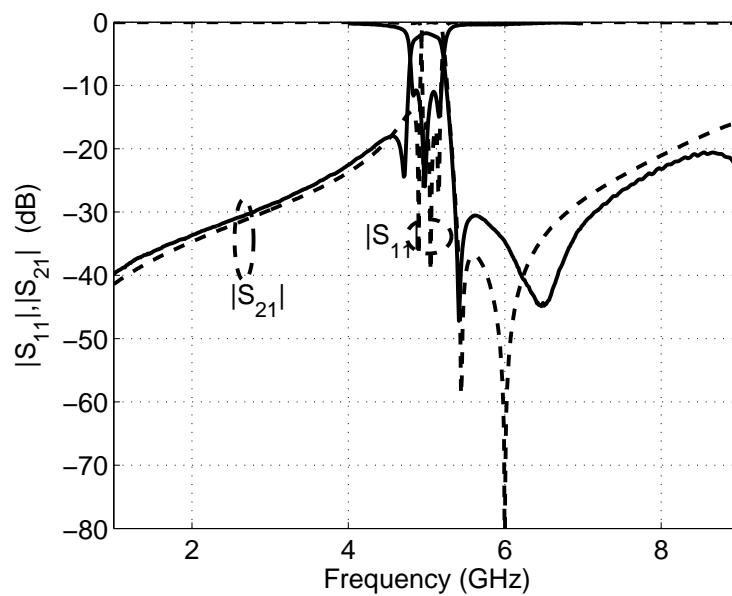


Figure 5.20: Simulated(dashed) and measured (solid) insertion and return loss of trip-mode bandpass filter with three transmission zeroes .

5.2 Dual-Mode Suspended Stripline Filters

Dual-mode resonators have not been introduced for suspended stripline technique with their classical structure. Since they require increasing the cross section of suspended stripline, that will increase the size of the overall filter structure. Due to the large cross-section, the waveguide mode may not allow a wide stopband. Up to now, the filters designed using suspended stripline are done using either the folded transmission lines, or by using quasi-lumped elements.

In this section a dual-mode suspended stripline resonator is introduced. The resonator is realized by combining quasi-lumped suspended stripline parallel resonator with open-loop resonator. These two resonators were chosen to be combined with each other because they have nearly the same size at the corresponding resonance frequency. A second order, and two fourth order filters are realized using this resonator. The realized filters are very compact compared to those realized by quasi-lumped resonators.

5.2.1 Quasi-Lumped Parallel Resonator

The parallel resonator has been introduced first in [114]. The resonator consists of a narrow strip connected to the side wall of the metal housing and patch at the other end, see Fig. 5.21a. The narrow stripline represents a shunt inductance, while the coupling between the patch and the walls of the mount represents a shunt capacitance, see Fig. 5.21b. The resonance frequency of the resonator can be controlled either by changing the length of the narrow stripline, or by changing its width. The other parameter that plays a role in controlling the resonance frequency of the resonator is the spacing between the patch and the housing mount. Locating the narrow stripline on the same side induces an additional inductive coupling between the two resonators, which in turn, introduces a transmission zero to the filter response [115]. The position of the transmission zero can be easily adjusted by increasing or decreasing the distance between these strips. Different filter types, broadband bandpass filters, ultra-wideband bandpass filters, and high-pass filters have been designed using this resonator. [24], [90], and [115].

5.2.2 Open-Loop Resonator

Open-loop resonator also known in the literature as split-ring resonator. This resonator resonates when the length of the resonator corresponds to $\lambda/2$ [2], [4], and [116–118]. The open end of resonator provides a capacitive coupling in parallel to the main path that provides a transmission zero at the higher stopband [116]. Due to the fact that the electric field at the open sides of the open-loop resonator is maximum at the resonance frequency of the resonator, and the magnetic field is maximum at the center of the resonator ; the coupling nature between two open-loop depends on the

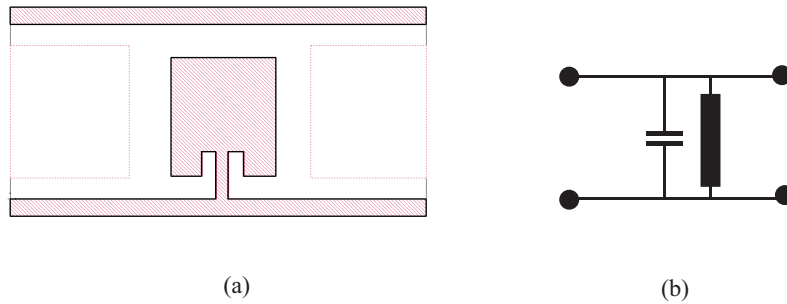


Figure 5.21: (a) Layout of suspended stripline quasi-lumped resonator, (b) equivalent circuit of the suspended stripline resonator .

neighboring sides [4]. Thus, by having the resonators coupled from the open-ends, capacitive coupling is generated, see Fig. 5.22a, while having the resonators coupled from the opposite sides, an inductive coupling is generated, see Fig. 5.22b. To generate a mixed coupling between the resonators, the resonators can be built keeping open ends on one side, or by keeping the open ends antipodal, see Fig. 5.22c and Fig. 5.22d. Size reduction has been already done by extending the loop in idle area inside the resonator itself and by increasing the capacitive coupling between the open ends [8]. The open-loop resonator can be easily realized using suspended stripline technique, see Fig.5.23

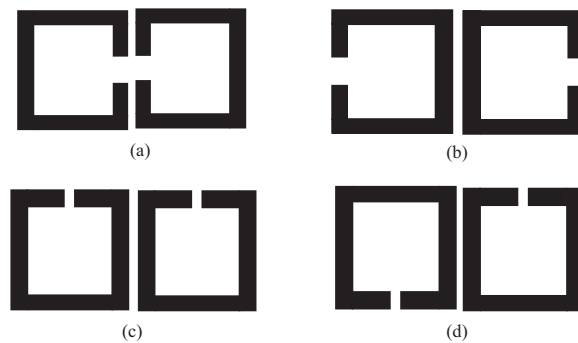


Figure 5.22: Coupling structures for microstrip open-loop resonator (a) capacitive coupling structure, (b) inductive coupling structure, (c) mixed coupling structure, (d) mixed coupling structure [4].

5.2.3 Resonators Combination

Combining both quasi-lumped resonator with open-loop, an SSL dual mode resonator can be realized. The new resonator is realized by adding a narrow stripline to the open-loop resonator, as shown in Fig. 5.24. Using this configuration, the quasi-lumped resonance in addition to the open-loop resonant mode is generated. Fig 5.25

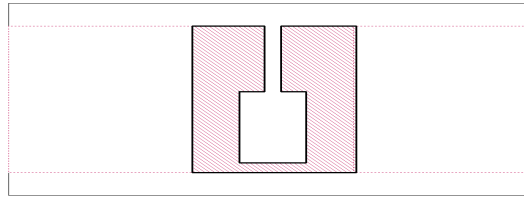


Figure 5.23: Suspended stripline open-loop resonator.

shows the return loss of the new resonator capacitively coupled to the feeding lines in comparison with return loss of the open-loop resonator. Controlling the resonant frequencies of the resonators must be done in such a way that it does not affect the size or the shape of the resonator, because this will affect both resonances, which makes it difficult to adjust the center frequency of the filter, and increases the difficulties in achieving a good matching at the passband of the filter.

The parameters that control the resonance frequencies are:

1. The width of the narrow stripline w , see Fig. 5.24, which affects only the quasi-lumped resonance without main change of the open-loop resonance, so by increasing w , the inductive value of the stripline is decreased, that will shift the quasi-lumped resonance to a higher frequency band, and vice versa.
2. The other parameters that mainly affect the open-loop resonance are, the spacing between the open ends of the resonator s , and the width of the open ends x , see Fig. 5.24. Decreasing s decreases the capacitive coupling between the open ends of the resonator, which shifts the open-loop mode to a higher frequency, and vice versa. On the other hand, increasing x increases the capacitive value between the open ends which shifts the open-loop mode to lower frequency band.

An easy way to design a filter using this resonator is to design two filters on the same frequency band. The first one by quasi-lumped resonator, and the second by open-loop. The size of the two resonators must be kept the same, in other words, the size of the patch must be equal to the outer frame of the open-loop resonator.

Coupling between the two modes of the dual-mode resonator is the next step. For this resonator the modes can be coupled by two ways. The first one is realized by increasing external coupling, this can be easily done using suspended stripline, since overlapping between the metallization on both sides of the substrate is allowed. A second order bandpass filter has been designed by using one resonator on the backside of the substrate coupled tightly with feeding lines that built on the topside of the substrate, the cross section of the transmission line used for this filter is shown in

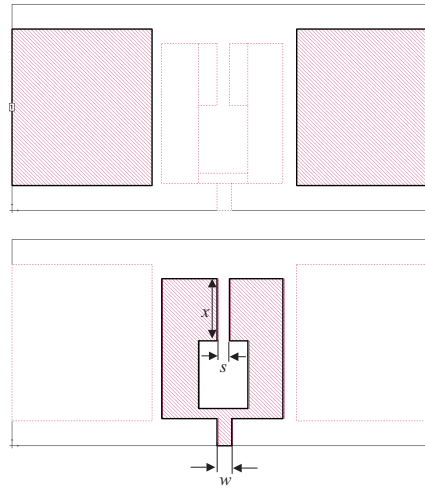


Figure 5.24: Suspended stripline open-loop resonator.

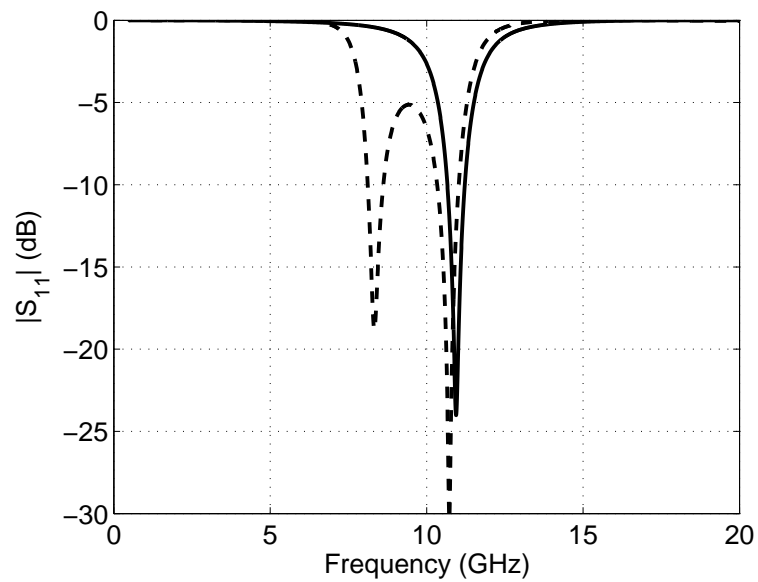


Figure 5.25: Simulated return loss of the dual-mode resonator (dashed) in comparison with the return loss of the open-loop (solid).

Fig.3.31. Fig. 5.26 shows a 3D view of the filter, while Fig. 5.27 shows the simulated insertion and return loss of the filter.

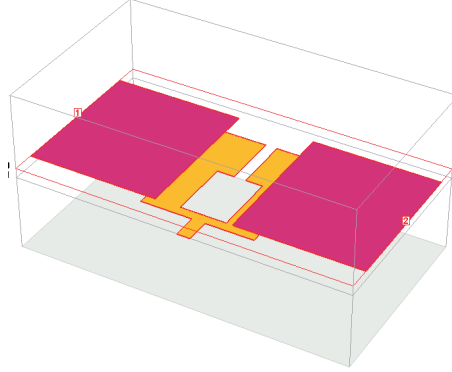


Figure 5.26: 3D view of a second order bandpass filter using SSL dual-mode resonator intensively coupled with the feeding lines.

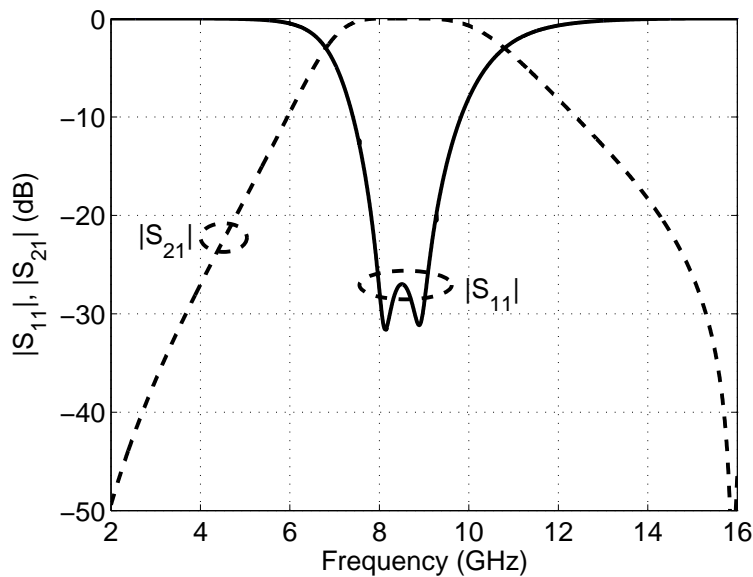


Figure 5.27: Simulated insertion and return loss of a second order bandpass filter using SSL dual-mode resonator intensively coupled with the feeding lines.

The second parameter that increases the coupling between the resonator modes is the position of the narrow stripline. Having asymmetry of the inductive strip, the modes of the resonators will be coupled and matched better than implementing the inductive strip at the center of the resonator. This principle is used to the design of a fourth order bandpass filter. Two coupled SSL dual-mode resonators have been implemented on the backside of the substrate. Each of these resonators is coupled to the neighboring port, which is implemented on the topside of the substrate. The parallel inductive strips are located on different sides of the substrate to avoid any

inductive coupling between both resonators (see [24], [115]). Fig. 5.28 shows a 3D view of the fourth order bandpass filter structure, the filter has a length of 7.25 mm, which is much smaller than the fourth order that is designed using quasi-lumped elements, see [24]. Fig. 5.29 shows the simulated return and insertion losses of the filter. The four return-loss poles can be observed clearly. In addition, a transmission zero occurs at about 14 GHz. This occurs due to the slot that is in parallel to the narrow stripline at the other side of the resonator. The filter has a bandwidth of about 2 GHz, and a center frequency of 10.8 GHz.

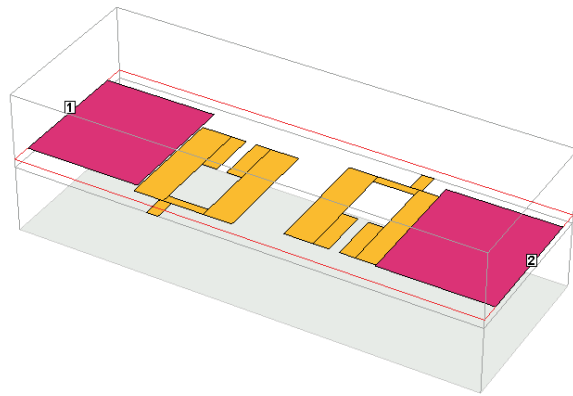


Figure 5.28: 3D view of fourth order bandpass filter using two dual-mode resonators.

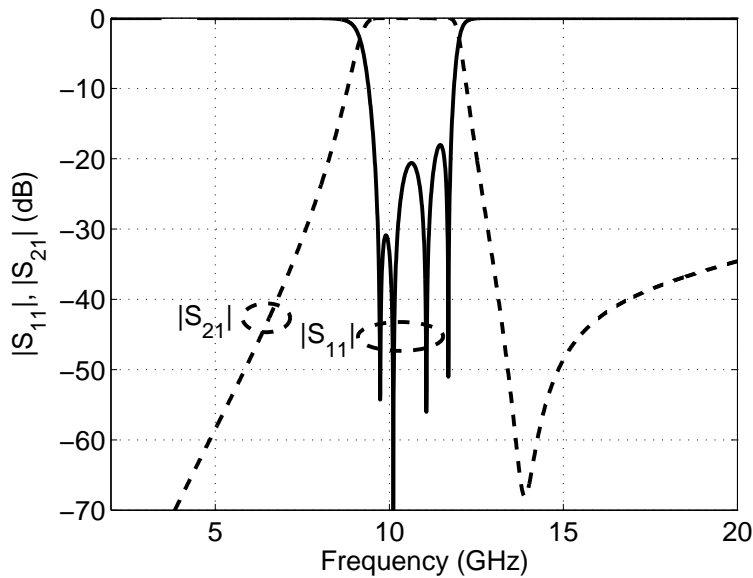


Figure 5.29: Simulated insertion and return loss of a fourth order bandpass filter using SSL dual-mode resonator.

As it has been already demonstrated in [24], [115], locating the parallel inductive strips of two resonators on the same side of the substrate, introduces an inductive

coupling in parallel to the original capacitive coupling. This causes an additional transmission zero. The same principle has been transferred to our design. An additional transmission zero has been introduced below the passband. The transmission zero which was introduced in the last structure is splitted now into two zeroes. Fig. 5.30 shows the simulated filter structure, while Fig. 5.31 shows a photograph of the measured structure, the filter is 6.45 mm in length, Fig.5.32 shows the simulated and the measured return and insertion losses of this filter. The general behavior of the insertion loss is well met. A slight frequency shift is due to the increased resonator inductance caused by a groove in the mount clamping the substrate. The maximum return loss is about 9 dB. This is due to fabrication errors, combined with the relatively high sensitivity of this type of filters. The measured insertion loss is smaller than 1.8 dB where most of this is caused by the problem in the return loss.

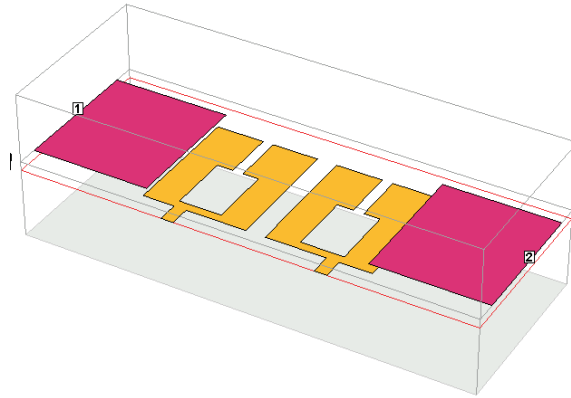


Figure 5.30: 3D sketch of a fourth order SSL bandpass filter using two dual-mode resonators with parallel inductive strips on one side.

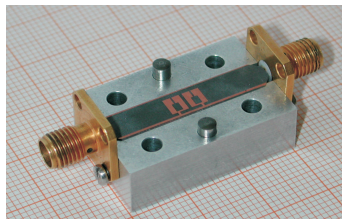


Figure 5.31: Photograph of fourth order bandpass filter structure.

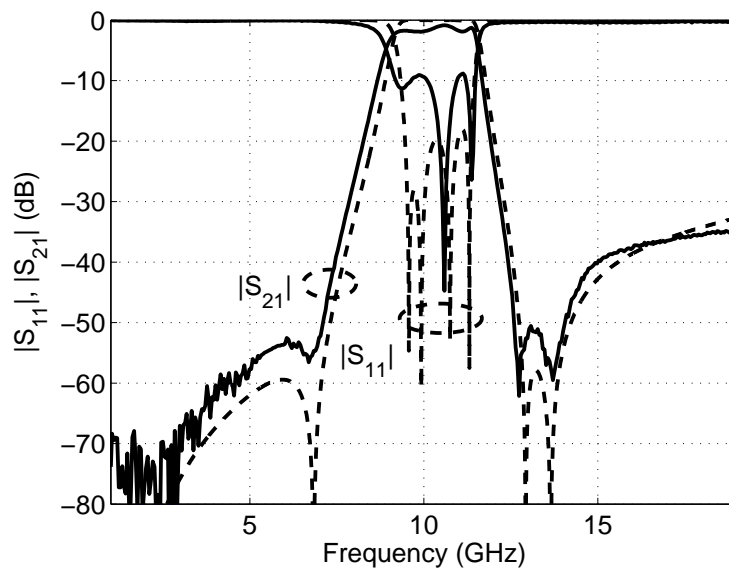


Figure 5.32: Measured (solid) and simulated (dashed) return and insertion losses of the fourth order bandpass filter with additional transmission zero.

Chapter 6

Dual-Band Bandpass Filters Using Dual-Mode Resonator

Dual-band filters have gained much interest in the recent years. Different filter approaches have been introduced during the last ten years to meet the demand of the modern wireless communication systems e.g., [46–52] and [119–125]. The classical dual-band bandpass filter approach has been achieved by connecting two individual bandpass filters with each other in parallel. However, such approach needs additional matching network that increases the size of the overall filter structure [46], [123] and [124]. Another approach using the dual-band stubs [47], however, due to the inductive coupling between these stubs, the filter has also transmission at low frequency, and attenuating lowpass band has not been reported so far. In [52] and [119–121], dual-band filter structures have been introduced using stepped impedance resonator (SIR), but due to the long transmission line sections used in this class of filters, the filter response does not have wide upper stopband. In addition, high losses are introduced to the filter response. Dual-band filter has been also achieved by using dual-mode resonators. In [125] a CPW dual-band filter has been designed by using two dual-mode resonators each of the resonators resonates at different frequency band. The resonators have been built using back-to-back microstrip ring resonator, this filter has a main advantage, which is the center frequency of each band is independent on the other. Moreover, the filter has been modified by building the smaller resonator inside the bigger one, by this configuration the filter has smaller volume. However, realizing this structure in microstrip technology requires to have cuts at the feeding line sides and to let the feeding lines pass the dual-mode resonators under air bridges [122]. By this configuration the coupling between the resonators and the feed lines can be easily controlled, however, this will increase the fabrication cost and the fabrication tolerance.

In this chapter, two simple, low-loss dual-band bandpass filters using the dual-mode resonators are proposed. The first filter is a microstrip one, and it is design by introducing transmission zeros inside the passband of broadband bandpass filter using

dual-mode resonator. The second one is a suspended stripline filter, it is realized by splitting the modes of the dual-mode resonator into two bands.

6.1 Dual-Band Microstrip Filter

6.1.1 Filter Topology

Broadband bandpass filter using square loop is shown in Fig. 6.1. It is basically a form of multiple-mode resonator, which is coupled capacitively with input/output ports [11]-[13]. The resonator consists of a square-loop dual-mode resonator with a length of l_D instead of the low-impedance transmission line section, connected from both sides high transmission lines with the length of l_T . These transmission lines are coupled from the other side capacitively to two transmission lines having the same length and connected to the input/output ports from the other side. Fig. 6.2 shows the insertion loss of the filter.

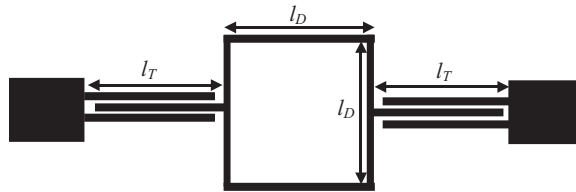


Figure 6.1: Layout of the broadband bandpass filter using multiple-mode resonator with a square-loop dual-mode resonator at the center of the filter.

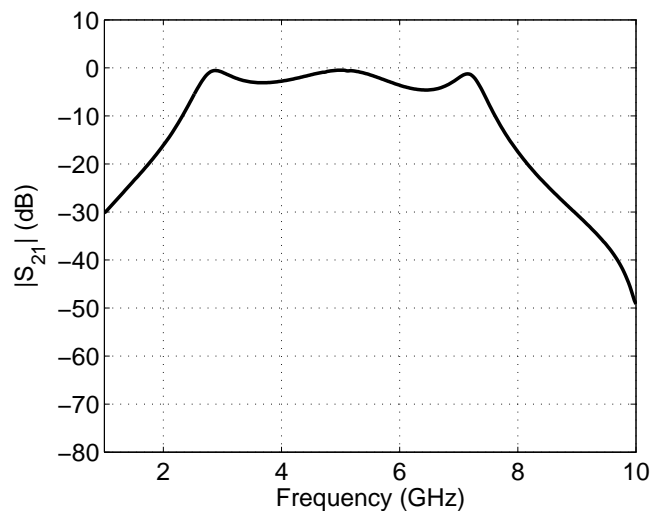


Figure 6.2: Insertion loss of the broadband bandpass filter with $l_D = l_T = 10$ mm.

Rotating one of the high impedance transmission line sections with one of the feeding lines 90° , as shown in Fig. 6.3, two transmission zeros are introduced in the

passband of the broadband bandpass filter. These two transmission zeros are splitting the passband of the filter into two passbands. Fig. 6.4 shows the insertion loss of the dual-band bandpass filter using dual-mode resonator. In case l_D is equal to l_T then the bandwidth of both bands is equal, since the transmission zeros are introduced in the middle of the passband of the original broadband filter.

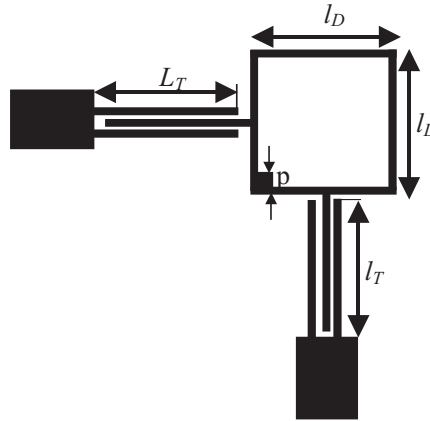


Figure 6.3: Layout of the dual-band bandpass filter using multiple-mode resonator with a square-loop dual-mode resonator at the center of the filter.

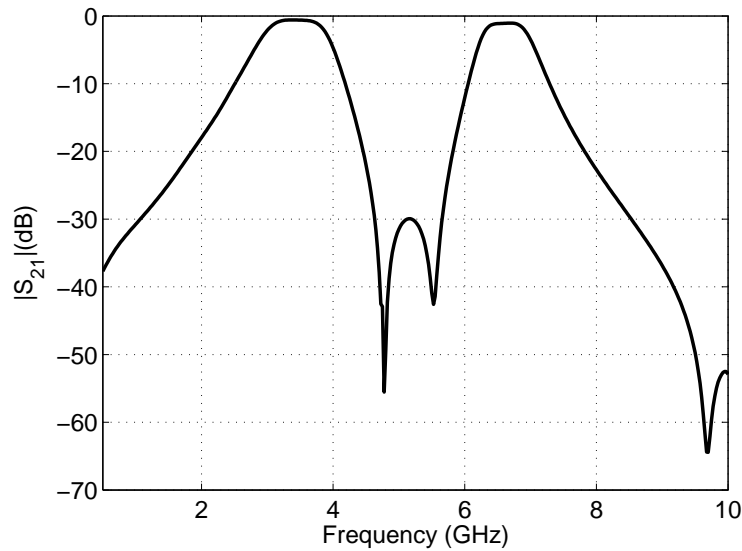


Figure 6.4: Insertion loss on dual-band bandpass filter with dimensions $l_D = l_T = 10$ mm, the width of all transmission lines is 0.3 mm.

6.1.2 Center Frequency and Bandwidth Control

The center frequencies of the filter can be easily shifted by changing the dimensions of both transmission lines length l_T and the length of dual-mode resonator arms l_D

with the same value, see Fig. 6.3. Fig. 6.5 demonstrates the relation of the insertion loss of the filter by choosing $l_D = l_T = 5$ mm, 10 mm, and 15 mm, respectively, while keeping the dimensions of the perturbation patch at $p = 0.5$ mm, and the width of the attached transmission line and the arms of square-loop resonator at 0.3 mm fixed.

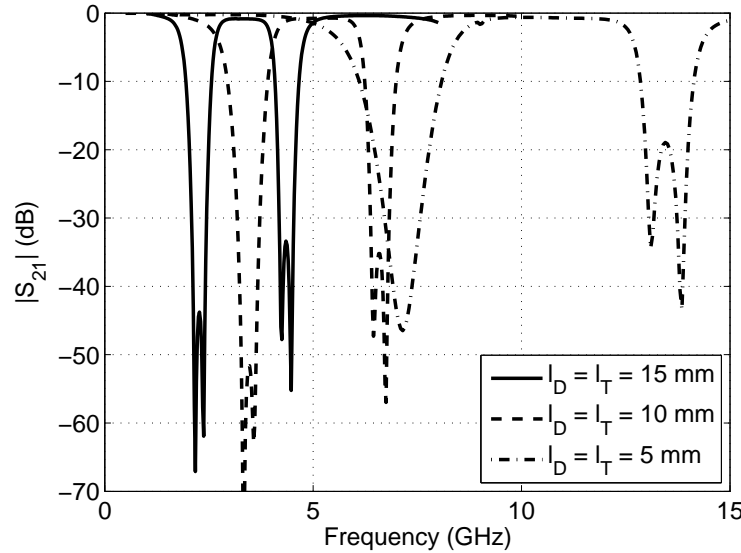


Figure 6.5: Simulated return loss of a dual-band bandpass filter with $l_D = l_T = 5, 10, 15$ mm.

One of the main advantages of this filter is that the bandwidths of both bands can be controlled by different parameters:

1. Bandwidth Control by Adjusting the Length of the Attached Transmission Lines l_T :

Changing the length of the attached transmission lines only affects the outer cut-off frequencies of the filter, while the transmission zeros remain unaffected, which leads to major effect on bandwidth of both bands. So by choosing l_T longer than the l_D , the bandwidth of the lower band increases and that of the higher band decreases. The opposite applies too, choosing the length of the attached transmission line l_T smaller than the length of arms of the dual-mode resonator decreases the bandwidth of the lower band and increases that of the higher band. This basically occurs due the transmission zeroes that remain fixed. This can be clearly seen in Fig. 6.6, which shows the simulated insertion loss of the filter for different transmission lines lengths l_T and keeping $l_D = 10$ mm.

2. Bandwidth Control by Adjusting the Length of the Square-Loop Resonator Arms l_D :

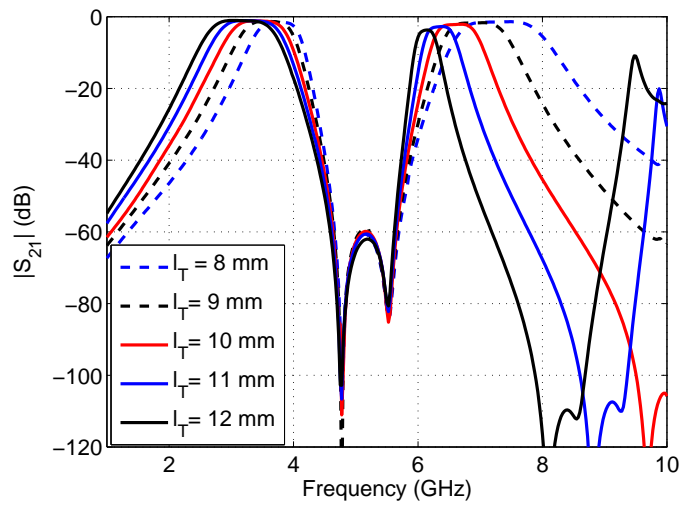


Figure 6.6: Simulated insertion loss of the dual-band bandpass filter with different l_T values, with $l_D = 10$ mm.

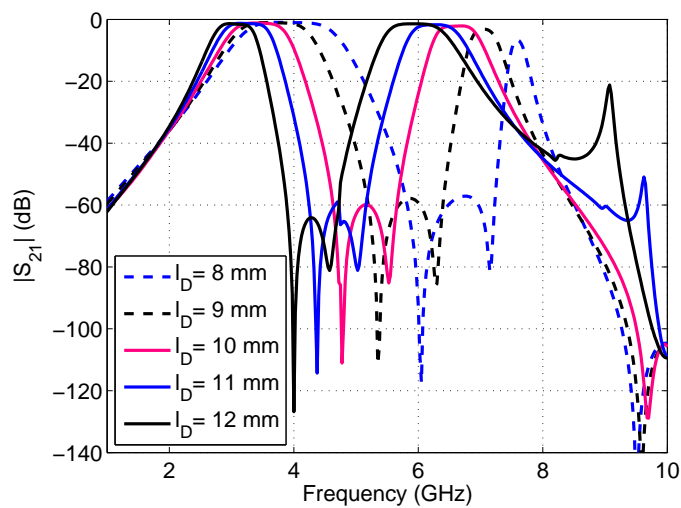


Figure 6.7: Simulated insertion loss of the dual-band bandpass filter with different l_D values with $l_T = 10$ mm.

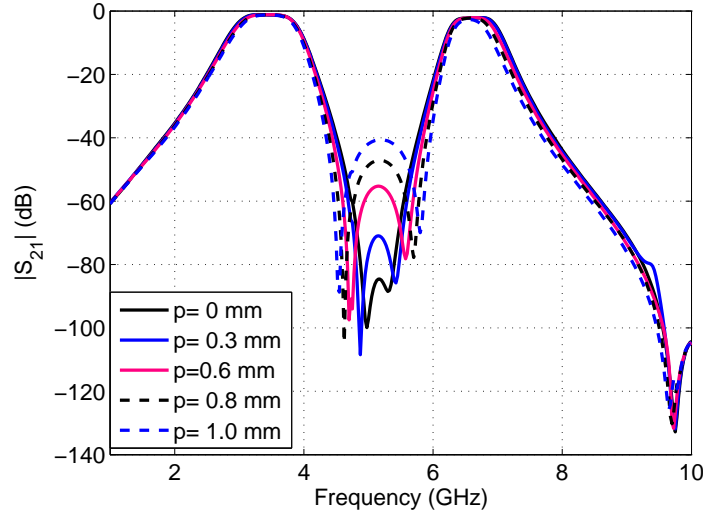


Figure 6.8: Simulated insertion loss of the dual-band bandpass filter with different p values, with $l_D = l_T = 10$ mm.

Changing the length of the dual-mode resonator arms will basically influence the position of the transmission zeroes. This in turn affects the bandwidth of the both bands. Increasing the length l_D , shifts the transmission zeroes to a lower band, which leads to having a narrower bandwidth of the lower band and wider bandwidth of the higher band. Shortening the arms shifts the transmission zeroes to a higher frequency band, which increases the bandwidth of the lower band and decreases that of the higher band. Fig. 6.7 shows the corresponding insertion loss.

3. Splitting the transmission zeroes can be easily done by increasing the dimensions of the square patch p attached to the inner side of the square-loop dual-mode resonator. Fig. 6.8 shows the effect of the square patch dimensions and the simulated insertion loss of the dual-band bandpass filter. It is clear from Fig. 6.8 that the longer the patch dimensions p , the more the transmission zeroes are splitted, which affects the sharpness of inner cut-off frequencies slopes of both bands, so by increasing the inner cut-off slopes become sharper, that may affect the bandwidth.

6.1.3 Experimental Results

A dual-band bandpass filter has been designed, fabricated and measured on RO4003c substrate. It has a thickness of 0.813 mm and a relative dielectric constant of 3.38. The width of the attached transmission line and the arms of the dual-mode resonator were chosen to be each 0.3 mm. The lengths $l_T = l_D = 10$ mm, and the dimension $p = 0.5$ mm. Fig. 6.9 shows the simulated and measured return and insertion loss of the

filter. The filter has center frequencies of 3.45 GHz, and 6.65 GHz, and bandwidths of 0.5 GHz and 0.55 GHz, respectively. The insertion loss within the pass bands is better than 0.7 dB for the lower band, and is better than 1.2 dB for the higher band. Good agreement between the measured and the simulated results is obtained.

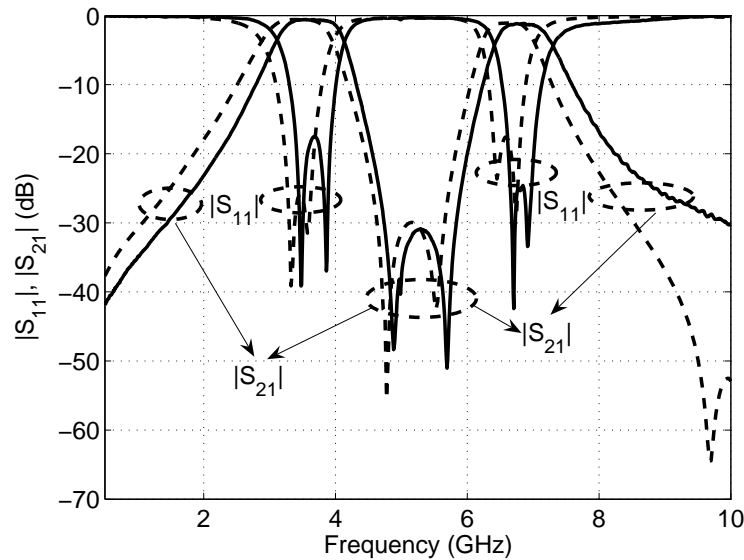


Figure 6.9: Simulated and measured return and insertion loss of a dual-band bandpass filter with dimensions $l_D = l_T = 10$ mm.

6.2 Dual-Band Suspended Stripline Filters Using Dual-Mode Resonator

In this section the suspended stripline dual-mode resonator that has been introduced in sec. 5.2 is used for dual-band filter realization. The modes of the resonator are splitted into two frequency bands. As it has been mentioned, this resonator generates two modes, the first one is quasi-lumped and the second one is open-loop mode. To split these modes, we have to choose the resonator dimensions in such a way that the quasi-lumped resonance is located at the lower frequency band and the open-loop resonant mode is located at higher frequency band.

To be able to split the modes and to shift them to a lower frequency band, we have used a housing mount with width of 10 mm. That gives us more space to enlarge our resonator, which makes it easy to shift the modes. the other dimensions are kept the same as in Fig. 3.31.

Many dimensions affect the resonant frequencies of the filter. However, changing the outer dimensions of the resonator affects both mode resonances, which makes it difficult to fix one band on a certain frequency and tune the other. In order to do so,

there are two parameters that affect only one mode or one band. The first parameter is the width of the inductive transmission line (w), which affects the quasi-lumped resonance, the wider the inductive strip is the lower the inductive value provided by this strip is, thus, the band is shifted to higher band by having wider strip line and vice versa. Fig. 6.10 shows the top and backside layouts of dual-band bandpass filter using splitted mode of dual mode suspended stripline resonator. The feeding lines are built on the topside of the substrate, while the resonators are constructed on the backside of the substrate. Fig. 6.11 shows the insertion loss of the dual-band filter with different inductive stripline widths. As it is shown in the Figure, changing the width of the inductive strip line affects only the lower band without any effect on the higher one. The other parameter is the length of the open-loop resonator, which

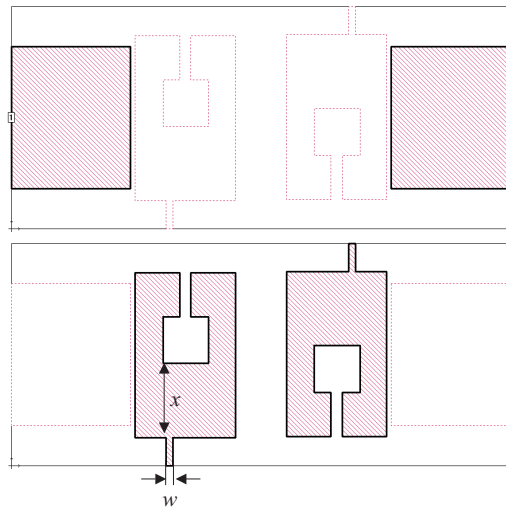


Figure 6.10: Top (up) and backside of dual-bandpass filter using splitted mode of suspended stripline dual-mode resonator.

affects the open loop-mode. To avoid the influence of this parameter on the quasi-lumped resonance, the length of the open-loop resonator is shortened by increasing the width of the resonator (x) from the middle side and from the inner side, see Fig. 6.10. Fig. 6.12 shows the insertion loss of the filter with different (x) values, as it is shown the upper band of the filter is moved to a higher frequency band by increasing the value of the dimension (x).

With this configuration, a second order dual-band bandpass filter has been designed using this kind of resonators. The filter has center frequencies of 3.8 GHz and 8.85 GHz, with bandwidths of 200 MHz and 300 MHz, respectively. The length of the filter is 9.65 mm. Since the filter has been designed using two splitted-modes dual-mode resonators, each band of the filter can be considered second order bandpass filter. Fig. 6.13 shows the simulated and measured insertion and return loss of the filter. The measured insertion loss at both passbands is better than 0.5 dB.

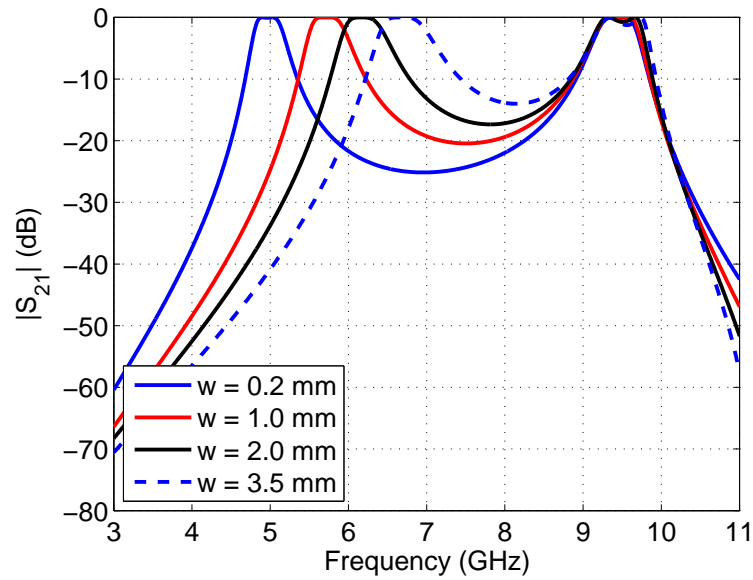


Figure 6.11: Insertion loss of the dual-band bandpass filter with different inductive stripline widths (w).

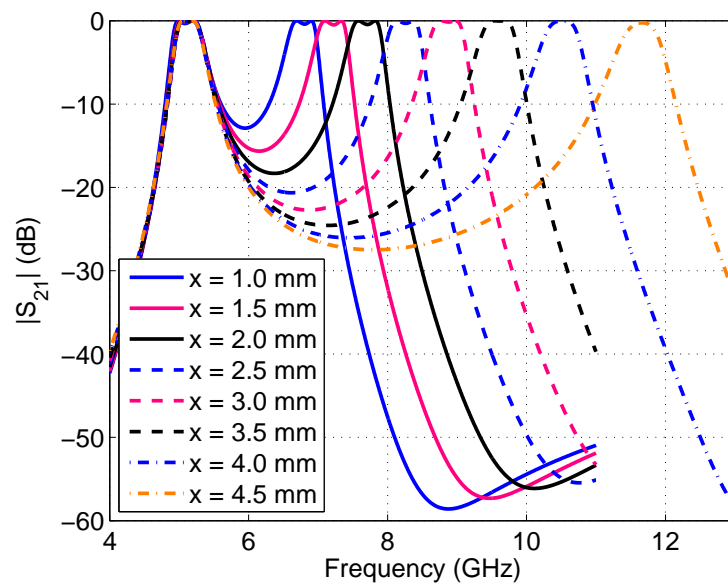


Figure 6.12: Insertion loss of the dual-band bandpass filter with different x dimension values.

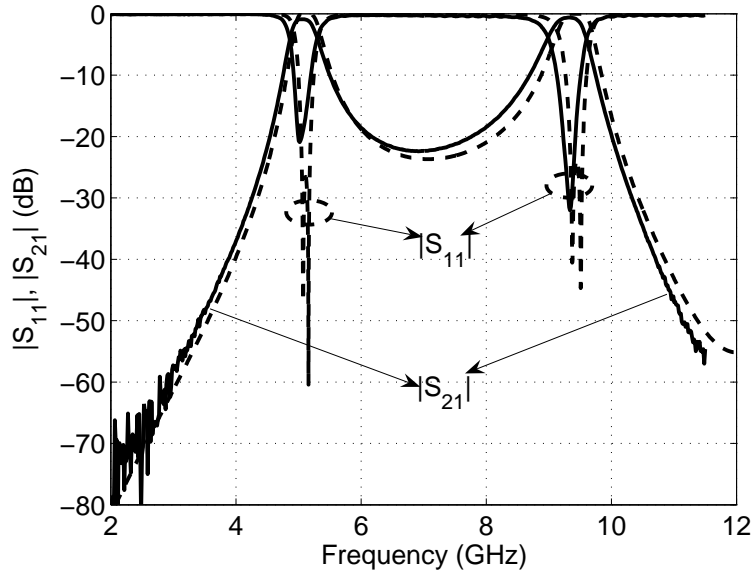


Figure 6.13: Simulated (dashed) and measured (solid) Insertion loss and return loss of the dual-band bandpass filter.

As it was shown in the same Figure, the stopband attenuation between the two passbands is about 23 dB, this rejection might not be sufficient for some application. Therefore transmission zeroes are needed between the passbands to improve the attenuation between the passbands. A transmission zero can be introduced there by applying additional inductive coupling between the resonators. This can be easily done by flipping one resonator by 180° , see Fig. 6.14. By this arrangement, the parallel inductive strips are now located on one side of the mount. A transmission zero is introduced at about 5.5 GHz. The measured and simulated return and insertion losses are shown in Fig. 6.15. An excellent agreement between the experimental and the theoretical results has been achieved.

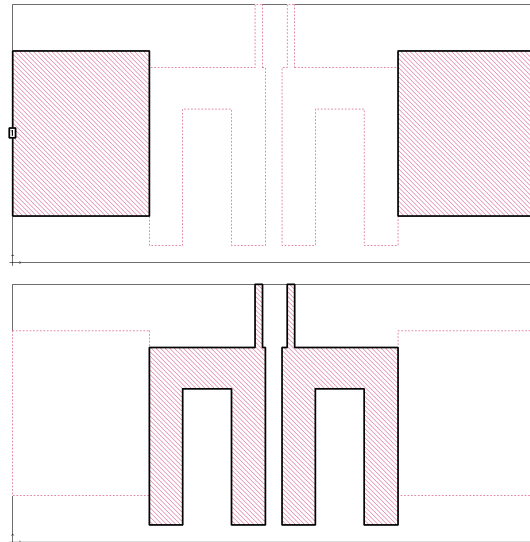


Figure 6.14: Top (up) and backside (down) layouts of a suspended stripline filter with inductive stripline at one side of the substrate.

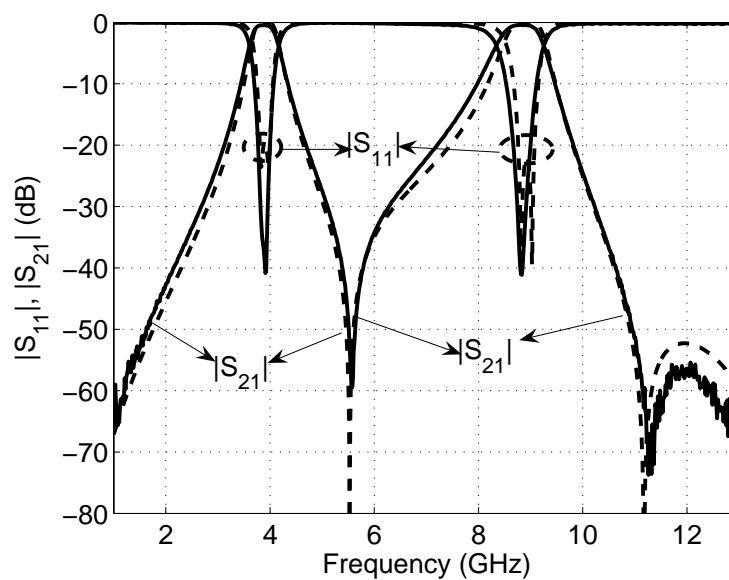


Figure 6.15: Simulated (dashed) and measured (solid) insertion and return loss of the dual-band bandpass filter with additional transmission zero.

Chapter 7

Conclusions and Future Work

7.1 Thesis Summary

The thesis has discussed and introduced different filter and resonator types. Chapter three has investigated a modified cross-section of the multilayer coplanar line and applied it for filter applications. The advantages of this modified multilayer coplanar lines are the high capacitive coupling that it provides, furthermore it can easily be integrated with CPW, microstrip line, or both. Compact filters have been introduced using this cross-section. Low-pass filter has been introduced using this cross section by adding wide patches to the classical CPW lowpass filter at the back side of the substrate and under the capacitive lines different compact filters have been introduced using this cross-section. Bandpass filters have been introduced using quasi-lumped elements, these filters have been constructed to be integrated with microstrip line, CPW, and both. Moreover, a suspended stripline UWB filter with a very wide stop-band has been introduced by coupling lowpass filter capacitively with the I/O feeding lines.

In chapter four an interdigital DGS slot has been introduced. The slot is very compact compared to the other known slot structures, up to now. Controlling the resonant frequency of the slot is done by changing the metallic finger lengths, spacing between fingers, or by changing the number of the fingers. Two lowpass filters have been presented using this slot showing the advantage of the compact slot. Moreover, the chapter has discussed the packaging difficulties of this technique and presented a solution to reduce the packaging difficulties by keeping the ground plane of the circuit fully metallized and etching the slots on the superstrate, which is directly laid on the top of the substrate. The metal of the superstrate is connected by via holes to the ground plane. The structure has the great advantage in reducing the packaging complexity, since it can be directly based on the carrier block without the need of machining a recessed region in it.

Chapter five introduced the first microstrip realization of triple-mode resonator.

This resonator was realized by adding an additional meander half wavelength microstrip line connected to two opposite corners of the original microstrip square-loop dual-mode resonator. The resonator was coupled capacitively by two perpendicular feeding lines. The position of the transmission zeros depends on the connection positions of the feeding lines. In the centered case, the filter shows one attenuation pole and two complex transmission zeros. By introducing a non-symmetry into the positions of the feeding lines, the transmission zeros are moved on to the imaginary axis of the s -plane. Equivalent circuit and coupling scheme has been presented. Two different third-order band pass filters were designed, fabricated, and measured. Good agreement has been obtained between the measured and theoretical results. In the same chapter, a realization suspended stripline dual-mode resonator has been introduced, which is the first dual-mode resonator for this technique. The resonator was realized by combining quasi-lumped parallel resonator with open-loop resonator. The resonator was applied to filter design. Very compact bandpass filters have been designed fabricated and tested. Transmission zeroes have been introduced to the filter response by applying additional inductive coupling between the resonators.

In chapter six dual-band bandpass filters have been realized by using dual-mode resonators. The first filter is a microstrip one, it has been realized by introducing transmission zeros in the passband of a broadband bandpass filter by using square-loop dual-mode resonator. controlling the center frequencies of both bands can be done by changing the length of the attached transmission lines and the length of the arms of the loop resonator equally. Controlling the bandwidth of both bands can also be done by either by changing the length of the attached transmission lines and fixing the length of the arms loop resonator, or by changing the length of the arms of the loop resonator and keeping the attached transmission line lengths fixed. The second introduced filter in this chapter was a suspended stripline one. the filter was realized by splitting the modes of the dual-mode resonator that is introduced in the last chapter into two frequency bands. transmission zero has been introduced between the two frequency bands by applying additional inductive coupling between the reosnotors. The dual-mode resonator has shown that it is an excellent resonator for filter applications especially for dual-band bandpass filter application.

7.2 Suggestions for Future Work

This thesis has presented and investigated different filter topologies and responses for different planar techniques. Since the development of the communication systems is increasing rapidly, and since the filters are essential component in any communication system, the author would like to suggest some ideas for future work.

1. For the DGS structure, it is an important issue to investigate broadband filters using this technique. Moreover, the thesis have introduced a packaging solution

for the DGS, it might be also important to introduce and investigate other packaging solutions.

2. Quadra-mode bandpass resonator may be realized by adding an additional path to the triple-mode resonator, which can decrease the size of the filter, and may increase the number of transmission zeros introduced in the stopband of the filter. For the suspended stripline, more investigation is needed on the triple-mode resonators.
3. In the dual-band bandpass filters, it might be interesting to introduce and investigate new tunable dual-band filters. Moreover, it might also be interesting to investigate a quadrable band diplexers using two dual-bandbandpass filters.

Bibliography

- [1] G. Mahttei, L. Young, and E. M. T. Jones, *Microwave Filters, Impedance Matching Networks and Coupling Structures*. Norwood, MA: Artech House, 1980.
- [2] J. S. Hong and M. J. Lancaster, *Microwave Filters for RF/Microwave Applications*. New York: John Wiley & Sons, 2001.
- [3] A. Gorur, "Description of coupling between degenerate modes of a dual-mode microstrip loop resonator using a novel perturbation arrangement and its dual-mode bandpass filter applications," *IEEE Trans. Microwave Theory Tech.*, vol. 52, no. 2, pp. 671–677, Feb. 2004.
- [4] J. S. Hong and M. J. Lancaster, "Couplings of microstrip square open-loop resonator for cross-coupling planar filters," *IEEE Trans. Microwave Theory Tech.*, vol. 44, no. 12, pp. 2099–2109, Dec. 1996.
- [5] R. E. Collin, *Foundations for Microwave Engineering*. New York: McGraw-Hill, Inc., 1992.
- [6] B. Strassner and K. Chang, "Wide low-loss high isolation microstrip periodic-stub diplexer for multiple frequency applications," *IEEE Trans. Microwave Theory Tech.*, vol. 49, no. 10, pp. 1818–1820, Oct. 2001.
- [7] W. Chen, *The circuits and filters handbook*. CRC Press, Inc.: Artech House, 1995.
- [8] M. G. Banciu, R. Ramer, and A. Ioachim, "Compact microstrip resonators for 900 MHz frequency band," *IEEE Microwave Wireless Compon. Lett.*, vol. 13, no. 5, pp. 175–177, May 2003.
- [9] I. Wolf, "Microstrip bandpass filter using degenerate modes of ring resonator," *Electronic Letters*, vol. 8, no. 12, pp. 302–303, June 1972.
- [10] J. S. Hong and M. J. Lancaster, "Bandpass characteristics of new dual-mode microstrip square loop resonators," *Electronic Letters*, vol. 31, no. 11, pp. 891–892, May 1995.

-
- [11] —, “Microstrip bandpass filter using degenerate modes of a novel meander loop resonator,” *IEEE Microwave Guided Wave Letters*, vol. 5, no. 11, pp. 371–371, Nov. 1995.
- [12] L. Zhu and W. Menzel, “Compact microstrip bandpass filter with two transmission zeroes using a stub-tapped half-wavelength line resonator,” *IEEE Microwave Wireless Compon. Lett.*, vol. 13, no. 1, pp. 16–18, Jan. 2003.
- [13] M. H. Ren, D. Chen, and Chrng, “A novel wideband bandpass filter using a cross-shaped multiple-mode resonator,” *IEEE Microwave Wireless Compon. Lett.*, vol. 18, no. 1, pp. 13–15, Jan. 2008.
- [14] U. H. Lok, Y. C. Chiou, and J.-T. Kuo, “Quadruple-mode coupled-ring resonator bandpass filter with quasi-elliptic function passband,” *IEEE Microwave Wireless Compon. Lett.*, vol. 18, no. 3, pp. 179–181, Mar. 2008.
- [15] L. Zhu, S. Sun, and W. Menzel, “Ultra-wideband (UWB) bandpass filters using multi-mode resonator,” *IEEE Microwave Wireless Compon. Lett.*, vol. 15, no. 11, pp. 796–798, Nov. 2005.
- [16] D. Ahn, J. S. Seok, C. S. Kim, J. Kim, Y. Qian, and I. Itoh, “A design of low-pass filter using the novel microstrip defected ground structure,” *IEEE Trans. Microwave Theory Tech.*, vol. 49, no. 1, pp. 86–93, Jan. 2001.
- [17] A. B. Rahman, A. K. Verma, A. Boutejdar, and A. S. Omar, “Control of bandstop response of hi-lo microstrip low-pass filter using slot in ground plane,” *IEEE Trans. Microwave Theory Tech.*, vol. 52, no. 3, pp. 1008–1013, Mar. 2004.
- [18] D. J. Woo, T. K. Lee, J. W. Lee, C. S. Pyo, and W. K. Cho, “Novel U-slot and V-slot dgss for bandstop filter improved Q factor,” *IEEE Trans. Microwave Theory Tech.*, vol. 54, no. 6, pp. 2840–2847, June 2006.
- [19] J. S. Yun, G. Y. Kim, J. S. Park, D. Ahn, K. W. Kang, and J. B. Lim, “A design of the novel coupled line bandpass filter using defected ground structure,” in *2000 IEEE MTT-S Int. Microw. Symp. Digest*, 2000, pp. 327–330.
- [20] C. S. Kim, J. S. Lim, J. H. Kim, and D. Ahn, “a design of a miniaturized 2-pole bandpass filter by using slot and hair-pin line,” in *2006 IEEE MTT-S Int. Microw. Symp. Digest*, 2006, pp. 1983–1986.
- [21] H. W. Liu, Z. F. Li, W. Sun, and J. F. Mao, “An improved 1-D periodic defected ground structure for microstrip line,” *IEEE Microwave Wireless Compon. Lett.*, vol. 14, no. 4, pp. 180–182, Apr. 2004.

- [22] S. W. Ting, K. W. Tam, and R. P. Martins, "Compact microstrip quasi-elliptic bandpass filter using open-loop dumbbell shaped defected ground structure," in *2006 IEEE MTT-S Int. Microw. Symp. Digest*, 2006, pp. 527–530.
- [23] H. J. Chen, T. H. Huang, C. S. Chang, L. S. Chen, N. F. Wang, Y. H. Wang, and M. P. Houn, "A novel cross-shap DGS applied to design ultra-wide stopband low-pass filters," *IEEE Microwave Wireless Compon. Lett.*, vol. 16, no. 5, pp. 252–254, May 2006.
- [24] W. Menzel and A. Balalem, "Quasi-lumped suspended stripline filters and diplexers," *IEEE Trans. Microwave Theory Tech.*, vol. 53, no. 10, pp. 134–142, Oct. 2005.
- [25] S. S. Liao and J. T. Peng, "Compact planar microstrip branch-line couplers using quasi-lumped elements approach with nonsymmetrical and symmetrical T-shaped structure," *IEEE Trans. Microwave Theory Tech.*, vol. 54, no. 9, pp. 3508–3514, Sept. 2006.
- [26] L. Zhu and K. Wu, "Accurate circuit model of interdigital capacitor and its application to design of new quasi-lumped miniaturized filters with suppression of harmonic resonance," *IEEE Trans. Microwave Theory Tech.*, vol. 48, no. 3, pp. 347–356, Mar. 2000.
- [27] S. C. Lin, C. H. Wang, and C. H. Chen, "Novel patch-via-spiral resonators for the development of miniaturized bandpass filters with transmission zeros," *IEEE Trans. Microwave Theory Tech.*, vol. 55, no. 1, pp. 137–146, Jan. 2007.
- [28] L. Young, "Stepped-impedance transformations and filter prototypes," *IRE Trans. Microwave Theory Tech.*, vol. 10, no. 5, pp. 339–359, Sept. 1962.
- [29] G. T. Roan and K. A. Zaki, "Computer-aided design of microstrip filters by iterated analysis," *IEEE Trans. Microwave Theory Tech.*, vol. 36, no. 11, pp. 1482–1487, Nov. 1988.
- [30] R. N. Martins and H. Abdalla, "Design of low-pass microstrip filter with equal-ripple passband and finite attenuation poles," in *2001 SBMO/IEEE MTT-S International*, Aug. 2001, pp. 71–74.
- [31] H. Hsieh and C. K, "Compact, broad-stopband elliptic-function lowpass filters using microstrip stepped impedance hairpin resonators," in *2003 IEEE MTT-S Int. Microw. Symp. Digest*, 2003, pp. 1775–1778.
- [32] W. Menzel and A. Balalem, "Compact suspended stripline quasi-elliptic low-pass filters," in *German Microwave Conf*, Apr. 2005, pp. 61–64.

- [33] M. Miyazaki, H. Asao, and O. Ishida, "A broadband dielectric diplexer using a snaked strip-line," in *1991 IEEE MTT-S Int. Microw. Symp. Digest*, 1991, pp. 551–554.
- [34] W. H. Tu and K. Chang, "Microstrip elliptic-function low-pass filters using distributed elements or slotted ground structure," *IEEE Trans. Microwave Theory Tech.*, vol. 54, no. 10, pp. 3786–3792, Oct. 2006.
- [35] J. S. Lim, C. S. Kim, D. Ahn, Y. C. Jeong, and S. Nam, "Design of low-pass filters using defected ground structure," *IEEE Trans. Microwave Theory Tech.*, vol. 53, no. 8, pp. 2539–2545, Aug. 2005.
- [36] J. Yang and W. Wu, "Compact elliptic-function low-pass filter using defected ground structure," *IEEE Microwave Wireless Compon. Lett.*, vol. 18, no. 9, pp. 578–580, Sept. 2008.
- [37] J. S. Lim, C. S. Kim, D. Ahn, Y. C. Jeong, and S. Num, "Design of low-pass filter using defected ground structure," *IEEE Trans. Microwave Theory Tech.*, vol. 53, no. 8, pp. 2539–2545, Aug. 2005.
- [38] E. H. Bradley, "Design and development of strip-line filters," *IRE Trans. Microwave Theory Tech.*, vol. 4, no. 2, pp. 86–93, Apr. 1956.
- [39] S. B. Cohn, "Parallel-coupled transmission-line-resonator filters," *IRE Trans. Microwave Theory Tech.*, vol. 6, no. 2, pp. 223–231, Apr. 1958.
- [40] W. Shwab, F. Boegelsack, and W. Menzel, "Multilayer suspended stripline and coplanar line filters," *IEEE Trans. Microwave Theory Tech.*, vol. 46, no. 7, pp. 1403–1407, 1994.
- [41] L. Zhu, H. Bu, and K. Wu, "Aperture compensation technique for innovative design of ultra-broadband microstrip bandpass filter," in *2000 IEEE MTT-S Int. Microw. Symp. Digest*, vol. 2, 2000, pp. 315–318.
- [42] F. C. Commission, "Revision of part 15 of the commissions rules regarding ultraudiband transmission systems," in *Tech. Rep. ET-Docket 98-153 FCC02-48*, Apr. 2002, pp. 98–153.
- [43] L. Zhu and S. S. anf W. Menzel, "Ultra-wideband bandpass filter with hybrid microstrip/CPW structure," *IEEE Microwave Wireless Compon. Lett.*, vol. 15, no. 12, pp. 844–846, Dec. 2005.
- [44] G. M. Yang, R. Jin, C. Vittaria, V. G. Harros, and N. X. Sun, "Small ultra-wideband (UWB) bandpass filter with notched band," *IEEE Microwave Wireless Compon. Lett.*, vol. 18, no. 3, pp. 176–178, Mar. 2008.

- [45] S. W. Wong and L. Zhu, "EBG-embedded multiple-mode resonator for UWB bandpass filter with improved upper-stopband performance," *IEEE Microwave Wireless Compon. Lett.*, vol. 17, no. 6, pp. 421–423, June 2007.
- [46] H. Miyake, S. Kitazawa, T. Ishizaki, T. Yamada, and Y. Nagatom, "A miniaturized monolithic dual band filter using ceramic lamination technique for dual mode portable telephones," in *1997 IEEE MTT-S Int. Microw. Symp. Digest*, vol. 2, 1997, pp. 789–792.
- [47] C. Quendo, E. Rius, and C. Person, "An original topology of dual-band filter with transmission zeros," in *2003 IEEE MTT-S Int. Microw. Symp. Digest*, vol. 2, 2003, pp. 1093–1096.
- [48] V. Palazzari, S. Pinel, J. Laskar, L. Roselli, and M. M. Tentzeris, "Design of an asymmetrical dual-band wlan filter in liquid crystal polymer (LCP) system-on-package technology," *IEEE Microwave Wireless Compon. Lett.*, vol. 15, no. 3, pp. 165–167, Mar. 2005.
- [49] S. F. Chang, J. L. Chen, and S. C. Chang, "New dual-band bandpass filters with step-impedance resonators comb and hairpin structures," in *Asia Pacific Microw. Conf*, Dec. 2003, pp. 793–796.
- [50] S. F. Chang, Y. H. Jeng, and J. L. Chen, "Dual-band step-impedance bandpass filter for wireless LANs," *Electronic Letters*, vol. 40, no. 1.
- [51] H. M. Lee, C. R. Chen, and C. C. Tsa, "Dual-band coupling and feed structure for microstrip filter design," in *2004 IEEE MTT-S Int. Microw. Symp. Digest*, vol. 2, 2004, pp. 1971–1974.
- [52] S. Sun and L. Zhu, "Compact dual-band microstrip bandpass filter without external feeds," *IEEE Microwave Wireless Compon. Lett.*, vol. 15, no. 10, pp. 644–646, Oct. 2005.
- [53] L. D. Paarmann, *Design and Analysis of Analog Filters*. Norwell: KLUWER ACADEMIC PUBLISHERS, 2001.
- [54] I. Hunter, *Theory and Design of Microwave Filters*. London: Institution of Engineering and Technology *IET*, 2001.
- [55] H. A. Wheeler, "Transmission-line properties of parallel wide strips by a conformal mapping approximation," *IEEE Trans. Microwave Theory Tech.*, vol. 12, no. 3, pp. 172–185, May 1964.
- [56] —, "Transmission-line properties of parallel strips separated by a dielectric sheet," *IEEE Trans. Microwave Theory Tech.*, vol. 13, no. 2, pp. 1800–1805, 1965.

- [57] M. V. Schneider, "Microstrip lines for microwave integrated circuits," *Bell Syst. Tech. Journal*, vol. 48, pp. 1421–1444, May 1969.
- [58] R. N. Simons, *Coplanar Waveguide Circuits, Components, and Systems*. New York: John Wiley & Sons, 2001.
- [59] J. D. Rhodes, "Suspended substrates provide alternative to coax," *Microwave Systems News*, vol. 9, no. 8, pp. 134–143, Aug. 1979.
- [60] E. Yamasita, B. Y. Wang, and K. Atsuki, "Effects of side-wall grooves on transmission characteristic of suspended strip lines," in *1985 IEEE MTT-S Int. Microw. Symp. Digest*, 1985, pp. 145–147.
- [61] —, "Effects of side-wall grooves on transmission characteristic of suspended strip lines," *IEEE Trans. Microwave Theory Tech.*, vol. 33, no. 12, pp. 323–328, Dec. 1985.
- [62] E. Yamasita, M. Nakajima, and K. Atsuki, "Analysis method for generalized suspended strip lines," in *1986 IEEE MTT-S Int. Microw. Symp. Digest*, 1986, pp. 261–264.
- [63] —, "Analysis method for generalized suspended strip lines," *IEEE Trans. Microwave Theory Tech.*, vol. 34, no. 12, pp. 3370–3374, Dec. 1986.
- [64] W. Menzel, "Broadband filter circuits using an extended suspended substrate transmission line configuration," in *22nd European Microwave Conference*, Oct. 1992, pp. 459–463.
- [65] W. Menzel and F. Boegelsack, "Folded stubs for compact suspended stripline circuits," in *1993 IEEE MTT-S Int. Microwave Symp. Digest*, 1993, pp. 593–596.
- [66] W. Menzel and M. S. Tito, "A miniaturized suspended stripline filters for integration into extended circuits," in *36 European Microwave Conference*, 2006, pp. 909–912.
- [67] L. C. A. Lehtovuori, *Model for Shielded Suspended Substrate Microstrip Line*. Circuit Theory Laboratory Report Series: Helsinki University of Technology, 1998.
- [68] S. Geelani, *High Q-factor Metamaterial Duplex Filters in Suspended Stripline Technology*. Ph.D. Thesis: Erlangen-Nuernberg university, March, 2009.
- [69] S. Banba, T. Hasegawa, and H. Ogawa, "Multilayer MMIC branch-line hybrid using thin dielectric layers," *IEEE Microwave Guided Wave Letters*, vol. 1, no. 11, pp. 346–347, Nov. 1991.

- [70] W. Menzel, W. Schwab, and G. Strauss, "Investigation of coupling structure for coplanar bandpass filter," in *1995 IEEE MTT-S Int. Microwave Symp. Digest*, June 1995, pp. 1407–1410.
- [71] C. Warns, W. Menzel, and H. Schumacher, "Transmission lines and passive elements for multilayer coplanar circuits on silicon," *IEEE Trans. Microwave Theory Tech.*, vol. 46, no. 5, pp. 616–625, May 1998.
- [72] H. Okazaki and T. Hirota, "Multilayer MMIC broad side coupler with a symmetric structure," *IEEE Microwave Guided Wave Letters*, vol. 7, no. 6, pp. 145–146, June 1997.
- [73] L. Zhu, H. Bu, and K. Wu, "Unifield CAD model of microstrip line with rear side aperture for multilayer integrated circuits," in *2000 IEEE MTT-S Int. Microw. Symp. Digest*, vol. 2, 2000, pp. 981–984.
- [74] K. J. H. an T. A. Schwarz and L. P. B. Katehi, "Si micromachined coplanar waveguides for use in high-frequency circuits," *IEEE Trans. Microwave Theory Tech.*, vol. 46, no. 6, pp. 762–768, June 1998.
- [75] J. Papapolymerou, F. Brauchler, J. East, and L. P. B. Katehi, "W-band finite ground coplanar monolithic multipliers," *IEEE Trans. Microwave Theory Tech.*, vol. 47, no. 5, pp. 614–619, May 1999.
- [76] H. Joshi and W. J. Chappell, "Dual-band lumped-element bandpass filter," *IEEE Trans. Microwave Theory Tech.*, vol. 54, no. 12, pp. 4169–4177, Dec. 2006.
- [77] M. S. W. S. G. Mao, "Design of artificial lumped-elements coplanar waveguide filters with contrrollable dual-passband responses," *IEEE Trans. Microwave Theory Tech.*, vol. 56, no. 7, pp. 1684–1692, July 2008.
- [78] A. Balalem, I. Hamad, J. Machac, and A. S. Omar, "Bandpass filters on a modified multilayer coplanar line," in *2006 IEEE MTT-S Int. Microw. Symp. Digest*, vol. 2, 2006, pp. 531–534.
- [79] R. A. Pucel, "Design considerations for monolithic microwave circuits," *IEEE Trans. Microwave Theory Tech.*, vol. 29, no. 6, pp. 513–534, June 1981.
- [80] E. Pettenpaull, H. Kapusta, A. Weisgerber, H. Mampe, J. Luginsland, and I. Wolff, "CAD models of lumped elements on gaas up 18 ghz," *IEEE Trans. Microwave Theory Tech.*, vol. 36, no. 2, pp. 294–304, Feb. 1986.
- [81] SONNET, *Version 10.52*. Sonnet Software Inc.: www.sonnetsoftware.com.
- [82] M. O. 2002, *version 5.53*. Applied Wave Research, Inc.

-
- [83] C. A. Balalanis, *Antenna Theory Analysis and Design*. New York: John Wiley & Sons LTD, 1997.
- [84] T. A. Milligan, *Modern antenna design*. New York: J. Wiley & Sons, 2005.
- [85] E. O. Hammerstadt, "Equations for microstrip circuit design," in *5th European Microwave conf*, 1975, pp. 268–272.
- [86] C. I. Mobbs and J. D. Rhodes, "A generalized chebyshev suspended substrate stripline bandpass filter," *IEEE Trans. Microwave Theory Tech.*, vol. 31, no. 5, pp. 397–402, May 1983.
- [87] E. Yamashita, B. Y. Wang, and K. Atsuki, "Effect of side-wall grooves on transmission characteristics of suspended striplines," in *1985 IEEE MTT-S Int.Microw. Symp. Digest*, vol. 2, 1985, pp. 145–148.
- [88] E. Yamashita, M. Nakajima, and K. Atsuki, "Analysis method for generalized suspended striplines," *IEEE Trans. Microwave Theory Tech.*, vol. 34, no. 12, pp. 1457–1463, Dec. 1986.
- [89] Y. S. Lin, W. C. Ku, C. H. Wang, and C. H. Chin, "Wideband coplanar-waveguide bandpass filters with good stopband rejection," *IEEE Microwave Wireless Compon. Lett.*, vol. 14, no. 9, pp. 422–424, Sept. 2008.
- [90] W. Menzel, M. S. Tito, and L. Zhu, "Low-loss ultra-wideband (UWB) filters using suspended stripline," in *Asia Pacific Microw. Conf*, Dec. 2005, pp. 2148–2151.
- [91] H. Ishida and K. Araki, "Design and analysis of UWB bandpass filter with ring filter," in *2004 IEEE MTT-S Int.Microw. Symp. Digest*, vol. 2, 2004, pp. 1307–1310.
- [92] T. N. Kuo, S. C. Lin, and C. H. Chen, "Compact ultra-wideband bandpass filters using composite microstrip-coplanar-waveguide structure," *IEEE Trans. Microwave Theory Tech.*, vol. 54, no. 10, pp. 3772–2778, Oct. 2006.
- [93] A. M. E. Safwat, F. Podevin, P. Ferrari, and A. Vilcot, "Tunable bandstop defected ground structure resonator using reconfigurable dumbbell-shaped coplanar waveguide," *IEEE Trans. Microwave Theory Tech.*, vol. 54, no. 9, pp. 3559–3564, Sept. 2006.
- [94] A. R. Ali, A. Abdel-Rahman, A. Amari, and A. S. Omar, "Direct and cross-coupled resonator filters using defected ground structure (DGS) resonators," in *35th European Microwave conf*, Oct. 2005, pp. 1275–1278.

-
- [95] C. Lugo and J. Papapolymerou, "Bandpass filter design using a microstrip triangular loop resonator with dual-mode operation," *IEEE Microwave Wireless Compon. Lett.*, vol. 15, no. 7, pp. 475–477, July 2005.
- [96] R. J. Mao and X. H. Tang, "Novel dual mode bandpass filters using hexagonal loop resonators," *IEEE Trans. Microwave Theory Tech.*, vol. 54, no. 9, pp. 3526–3533, Sept. 2006.
- [97] M. H. Awida, A. M. Safwat, and H. El-Hinnawy, "Dual-mode microstrip bandpass filter using ring of arrows resonator," *Electronic Letters*, vol. 41, no. 24, pp. 1335–1336, Nov. 2005.
- [98] A. Gorur, "A novel dual-mode bandpass filter with wide stopband using the properties of microstrip open-loop resonator," *IEEE Microwave Wireless Compon. Lett.*, vol. 12, no. 10, pp. 386–388, Oct. 2002.
- [99] A. Gorur and C. Karpuz, "A reduction-size dual-mode bandpass filter with capacitive loaded open-loop arms," *IEEE Microwave Wireless Compon. Lett.*, vol. 13, no. 9, pp. 386–387, Sept. 2003.
- [100] —, "Miniature dual-mode microstrip filter," *IEEE Microwave Wireless Compon. Lett.*, vol. 17, no. 1, pp. 37–39, Jan. 2007.
- [101] J. S. Hong and S. Li, "Theory and experiment of dual-mode microstrip triangular patch resonators and filters," *IEEE Trans. Microwave Theory Tech.*, vol. 52, no. 4, pp. 1237–1243, Apr. 2004.
- [102] R. R. Mansour, "Design of superconductive multiplexers using single-mode and dual-mode filters," *IEEE Trans. Microwave Theory Tech.*, vol. 42, no. 7, pp. 1411–1418, July 1994.
- [103] A. C. Kundu and I. Awai, "Control of attenuation pole frequency of a dual-mode microstrip ring resonator bandpass filter," *IEEE Trans. Microwave Theory Tech.*, vol. 49, no. 6, pp. 1113–1117, June 2001.
- [104] L. H. Chuna and D. Mirshekar, "Analysis of dielectric loaded cubical cavity for triple-mode filter design," in *Proc. Inst. Eng. -Microwave, antenna, Propagation*, vol. 151, Feb. 2004, pp. 61–66.
- [105] J. Hattori, H. Wakamatsu, H. Kubo, and Y. Ishikawa, "2 GHz band triple mode dielectric resonator duplexer for digital cellular base station," in *Asian Pacific Microwave Conf.*
- [106] I. C. Hunter, J. D. Rhodes, and V. Dassonville, "Triple mode dielectric resonator hybrid reflection filters," in *Proc. Inst. Eng. -Microwave, antenna, and Propagation*, Aug. 1998, pp. 337–343.

- [107] C. Lugo and J. Papapolymerou, "Planar realization of a triple-mode bandpass filter using a multilayer configuration," *IEEE Trans. Microwave Theory Tech.*, vol. 55, no. 2, pp. 296–301, Feb. 2007.
- [108] S. Amari, "Comments on description of coupling between the degenerate modes of a dual-mode microstrip loop resonator using a novel perturbation arrangement and its dual-mode bandpass filter applications," *IEEE Trans. Microwave Theory Tech.*, vol. 52, no. 9, pp. 2190–2192, Sept. 2004.
- [109] R. Cameron, "Advanced coupling matrix synthesis techniques for microwave filters," *IEEE Trans. Microwave Theory Tech.*, vol. 51, no. 1, pp. 1–10, Jan. 2003.
- [110] S. Amari, "Synthesis of cross-coupled resonator filters using an analytical gradient-based optimization technique," *IEEE Trans. Microwave Theory Tech.*, vol. 48, no. 9, pp. 1559–1564, Sept. 2000.
- [111] S. Amari, U. Rosenberg, and J. Bornemann, "Adaptive synthesis and resonator filters with source/load-multiresonator coupling," *IEEE Trans. Microwave Theory Tech.*, vol. 50, no. 8, pp. 1969–1978, Aug. 2002.
- [112] I. Awai and T. Yamashita, "Two-stage bandpass filters based on rotated excitation of circular dual mode resonators," *IEEE Microwave Guided Wave Letters*, vol. 7, no. 8, pp. 212–213, Aug. 1997.
- [113] , *Advanced Design System ADS*. Agilent Technology.
- [114] W. Menzel, "A novel miniature suspended stripline filter," in *33rd European Microwave conf*, Oct. 2003, pp. 1047–1050.
- [115] W. Menzel and M. Berry, "Quasi-lumped suspended stripline filters with adjustable zeroes," in *2004 IEEE MTT-S Int. Microw. Symp. Digest*, June 2004, pp. 1601–1604.
- [116] E. G. Cristal and S. Frankel, "Hairpin-line and hybrid hairpin-line/half-wave parallel-coupled-line filters," *IEEE Trans. Microwave Theory Tech.*, vol. 20, no. 11, pp. 719–728, Nov. 1972.
- [117] M. Makimoto and M. Sagawa, "Varactor tuning bandpass filter using microstrip-line ring resonator," in *1986 IEEE MTT-S Int. Microw. Symp. Digest*, June 1986, pp. 411–414.
- [118] K. Takahashi, M. Sagawa, and M. Makimoto, "Miniaturized hair-pin resonator and their applications to receiver front-end MICs," in *1989 IEEE MTT-S Int. Microw. Symp. Digest*, June 1989, pp. 667–670.

- [119] J. T. Kuo, T. H. Yeh, and C. C. Yeh, "Design of microstrip bandpass filters with a dual-passband response," *IEEE Trans. Microwave Theory Tech.*, vol. 53, no. 4, pp. 1331–1337, Apr. 2005.
- [120] H. M. Lee and C. M. Tsai, "Dual-band filter design with flexible passband frequency and bandwidth selections," *IEEE Trans. Microwave Theory Tech.*, vol. 55, no. 5, pp. 1002–1009, Apr. 2007.
- [121] Y. P. Zhang and M. sun, "Dual-band microstrip bandpass filter using stepped-impedance resonators with new coupling schemes," *IEEE Trans. Microwave Theory Tech.*, vol. 54, no. 10, pp. 3779–3785, Oct. 2006.
- [122] A. Gorur and C. Karpuz, "Compact dual-band bandpass filter using dual-mode resonators," in *2007 IEEE MTT-S Int. Microw. Symp. Digest*, vol. 2, 2007, pp. 905–908.
- [123] C. Y. Chen, C. Y. Hsu, and H. R. Chuang, "Design of miniature planar dual-band filter using dual-feeding structures and embedded resonators," *IEEE Microwave Wireless Compon. Lett.*, vol. 16, no. 12, pp. 669–671, Dec. 2006.
- [124] C. Y. Chen and S. Y. Hsu, "A simple and effective method for microstrip dual-band filters design," *IEEE Microwave Wireless Compon. Lett.*, vol. 16, no. 5, pp. 246–248, May 2006.
- [125] X. Y. Zhang and Q. Xue, "Novel dual-mode dual-band filters using coplanar-waveguide-fed ring resonators," *IEEE Trans. Microwave Theory Tech.*, vol. 55, no. 10, pp. 2183–2190, Oct. 2007.

Curriculum Vitae

Name: Atallah Balalem
Date of Birth: January 15, 1978 in Nablus, Palestine
Nationality: Palestinian
Status: Married, 1 Child
Address: Listemannstr. 18
39104 Magdeburg, Germany
E-mail: atallah.balalem@ovgu.de

Education

- Since 06.2005: Working towards Ph.D. degree at the Institute for Electronics, Signal Processing, and Comm., University of Magdeburg, Germany.
- 04.2002 - 02.2005: M.Sc. in Communication Technology, University of Ulm, Ulm, Germany.
- 10.1996 - 06.2000: B.Sc. in Physics / Minor Electronics, An-najah National University, Nablus, Palestine.

Work Experience

- 01.2004 - 03.2005: Testing and integrating mobile phone software on various platforms, LogicaCMG Ulm, Ulm, Germany.
- 02.2003 - 08.2003: Thermal analysis with differential scanning calorimeter (DSC) Dept. of Advanced Materials, University of Ulm, Ulm, Germany.
- 02.2003 - 08.2003: Assistant lecturers for maths and physics Der Sharaf Secondary School, Nablus, Palestine.

Memberships

- Editorial Board Member of IEEE Microwave and Wireless Components Letters.
- Editorial Board Member of Journal of Electromagnetic Waves and Applications.

List of Publications

Journal Papers:

1. Atallah Balalem, Jan Machac, and Abbas Omar, "**Dual-Band Bandpass Filter Using the Microstrip Square-Loop Dual-Mode Resonator**", *Microwave and Optical Technology Letters*, Vol. 50, No. 6, pp. 1567-1570, June 2008.
2. Atallah Balalem, Wang Kim-Fai, Jan Machac, and Abbas Omar, "**Low-Loss Doubly Metallized CPW Low-Pass Filters with Additional Transmission Zeros**", *Microwave and Optical Technology Letters*, Vol. 50, No. 5, pp. 51-55, May 2008.
3. Atallah Balalem, Wolfgang Menzel, Jan Machac, and Abbas Omar, "**A Simple Ultra-Wideband Suspended Stripline Bandpass Filter with Very Wide Stop-band**", *IEEE Microwave and wireless components letters*, Vol. 18, No. 3, pp. 170-172, March 2008. (cited 5 times)
4. Atallah Balalem, Jan Machac, and Abbas Omar, "**Microstrip-CPW Bandpass Filter for Antenna Application**", *Microwave and Optical Technology Letters*, Vol. 50, No. 1, pp. 51-55, January 2008. (cited 2 times)
5. Atallah Balalem, Ali R. Ali, Jan Machac, and Abbas Omar, "**Quasi-Elliptic Microstrip Low-Pass Filters Using an Interdigital DGS Slot**", *IEEE Microwave and wireless components letters*, Vol. 17, No. 8, pp. 586-588, August 2007. (cited 8 times)
6. Wolfgang Menzel, Atallah Balalem, "**Quasi-Lumped Suspended Stripline Filters and Diplexers**", *IEEE Transactions on Microwave Theory and Techniques*, Vol. 53, No. 10, pp. 3230-3237, October 2005. (cited 9 times)

Conference Papers:

7. Adel Abdel-Rahmand, Atallah Balalem, Jan Machac, and Abbas Omar, "**UWB Bandpass Filter with Wide Stopband Using Lumped Coupling Capacitors**", *Asian Pacific Microwave Conf. 2009 (APMC 2009)*, Singapore, December 2009.
8. Atallah Balalem, Ali R. Ali, Smain Amari, Jan Machac, and Abbas Omar, "**Realization of a Planar Triple-Mode Resonator Using a Square-Loop Resonator**", *2009 IEEE MTT-S Int. Microwave symp. Digest*, Boston, USA, June 2009.
9. Atallah Balalem, Jan Machac, Abbas Omar, "**Inverted Defected Ground Structure for Microstrip Lines Filters Reducing Packaging Complexity**", *Proc. Asian Pacific Microwave Conf. (APMC) 2008*, Hong Kong, China, December 2008.
10. Atallah Balalem, Ali R. Ali, Jan Machac, Abbas Omar, "**Compact Band-stop Filters Using an Interdigital DGS Structure**", *Proceedings of 14th Microwave Techniques COMITE 2008*, Prague, Czech Republic, pp. 175-178, April 2008.
11. Ahmad Boutejdar, Adel Elsherbini, Atallah Balalem, Jan Machac and Abbas Omar, "**Design of New Hairpin Microstrip Bandpass Filter Using Coupling Matrix Method and Befected Ground Strustructure (DGS)**", *Progress in Electromagnetic Research Symposium 2007(PERS)*, Prague, Czech Republic, pp. 261-265 August 2007. (cited 1 time)
12. Atallah Balalem, Jan Machac, Abbas Omar, "**Quasi-Lumped bandpass filters using Doubly Metalized Lines**", *Proceedings of 17th International conference Radioelectronica 2007*, Berno, Czech Republic, April 2007.
13. Mohammed Awida, Atallah Balalem, Amr Safwat, Hadia El- Hinnawy, Abbas S. Omar, "**Combined lowpass-Bandpass Filter Response Using Different Shapes of Microstrip Dual-Mode Response**", *In Proc. European Mecrowave Asosiation EuMA*, Vol. 2, Issue 4, pp. 326-332, Dec. 2006.
14. Atallah Balalem, Wolfgang Menzel , Abbas Omar, "**Quasi- Lumped- Open-Loop Suspended Stripline Bandpass Filters**", *European Microwave Conf. 2006*, Manchester, UK, pp.568-571, September 2006.
15. Atallah Balalem, Ehab K. I. Hamad, Jan Machac, Abbas S. Omar, "**Bandpass Filters on a Modified Multilayer Coplanar Line**", *2006 IEEE MTT-S Int. Microwave symp. Digest*, san fransisco, USA, pp.531-534, June 2006. (cited 1 time)

16. Mohammed Awida, Atallah Balalem, Amr Safwat, Hadia El- Hinnawy, and Abbas S. Omar, "**Combined Low-Pass and Bandpass Response Using Microstrip Dual- Mode Resonators**", *2006 IEEE MTT-S Int. Microwave symp. Digest*, san francisco, USA, pp.701-704, June 2006.
17. Wolfgang Menzel, Atallah Balalem, "**Suspended Stripline Bandpass Filters with Inductive and Mixed Coupling**", *in Proc. German Microwave Conference GeMiC 2006*, Karlsruhe, Germany, pp.28-30, April 2006.
18. Wolfgang Menzel, Atallah Balalem, "**Compact Suspended Stripline Quasi-Elliptic Low-Pass Filters**", *in Proc. German Microwave Conference GeMiC 2005*, Ulm, Germany, pp.61-64, April 2005. (cited 2 times)

Atallah Balalem

30.10.2009, Magdeburg